NASA CONTRACTOR REPORT

NASA CR-1902

ATTITUDE-REFERENCED RADIOMETER STUDY

Part II - Primary Calibration System

by William R. Williamson and Allen A. Otte

Prepared by
HONEYWELL, INC.
Minneapolis, Minn.
for Langley Research Center

NATIONAL AERONAUTICS AND SPACE ADMINISTRATION • WASHINGTON, D. C. • DECEMBER 1971

1. Report No.	2. Government Accession No.	3. Recipient's Catalog No.
NASA CR-1902		

4. Title and Subtitle	5. Report Date
Attitude-Referenced Radiometer Study Part II - Primary Calibration System	December 1971 6. Performing Organization Code

7. Author(s)	8. Performing Organization Report No.
William R. Williamson and Allen A. Otte	10. Work Unit No.

9. Performing Organization Name and Address	11. Contract or Grant No.
Honeywell, Inc. Aerospace Division Minneapolis, Minnesota	NAS1-8801 13. Type of Report and Period Covered

12. Sponsoring Agency Name and Address	14. Sponsoring Agency Code
National Aeronautics and Space Administration Washington, D.C. 20546	Contractor Report

15. Supplementary Notes

16. Abstract

A Primary Calibration System, PCS, for infrared radiometers has been developed, built, and tested. The system allows radiometers to be calibrated with less than 1 percent error for use in earth coverage horizon measurements, earth resources surveys, and synoptic meteorological measurements. This document reports on the final design, fabrication and test of the PCS. A detailed description of the PCS construction is presented, along with the results of a complete series of functional tests. Test to verify the source thermal characteristics, collimator reflectance, and output beam characteristics are described and their results presented.

17. Key Words (Suggested by Author(s))	18. Distribution Statement
Infrared Radiometer Calibration System Radiance Calibration	Unclassified - Unlimited

19. Security Classif. (of this report)	20. Security Classif. (of this page)	21. No. of Pages	22. Price*
Unclassified	Unclassified	131	$3.00

*For sale by the National Technical Information Service, Springfield, Virginia 22151

1. Radiometers -- Calibration

FOREWORD

This report documents the results of an Attitude-Referenced Radiometer Study (ARRS), Part II, performed under National Aeronautics and Space Administration Contract No. NAS1-8801.

A previous design study under Contract NAS1-8801 (ARRS Part I) included the concept and layout design, and establishment of the design requirements for a Primary Calibration System (PCS) for high-accuracy calibration of infrared radiometers. The ARRS Part II program, documented in this volume, was devoted to the detailed design, construction, and evaluation of the PCS. Detailed test results are presented herein.

Honeywell Inc., Aerospace Division, performed this study program under the technical direction of Mr. J. C. Bates. The Part II effort was conducted from 1 December 1969 to 1 May 1971.

Acknowledgment is extended to Messrs. I. R. Abel and J. R. Thomas, Honeywell Inc., for analyses performed on the reflectometer and test radiometer to establish the design requirements for these portions of the system.

Gratitude is extended to NASA Langley Research Center, for their technical guidance, under the program technical direction of Mr. A. Jalink, Jr., with direct assistance from Mr. W.D. Hesketh.

CONTENTS

LIST OF ILLUSTRATIONS

LIST OF ILLUSTRATIONS (CONTINUED)

LIST OF ILLUSTRATIONS (CONCLUDED)

LIST OF TABLES

ATTITUDE-REFERENCED RADIOMETER STUDY
PRIMARY CALIBRATION SYSTEM

By: William R. Williamson and Allen A. Otte
Honeywell Inc.

SUMMARY

For earth coverage horizon measurements, earth resources surveys, and synoptic meteorological surveys, infrared radiometric sensors must be calibrated accurately. In the past, radiometer calibration for these measurements has been achieved at the 5 to 10 percent level, resulting directly in errors of this magnitude in the determined atmospheric temperatures and constituents and earth surface features and characteristics. A high-accuracy calibration system has been developed and evaluated to provide the required precision and accuracy for calibration of infrared radiometers to within 1 percent.

The system uses a point source projected to infinity to provide a well-defined collimated beam of long-wavelength infrared radiation (LWIR). Radiation emanates from an adjustable-temperature blackbody source with known emissivity and with a known and accurately controlled temperature. An off-axis parabolic collimator located with its focal point at the source aperture projects collimated radiation to the radiometer being calibrated. The system includes a liquid-nitrogen-cooled vacuum chamber to reduce stray radiation and atmospheric absorption effects to negligible levels. Radiometers with entrance apertures of up to 56 cm in diameter can be calibrated in this system.

To evaluate and prove the accuracy of the Primary Calibration System, a reflectometer system and a test radiometer were designed and constructed. As a necessary element in assuring an accurate calibration, the reflectometer system measured the reflectance of the large collimating mirror, at its operating temperature of $80^{\circ}K$, to an accuracy of 0.1 percent. The test radiometer was used to map the PCS collimator beam uniformity and system goniometric properties.

The system has been evaluated and test results show that it has a capability of less than 1 percent calibration error in the wavelength interval of 5 to 25 microns over the temperature range of $80^{\circ}K$ to $300^{\circ}K$.

INTRODUCTION

A Primary Calibration System for Infrared Radiometers has been developed during this and preceding contracts for NASA Langley Research Center. A preceding program, NAS 1-6010, established the need for a Primary Calibration System to provide absolute calibration of radiometers to within 1 percent error for use in earth coverage horizon measurements, earth resources surveys, and synoptic meteorological measurements. Feasibility of primary calibration to this required accuracy was also established.

The calibration system uses a controlled adjustable-temperature blackbody source projected to infinity by collimating optics. During the Attitude-Referenced Radiometer Study (ARRS) Part I (Contract NAS 1-8801), the configuration of all system elements was specified, including the blackbody source and temperature control, collimating optics, vacuum chamber, vacuum system, and cooling system. One of the tasks accomplished was determination of the feasibility of measuring collimator reflectance to the order of 0.1 percent. The knowledge of collimator reflectance to this accuracy is essential in determining total system calibration accuracy to the levels required.

The objective of the ARRS Part II program was to perform a detail design of the Primary Calibration System, based on the results of ARRS Part I, and then fabricate, assemble, and test an operational system which would satisfy the design requirements.

Included in the Part II activities were the detail design, supporting analyses, construction, and test of a reflectometer and test radiometer to verify the operational characteristics of the system--the reflectometer to measure the collimator reflectance insitu and the test radiometer to measure the PCS output beam characteristics. A complete series of functional tests was performed and the results documented to define the performance parameters in the areas of:

- Vacuum characteristics
- Cooldown characteristics
- Source thermal characteristics
- Collimator reflectance
- Output beam radiance characteristics

BACKGROUND AND GENERAL SYSTEM DESCRIPTION

This document reports on Part II of the Attitude-Referenced Radiometer Study, which consisted of the final design, fabrication, and test of the PCS. The system allows the calibration of IR radiometers with less than 1 percent error. This accuracy is desirable for radiometers used for earth coverage horizon definition measurements, earth resources surveys, and meteorological measurements. Previous studies (References 1 and 2) documented some of the important elements required to allow this level of accuracy in IR calibrations. The ARRS Part II program relied heavily on these background studies to guide the design and development of a Primary Calibration System.

Background

For the types of measurements indicated, a primary requirement is the ability to measure the radiance of interest with the maximum possible accuracy. Since the accuracy of measurement can be no greater than that of the primary calibration, the calibration source and method of calibration are extremely important. Previous studies (documented in Reference 1) indicated that the following conditions of calibration must be met to assure that the desired accuracy is achieved:

- The output of the radiation source within the calibration system must be known to within 1 percent of its actual value (accuracy), and its radiance from measurement to measurement must not vary more than 0.1 percent (precision).
- The calibration source must appear to be at infinity as viewed by the radiometer under test so that it simulates the conditions of field measurement and makes it possible to ascertain that no error is introduced by an uncertainty in the radiometer field of view.
- A means of varying the source radiance must be provided so the radiometer may be calibrated at radiance values equivalent to the radiance range of its intended operation.
- A known zero reference for calibration must be provided so the effect of thermally emitted radiation by the optical components of the radiometer may be evaluated.

From the above conditions, the basic criteria for a primary calibration system were established:

- An operable dynamic range up to a maximum of 10 w/m^2-sr over the spectral region 14.0 to 16.3 microns
- A system accuracy of 0.03 w/m^2-sr (1σ)
- A measurement repeatability of 0.005 w/m^2-sr (1σ)
- A source temperature of $80^{\circ}K$ to $300^{\circ}K$

- Operation in a vacuum to eliminate effects of atmospheric absorption
- Operation that simulates field measurement conditions, i.e., extended calibration source rather than a point source.

In Reference 1, the methods of mechanizing an extended-source calibration system were analyzed. There are basically two methods:

- The extended-source technique whereby the source is made sufficiently large that the source itself fills the radiometer aperture. For large instruments, this technique has the obvious disadvantage of requiring low thermal gradients over large areas.
- The source at infinity technique in which a relatively small source is placed at the focus of a collimating optical system. With sufficient diameter of the collimated beam to fill the optical aperture, the source is imaged as an extended source.

The latter of these two techniques (Figure 1) was selected for the calibration system. Within the system, the critical elements for accurate calibration are the source temperture, source emissivity and the reflectance of the collimating mirror. Precise knowledge of each of these quantities is required to ensure calibration of a radiometer to an accuracy with less than 1 percent error.

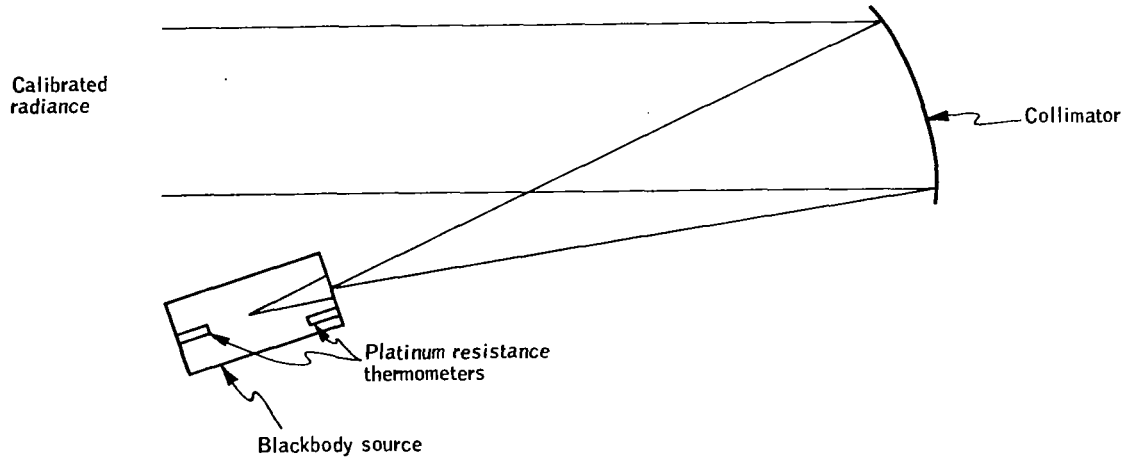

Figure 1. Primary Calibration System Concept

Reference 2 covers the development of a calibration source which included the construction and testing of a feasibility demonstration model of a blackbody source (Figure 2). Primary emphasis during this effort was placed on proving that the source temperature could be measured and controlled and that the temperatures being measured were those of the radiating body.

High-accuracy platinum resistance thermometers, traceable to standards of the National Bureau of Standards (NBS), were used in the configuration shown in Figure 2. Tests with this system demonstrated the practicality of obtaining a precise LWIR source continuously adjustable in temperature from 80°K to 300°K (Reference 2).

After establishing the capability to measure and control precisely the temperature of a radiating cavity, a study was undertaken to measure precisely the directional spectral emittance of blackbody cavities. Reference 3 reports on a measurement technique of blackbody cavities. Cavity emittance was determined from reflectance measurements of the cavities using a laser energy source (10.6 microns) and an integrating hemi-ellipsoid collector. It was demonstrated that this technique is capable of highly precise emittance measurements to a resolution of five significant figures for high-emittance cavities.

Emittance measurements were made of four different blackbody cavities: a cylinder, cone, off-axis cone (all with length-to-diameter ratios of 3), and an off-axis cone (length-to-diameter ratio of 12.45). Measurements were made of each cavity coated with nominally specular and diffuse reflecting black paints. Additional measurements were made of the 12.45 length-to-diameter ratio off-axis conical cavity without an internal paint coating.

Emittance values for these cavities varied from 0.94 for the cylinder painted with specular reflecting paint to greater than 0.99999 for the 12.45 length-to-diameter ratio, off-axis cavity when painted with either specular or diffuse reflecting paints. This latter cavity design, with diffuse reflecting paint, is employed in the Primary Calibration System blackbody.

During Part I of the ARRS (Reference 4), tests were conducted to determine a method of measuring the reflectance of off-axis collimating mirrors with an error of less than 0.1 percent. Tests were conducted in an atmospheric environment using 20-cm-diameter off-axis parabolic mirrors. A modified Strong method (test mirror in - test mirror out) was tested and indicated this potential accuracy could be achieved. Repetitive precision measurements could not be made during these tests due to atmospheric variations. Attempts were made to purge the system to a nitrogen atmosphere which indicated the system would perform as desired in the PCS vacuum environment planned.

Part I of the ARRS also included the concept and layout design of the PCS, including radiance, thermal, vacuum, and cooling system analyses and development of detailed design requirements. The ARRS Part II program then proceeded with the detailed design, construction, and evaluation of a complete operational Primary Calibration System.

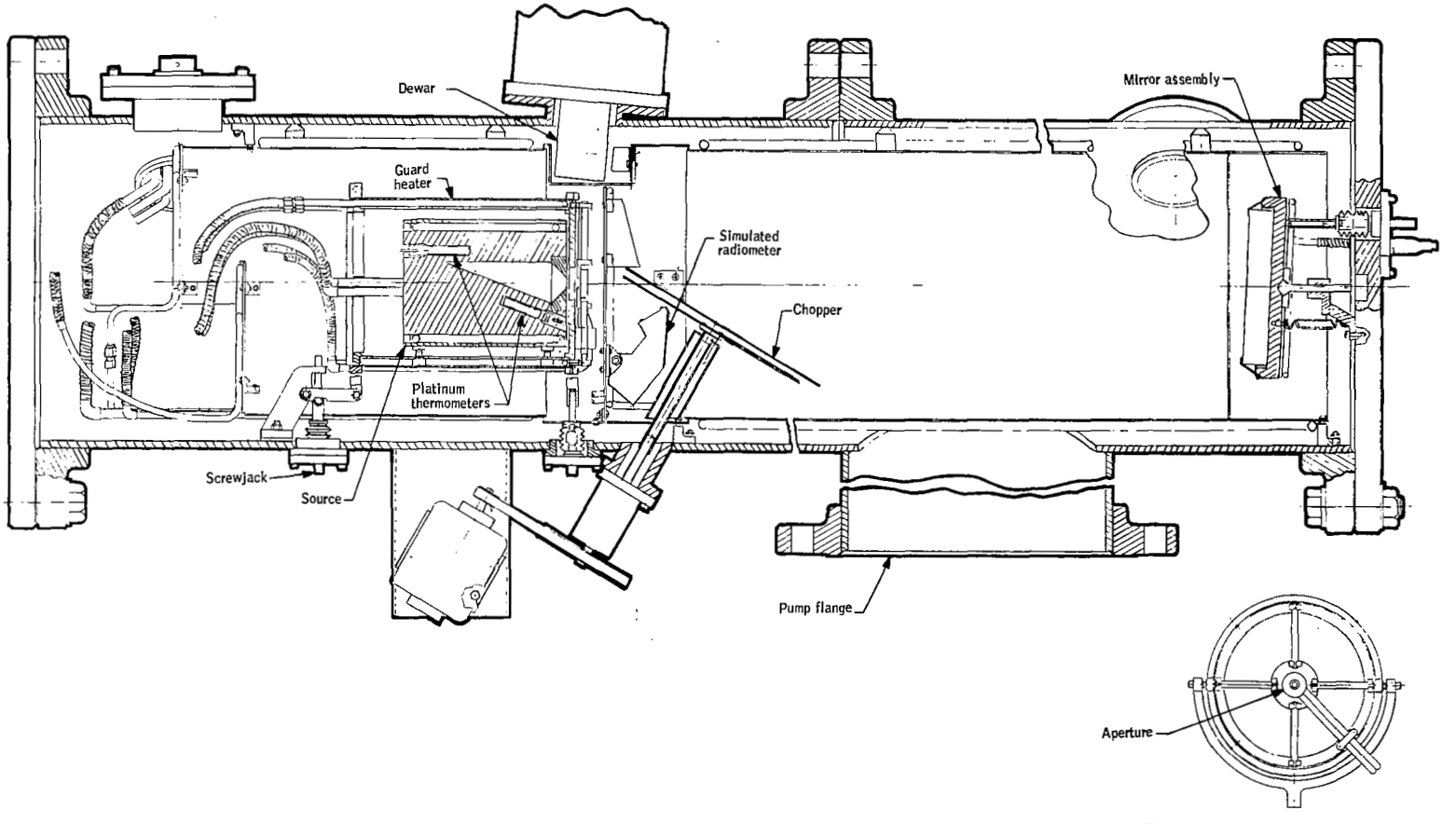

Figure 2. Variable-Temperature Source - Final Design

General System Description

The Primary Calibration System designed and constructed during the ARRS Part II contract is shown in Figure 3. The figure shows the external configuration of the system with the test radiometer and reflectometer chamber attached to the primary chamber. The test radiometer and reflectometer chamber are attached to the primary chamber only for test and checkout of the PCS. During actual calibration operation, the radiometer to be tested would be placed in a chamber and interfaced directly with the primary chamber 76-cm-diameter standard flange opening. Radiometers with entrance apertures up to 56 cm in diameter may be calibrated with the PCS.

Primary chamber. - The primary chamber (Figure 4) is a cylindrical, stainless steel, vacuum-sealed chamber, 106 cm in diameter by 4.87 meters long. The beam output end reduces down to a 76-cm-diameter opening. The chamber incorporates the following assemblies:

- Source-guard assembly
- Variable-temperature, variable-aperture plate
- Chopper assembly
- Access for an external alternate source
- Collimating mirror and mount
- Liquid-nitrogen-cooled baffles and shrouds
- Liquid nitrogen handling system
- Vacuum chamber
- A three-stage vacuum system.

The blackbody radiance source has a verified emissivity at 10.6 μm of 0.9999 ±0.0001 which can be varied in temperature over the range of 80°K to 300°K with a temperature measurement accuracy of better than 0.01°K. Directly in front of the source is a movable-aperture plate which defines the source radiance diameter, variable up to 1.0 cm. The aperture is located at the focus of the f/5, 61-cm-diameter collimator, whose output reflected radiance is then a collimated beam which appears to emanate from a blackbody source placed at infinity. A rotating chopper located in front of the aperture plate modulates the output beam to distinguish it from the background radiation.

The chamber internal elements are cooled to approximately 80°K with liquid nitrogen circulated through cooling passages in the baffles and shrouds. All internal elements are painted with diffuse black paint to reduce internal reflections and stray radiation. The chamber is evacuated with a mechanical roughing pump and by cryopumping of the baffles and shrouds, and ion pumps maintain pressure levels of 1.33×10^{-3} - 1.33×10^{-4} Newton/m^2 (10^{-5} - 10^{-6} torr).

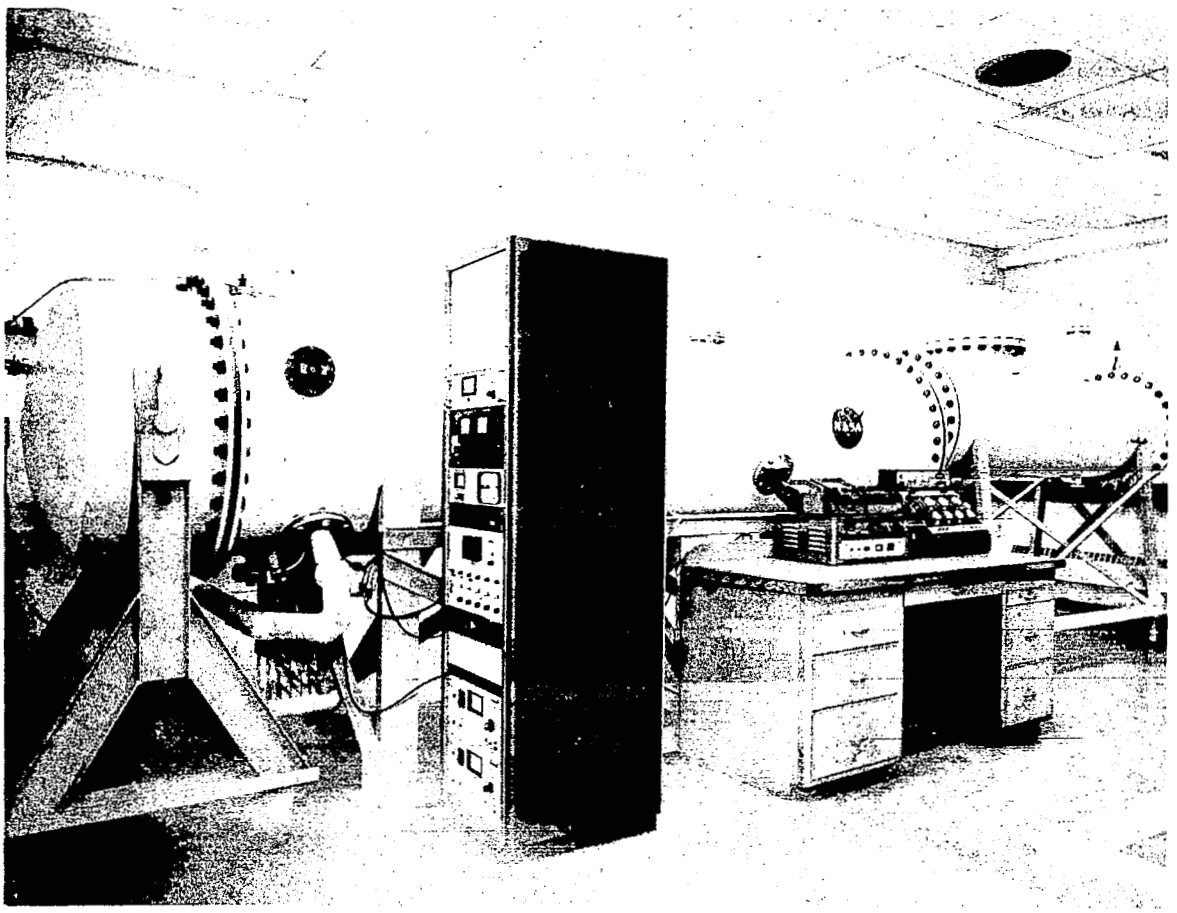

Figure 3. Primary Calibration System (PCS)

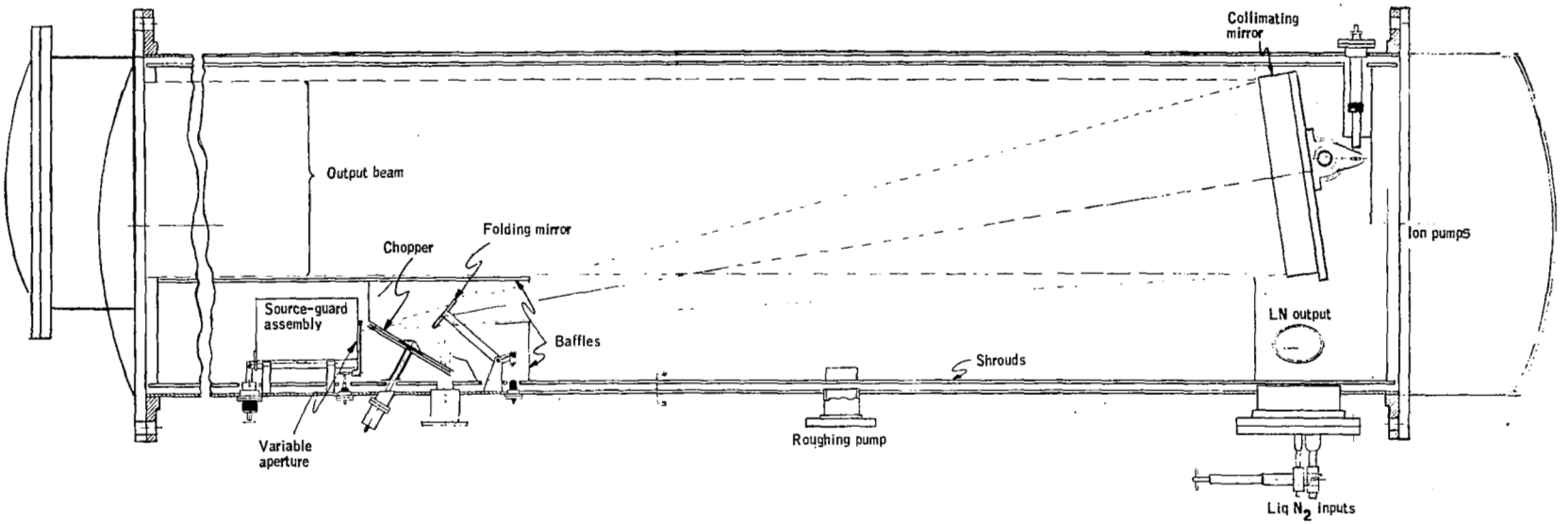

Figure 4. Primary Chamber

During normal operation, the chamber is sealed and pumped down to 1.33 N/m^2 (10^{-2} torr) pressure with the roughing pump. Main shrouds are then cooled to 250°K to condense out any residual water vapor. Mirrors and other elements in the chamber are then cooled, and the cryopumping effect from cooldown drops the chamber pressure to 1.33 x 10^{-2} N/m^2 (10^{-4} torr). Vacuum is then maintained by the ion pumps. Total cooldown time is approximately 12 hours. Calibration then proceeds by properly orienting the output beam relative to the radiometer, using collimating mirror adjustments accessible from outside the chamber, and by measuring the radiometer output with appropriate instrumentation for various desired temperatures of the blackbody source.

Reflectometer. - The reflectometer chamber, used for performing in situ reflectance measurements of the PCS collimator, is shown in Figure 5. It contains an 875°K blackbody source capable of rotating 180 degrees to perform the measurement, an auxiliary parabola with a 17.8-cm-diameter aperture for acceptance angle definition, a cooled 300-Hz chopper and cold trap, and an Hg-Cd-Te detector. The reflectometer optics are housed within an uncooled vacuum chamber which is attached directly to the reducer end of the primary chamber.

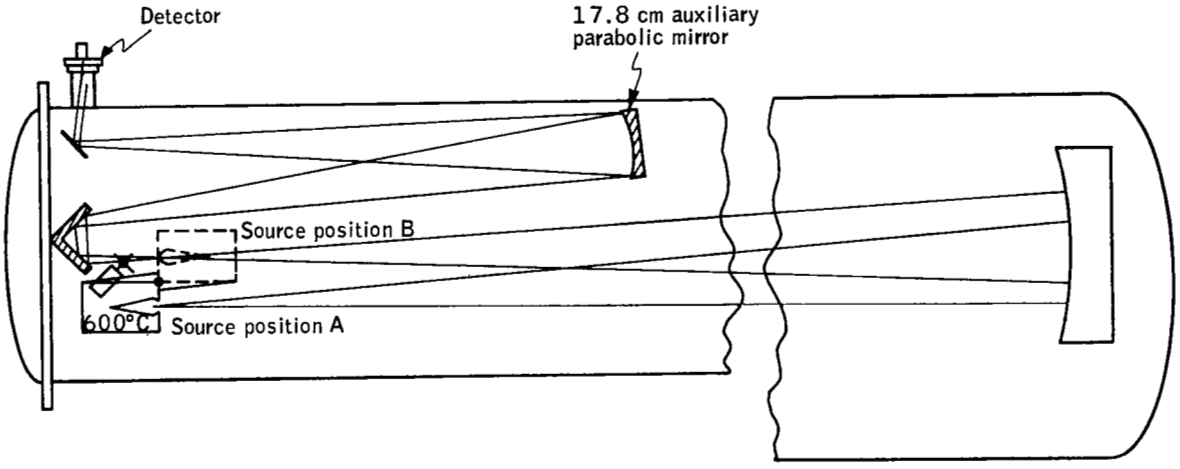

Figure 5. PCS Reflectometer

To perform the reflectance measurement, the combined chambers are pumped down with the PCS vacuum system, and the primary elements are cooled down in the normal sequence until the collimating mirror reaches a temperature of 150°K. The collimating mirror is rotated to a position such that the detector is imaged by the auxiliary parabola and the collimator into the reflectometer blackbody cavity located at the radius of curvature of the collimator and rotated to what is termed position A in Figure 5. The detector output signal, V_a, is measured. The reflectometer blackbody is then rotated 180 degrees to position B by a mechanism accessible from outside the chamber. The reflectometer detector is then imaged directly by the auxiliary parabola into the blackbody cavity. The detector output, V_b, is measured in this position, and the collimator reflectance, ρ_c, is then given by the ratio of the two signals $\rho_c = V_a/V_b$.

Sufficient signal-to-noise ratio exists and sufficient rejection of background radiation and stray light are designed into the reflectometer to permit reflectance measurement accuracy of better than one part in 1000.

Test radiometer. - The test radiometer, shown in Figure 6, is used to experimentally determine the PCS output beam characteristics, including beam uniformity across its defining aperture, and the beam angular or goniometric characteristics. The radiometer is mounted vertically within the reflectometer chamber in place of the reflectometer auxiliary parabola. An extended-length 50-cm-diameter cover accommodates the additional length within the chamber.

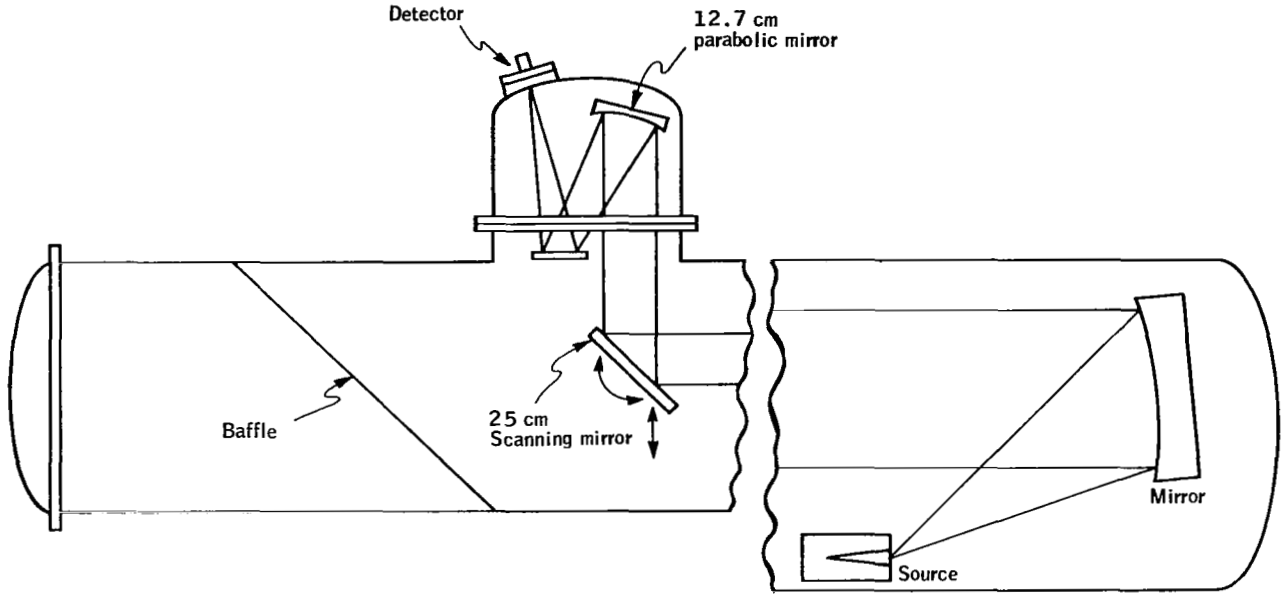

Figure 6. PCS Test Radiometer

The collecting optics of the radiometer include an off-axis parabola, a scanning mirror, a folding mirror, baffles and an Hg-Cd-Te detector. The 61-cm-diameter collimated beam from the PCS chamber is scanned by the radiometer by traversing the scanning mirror up and down on two linear guide rods. Goniometric or angular scanning is accomplished with the scanner centered in its traverse by tilting the scanning mirror ± 10 degrees. A fine-angular-scan capability is also included to allow multipoint scanning of the PCS blackbody source to determine its uniformity characteristics. Operation of the scanning mechanism is from outside the chamber by a rotational and translational bellows feedthrough flange assembly located on the bottom of the chamber. Beam scanning in two essentially perpendicular directions is accomplished by rotating the entire reflectometer/test radiometer chamber approximately 45 degrees off the vertical axis in each direction. This arrangement was employed to allow use of a standard gravity-feed Hg-Cd-Te detector dewar assembly without modification.

DETAILED SYSTEM DESCRIPTION

Primary Chamber

Source-guard assembly. - A detailed layout of the source-guard assembly is shown in Figure 7. The source is fabricated from high-purity, oxygen-free copper to assure minimum outgassing and minimum thermal gradient effects. A two-stage, recessed off-axis cone with a length-to-diameter (L/D) ratio of 12.45 and an aperture diameter of 1.75 cm is machined into the copper block. The reverse section of the cone is shrunk-fit into the block. The cavity was designed to be machined on-axis with respect to the block, with the result that, in the chamber installation, it is operated 9° off-axis, thus assuring proper emissivity characteristics. The cavity is coated with a nominally diffusely reflecting black paint with an emittance of at least 0.95. This paint, coupled with the cavity geometry, will provide a source emittance exceeding 0.9999. This extremely high emittance was experimentally verified at 10.6 μm by the Emittance Measurement Study on similar sources (Reference 3).

Platinum resistance thermometers are installed at opposite ends of the source to measure accurately the source temperature and gradient structure through the block. These thermometers were calibrated to the 1968 International Practical Temperature Scale and are traceable to the NBS. Calibration accuracy obtainable is shown in Figure 8. The thermometer installation utilizes an aluminum carrier with multiple convoluted corrugations around the thermometer to provide good thermal contact to the copper block. The thermometer is a tight slip fit in the carrier, which runs the length of the thermometer. This configuration provides good thermal contact from the thermometer to the copper block without unduely stressing the thermometer case. The thermometers are of a four-lead configuration designed for operation with a Mueller bridge, which eliminates leadwire resistance effects from the measurement. The leads, made of No. 33 solid copper wire, are heat stationed around the circumference and to the rear of the source block to minimize thermal electromotive force (emf) effects.

To achieve desired stability and minimize thermal gradients within the source, an active thermal insulator, or guard assembly, is used. The guard assembly surrounds the source and effectively thermally isolates it from the surrounding cold environment. The source temperature is maintained by controlling the guard temperature and radiatively coupling it to the source block.

Helical milled slots are provided around the circumference of the source block. These form cooling passages for liquid nitrogen flow around the source. An outer copper sleeve is shrink fitted, then silver soldered to the source block, which provides a sealed jacket around it. The source liquid nitrogen cooling lines are attached to this sleeve. Provisions for source heating are made by a 260-watt spray-on resistive heater applied to the outer

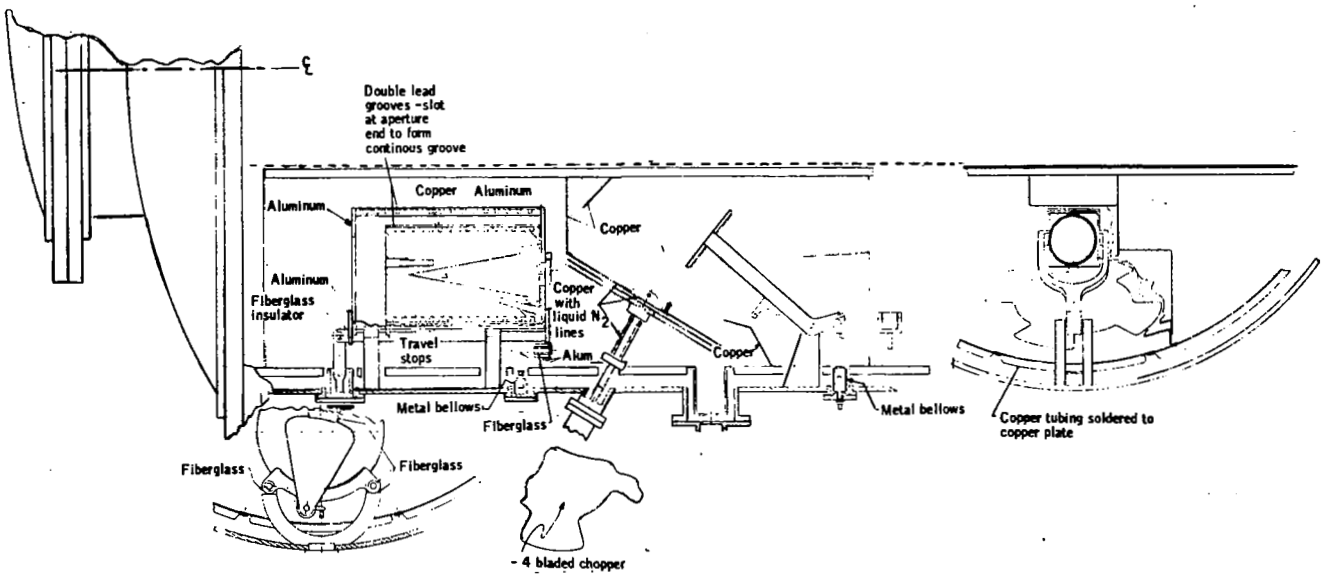

Figure 7. PCS Source-Guard and Chopper Assembly

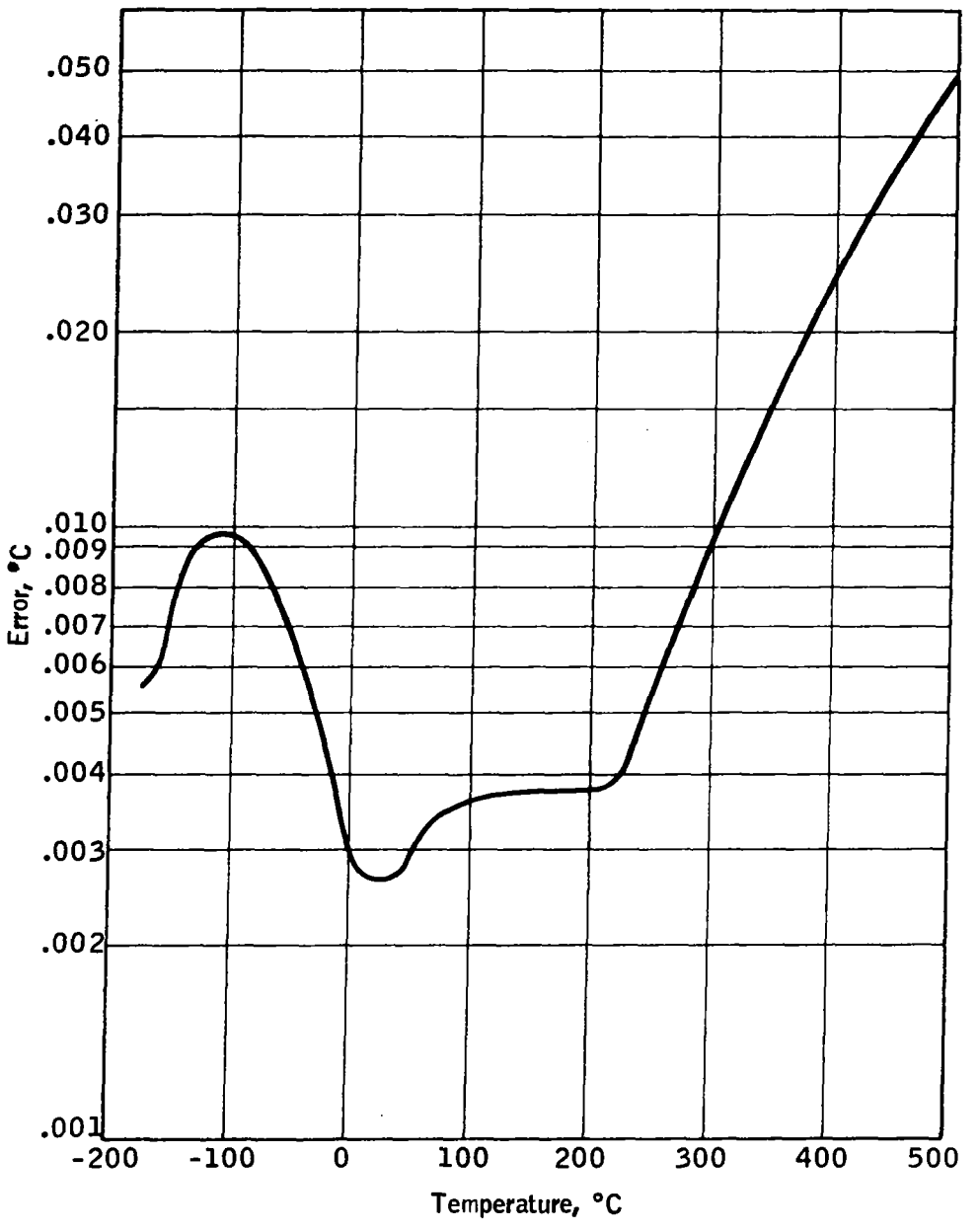

Figure 8. Calibration Accuracy of Platinum Thermometer

circumference of the copper sleeve. The outer surfaces are painted black to maximize the radiative coupling between the source and guard. The radiative coupling between the source and guard provides the stability and temperature uniformity needed for the desired source gradient structure. Stainless steel straps around the source, to which insulating fiberglass pads are attached, are used to mount the source within the guard assembly.

The guard assembly consists of a multi-element aluminum circular cylinder which surrounds the copper source. The guard cylinder contains milled helical slots similar to the source for liquid nitrogen coolant flow. An outer sleeve is welded to the slotted cylinder to seal the coolant passages. The inner surface of the cylinder and endcaps are painted black to maximize radiative coupling to the source. The guard cylinder OD and end caps are coated with a spray-on heater material to provide warmup and temperature control of the source-guard assembly. The guard heater is sized at 100 watts to provide desired warmup rates. The guard outer surfaces are covered with aluminum foil to reduce the radiative coupling to surrounding cold baffles and shrouds. A platinum resistance thermometer attached to the guard cylinder ID provides the sensing point to which the guard temperature is controlled.

Interconnecting inlet and outlet liquid nitrogen coolant tubes are isolated from the cold chamber walls with fiberglass spacers. Care is exercised in avoiding conducting heat losses from the source and guard to the surrounding elements.

Longitudinal movement of the source-guard assembly along the system optical axis allows the defining source aperture to be located at the collimating mirror focal point. This is provided by a sliding mount which is thermally stable yet well isolated from the outer chamber. The mount is constructed of stainless steel with fiberglass pads for thermal isolation. Adjustment from outside the chamber is accomplished through a sealed bellows linkage.

Variable aperture. - Figure 7 shows the layout of the source variable aperture that is used to vary the source radiance angle of subtense. This allows checking radiometer detector linearity over various aperture extents. A series of five precisely machined aperture holes are indexed in front of the source cavity. These hole diameters are: 1.0 cm, 0.33 cm, 0.12 cm, 0.043 cm, and 0.015 cm. The 1-cm diameter provides a 3.3-mr source extent. In addition, an incandescent light source with a defined diameter of 0.25 cm is attached to the aperture plate and is used to visually align radiometer optics to the blackbody source. Temperature control of the aperture plate is accomplished by flow-rate control of a liquid-nitrogen cooling line attached to the aperture plate. The plate is physically attached to the guard front endplate through fiberglass bushings. Control of the plate position is accomplished with a linkage through a sealed bellows to the outside of the chamber.

Chopper. - Figure 7 shows the chopper layout. The chopper is configured as a four-segment rotating blade which modulates the variable-temperature-source beam or an external radiation source (triple-point cell) alternatively. The dwell-to-rise time ratio of the blade with a 1-cm source diameter is 4 to 1. The chopper blade is supported in the chamber with two ball bearings and is driven by a vacuum-sealed bellows drive mechanism. Thermal isolation of the blade from the driving mechanism is accomplished by a fiberglass shaft

coupling. The chopping rate is variable up to 66 Hz with a servo-controlled motor drive assembly. The portion of the chopper blade intercepting the radiance beam is made highly specularly reflective to minimize blade self-emission and to direct the reflected intercepted rays to a cold trap so that they are absorbed away from the field of view of the optical system. This is accomplished by orienting the blade at a 60° angle with respect to the chopped radiation beam. The modulated output beam is then alternately the source-trap output radiance. A magnetic pickoff assembly, whose signal is also chopped by the blade, is used to provide a synchronous reference output signal for interfacing with a phase-lock electronics readout system.

The chopper blade is radiatively cooled with highly absorbant copper baffles located on both sides of the blade and around the drive shaft. Conductive cooling is accomplished through the bearings attached to the baffles and chopper drive shaft. Liquid nitrogen lines are soldered to the baffles for cooling.

Folding mirror. - Figure 7 shows the layout of the folding mirror and mount assembly. The mirror is rotated into the optical path of the primary chamber source cone such that an external radiation source -- i.e., the triple-point cell -- can be folded into the optical system. This mirror is 11.4 cm in diameter by 1.27 cm thick and is made of high reflective quality gold-coated CerVit, with a reflectance as shown in Table 1, accurate to 0.1 percent as measured by the Naval Weapons Center, China Lake, California.

TABLE 1. - FOLDING MIRROR MEASURED REFLECTANCE, R

Wavelength, λ	R
14	0.9889
15	0.9886
16	0.9888
	0.9888 average

The measured reflectance is that of a witness flat which was coated simultaneously with the folding mirror. The mirror is conductively cooled with liquid nitrogen circulated through its mounting plate. A fiberglass bushing provides thermal isolation to the outer chamber. Movement of the mirror is by an externally adjustable bellows-linkage mechanism.

External source interface. - A flanged interface connection is provided by the chamber to allow an external radiance source to be introduced into the PCS optical system. A variable-sized, cold aperture stop defines the radiance subtense of the source. The chopper blade is positioned to chop the radiation in a manner similar to its operation with the variable-temperature blackbody source. Possible alternate sources which may have application for an absolute temperature/emission comparison with the primary chamber source are a water triple-point cell, a monochromator, and an independent blackbody radiance source.

Collimating mirror and mount. - The collimating mirror is configured as an off-axis parabola with its centerline 9° off its optical axis and with a focal length of 3.02 meters. The mirror material is premium grade CerVit known for its extremely low thermal expansion coefficient. Dimensions of the mirror are 63.5 cm in diameter by 10.6 cm thick with a clear outside diameter of 61 cm. The mirror was ground and polished to a figure such that the blur circle is 0.127 mm in diameter. The top 2.5 cm of the mirror was overcorrected, and the aberrations due to this portion of the mirror are excessive. In the installation in the PCS, the mirror is mounted such that the top 2.5 cm of the mirror is masked off by the mirror baffle and the bottom 1.27 cm of the mirror is used by the system. Figure 9 shows that the mirror is diffraction limited above 10.3 microns. The mirror is coated with high-purity gold over chrome, with a reflectance of at least 0.985, calibrated to 0.1 percent. Measurements of the mirror reflectance have been made and are discussed later.

Figure 10 illustrates the method for mounting the mirror. The aluminum mirror-mounting plate is supported by a 5-cm OD, 0.48-cm wall stainless steel tube which runs through two aluminum pillow blocks with fiberglass thermal isolating inserts. At each end of the 5-cm tube are slip-fit steel extensions with a flattened shaft. These protrude through slotted plates which are bolted and vacuum-sealed to the chamber. Stainless steel bellows are welded to these pieces to achieve a vacuum seal. External adjustment screws are used to adjust for axial and/or angular azimuth position (±1 degree). Freedom of movement of 5 degrees in elevation is needed to perform the in situ reflectance measurement. Elevation adjustment is by an external differential adjustment screw which transmits vertical motion through a bellows seal to a crank arm fastened to the mirror-mounting plate. The crank arm pivots around the 5-cm support tube and gives angular motion to the mirror around this point. The vertical adjustment tube, shaft, and bellows are made of stainless steel. The crank arm is made of aluminum with fiberglass inserts. The mirror is supported on the mounting plate by means of a copper band strap and three spring-loaded clips.

For cooling the mirror, the mirror-mounting plate has milled passages in it through which liquid nitrogen flows. In addition, two passes of liquid nitrogen are made through copper tubes soldered to the support strap, cooling the circumference of the mirror. A monel mesh is located between the back of the mirror and its mounting plate to improve thermal conduction. The front surface of the mirror plate and the back surface of the mirror are painted black to maximize radiative coupling.

Shrouds and baffles. - Shrouds and baffles are placed throughout the primary chamber to eliminate stray radiation and emission from within the optical system FOV. These shrouds and baffles are shown in Figures 4, 7, and 10 and consist of the following:

- Main shroud, fabricated in one section with three parallel flow sections
- C-shaped shroud at the chamber source end
- Mirror front baffle

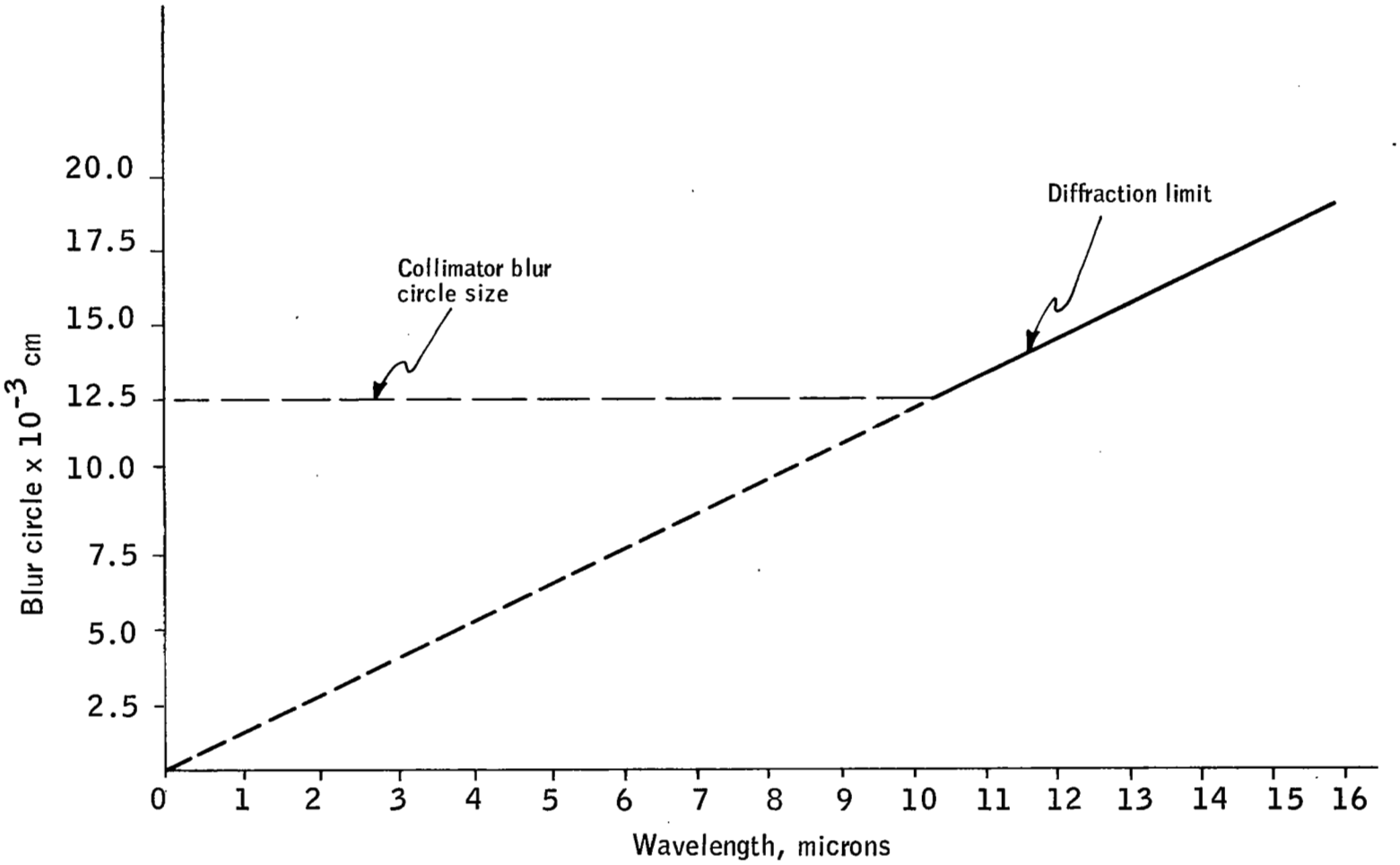

Figure 9. Collimator Blur Circle Size versus Diffraction Limit

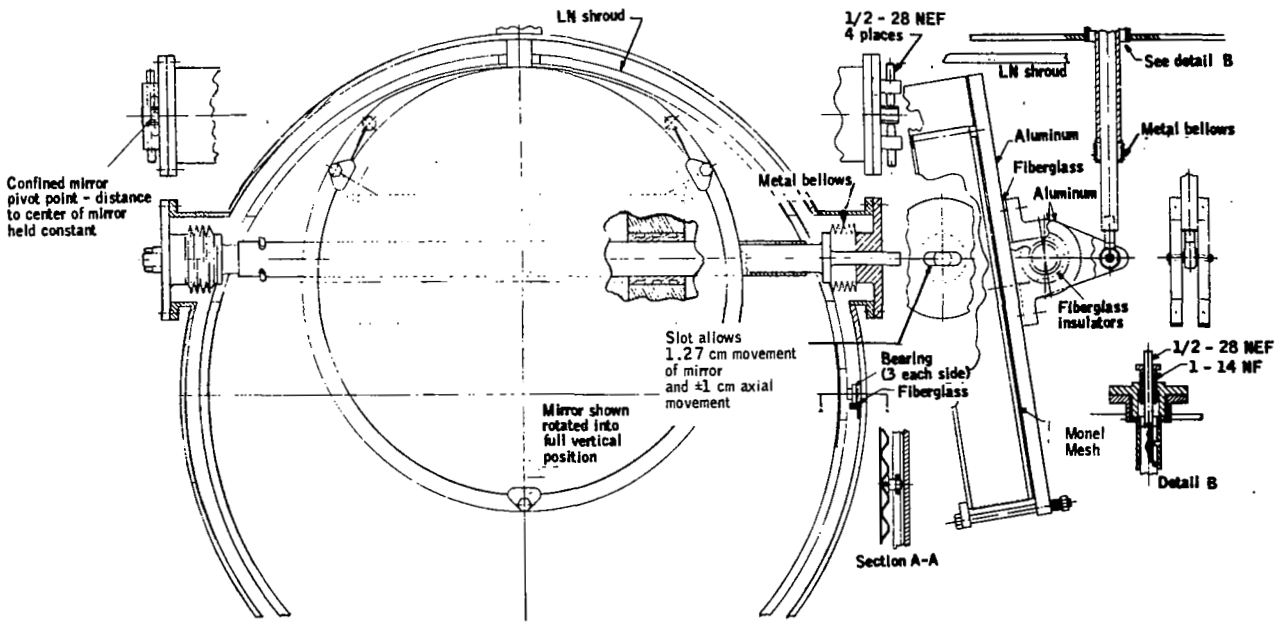

Figure 10. Collimating Mirror and Mount

- Rear ion pump split baffles
- Center baffle in front of the source
- Exit-beam baffle
- Baffle plate between the source and collimated beam.

Each of the above shrouds and baffles is made from two embossed, stainless steel sheets. When the sheets are electric-resistance welded together into a panel, the embossed areas become channels for liquid nitrogen coolant flow. In addition to the directly cooled shrouds and baffles, several other conductively cooled baffles are located within the chamber to eliminate stray radiation. Inner surfaces of all shrouds and baffles are coated with high-absorptivity paint ($\alpha > 0.9$) to provide as black a surface as possible. The shroud and baffle surfaces viewing the chamber walls are electropolished for low emissivity ($\epsilon < 0.1$) to minimize radiative coupling. The large circular shrouds are mounted to the chamber walls by ball bearings and fiberglass bushings resting on steel tracks, which provides a convenient means of installation.

Vacuum chamber. - The primary vacuum chamber consists of a 4-m long, 1.07-m diameter, 8 mm wall thickness cylinder with flat-faced vacuum-seal flanges at either end (see Figure 11). Standard vacuum flanges are provided for the vacuum roughing pump and liquid nitrogen header connections. A movable 61-cm long, 1.07-m diameter extension is provided at one end of the chamber to house the ion pumping modules. The opposite end contains a flanged reducer extension to which the 76-cm diameter reflectometer/test radiometer or test chamber is attached. Special machined flanges for adjustment linkages and mountings are welded to the chamber walls. Soft aluminum wire, 0.76 to 1.52 mm in diameter, welded into rings and positioned between the flange faces, are used to provide the seals between the flanged interface connections. All chamber materials are type 304 stainless steel for weldability and corrosion resistance. All interior surfaces are polished for cleanliness and low emissivity to reduce thermal loading on the shrouds. The exterior surfaces are painted with white enamel.

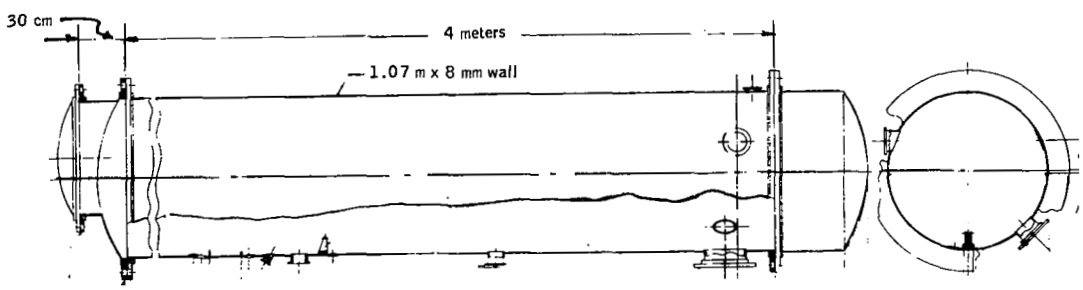

Figure 11. PCS Vacuum Chamber

The chamber is mounted on a stand of structurally-reinforced steel with leveling pads. The stand provides necessary access to the chamber adjustments. The chamber and stand are shown in Figure 12.

Cooling system. - The primary chamber cooling system is a recycling system consisting of a supply dewar, transfer line, phase separator, transfer pump, inlet manifold, 13 plumbing circuits, and outlet manifold (see Figure 13). The liquid nitrogen flows from the supply dewar at approximately 2×10^5 N/m^2 (30 psi) to the cooled elements in the chamber and then to the phase separator. Here the nitrogen gas is vented and the liquid nitrogen returned to the dewar by the transfer pump. Separate valves and lines control the coolant flow to each of the elements within the chamber. Figure 14 shows the interconnections for the internal coolant flow. The internal lines are made of rigid and flexible stainless steel tubing. Permanent joints are brazed together and removable connections are made with gyrolock fittings. A common manifold within the chamber combines all the exit lines to a single large 6.3-cm diameter line which exits through a header to the phase separator. The phase separator consists of two containers, one inside the other, with foamed polyurathane between them for insulation.

Vacuum system. - The primary chamber vacuum system consists of three stages -- a mechanical roughing pump, cryopumping by the cooled baffles and shrouds, and an ion pumping system. Figure 15 shows the vacuum system elements. A 2.26 m^3/min roughing pump pumps down to a level of 1.33 N/m^2 (10^{-2} torr); its flanged connection is midway between the optical elements of the primary chamber. A liquid-nitrogen-cooled trap prevents any oil from inadvertently backstreaming into and contaminating the chamber. Gate valves are located above and below the trap. The cryopumping action of the baffles and shrouds normally reduces the pressure level in the chamber to 6.6×10^{-2} N/m^2 (5×10^{-4} torr). The ion pumping system contains forty 25-liter-per-second pumping modules to achieve and maintain a pressure of less than 1.33×10^{-3} N/m^2 (1×10^{-5} torr). Figure 16 shows the location of the pumping modules within the flanged housing of the 61-cm chamber extension. Two rack-mounted power supplies energize the pumping modules. A 20-mesh stainless steel screen is located between the pumping modules and the rest of the chamber to contain corona discharge which may be present at higher pressure levels ($>1.33 \times 10^{-3}$ N/m^2).

Electrical system. - Figure 17 is the electrical schematic diagram for the primary chamber. Interconnections to the chamber are made through two hermetic-seal connectors.

A proportional temperature controller is provided to control the guard heater assembly power and temperature. A commutating Mueller bridge is used to measure precisely the platinum resistance thermometer resistances ($\pm$ 0.0001 ohm). Wheatstone bridges are used to measure the 14 nickel-iron temperature sensor resistances throughout the chamber, monitoring the temperatures of interest. A table-mounted rack (Figure 18) contains the temperature controller, source control switch, chopper pickoff output, and temperature-sensor switching and output jacks.

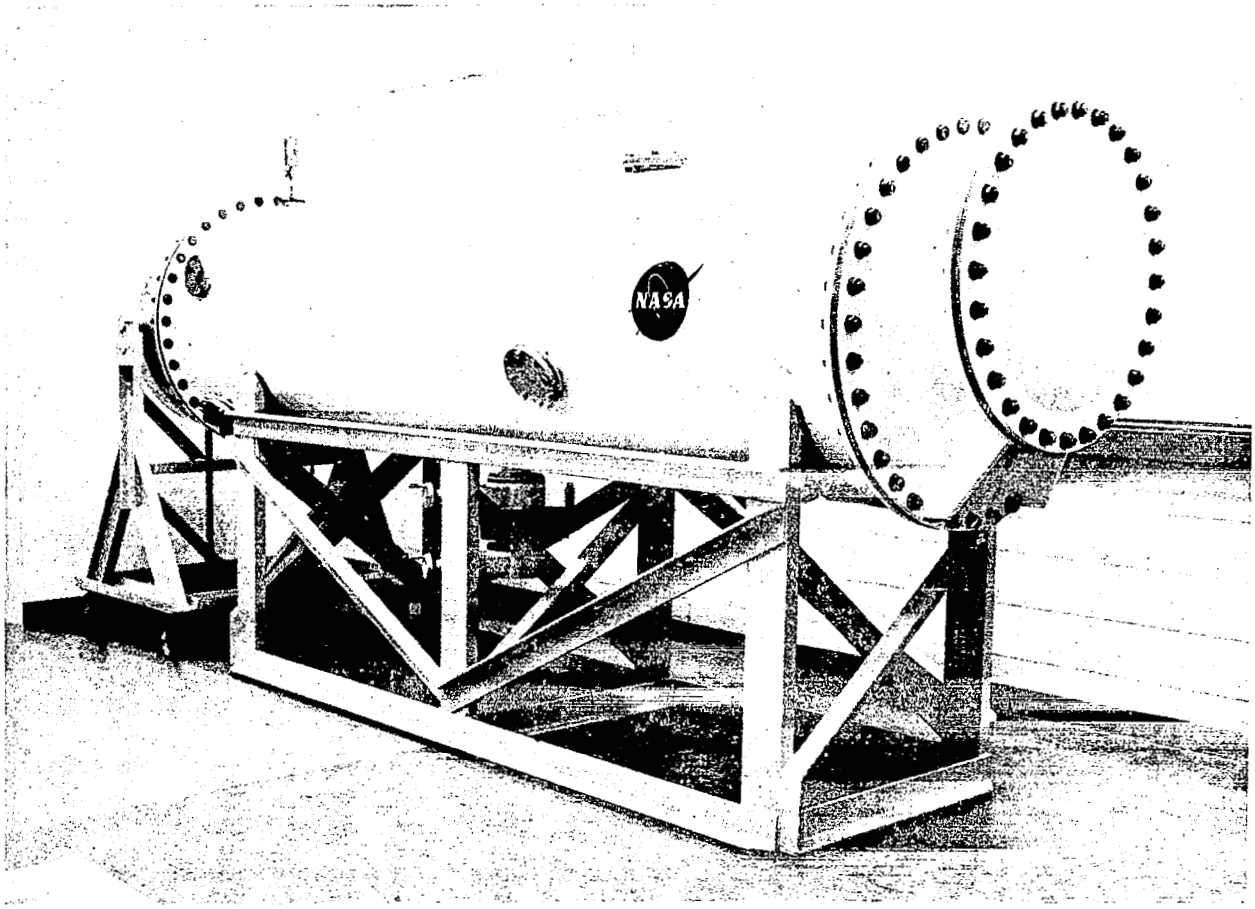

Figure 12. PCS Vacuum Chamber and Stand

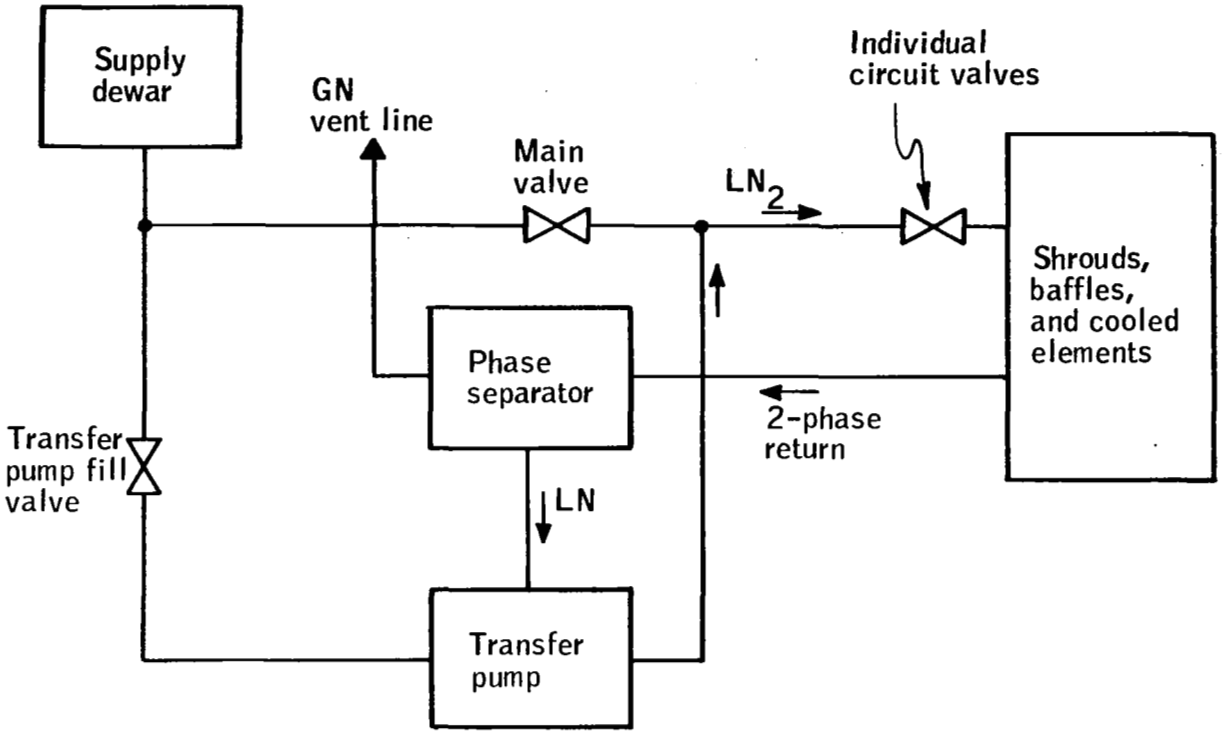

Figure 13. Liquid Nitrogen Handling System

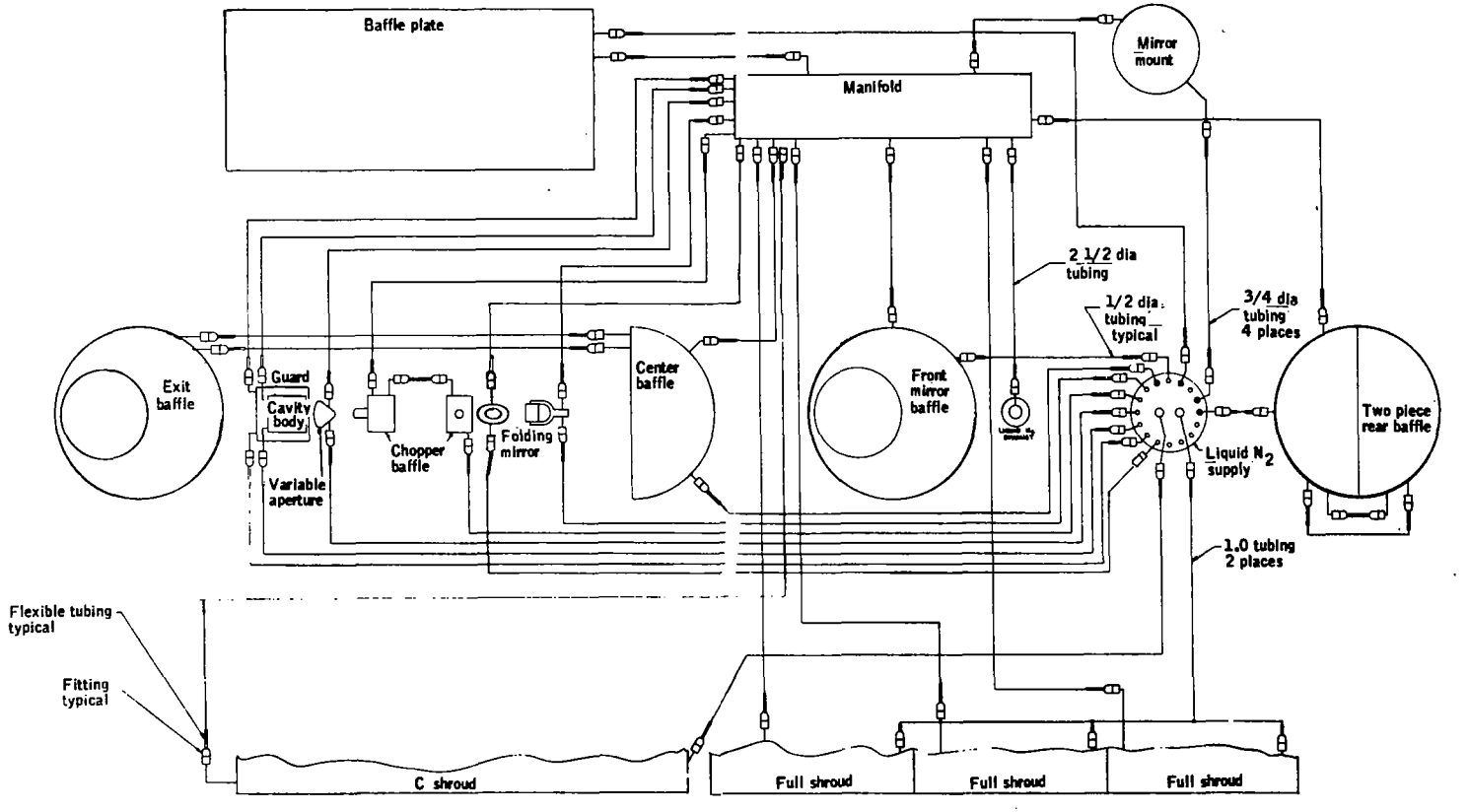

Figure 14. Liquid Nitrogen Tubing Schematic

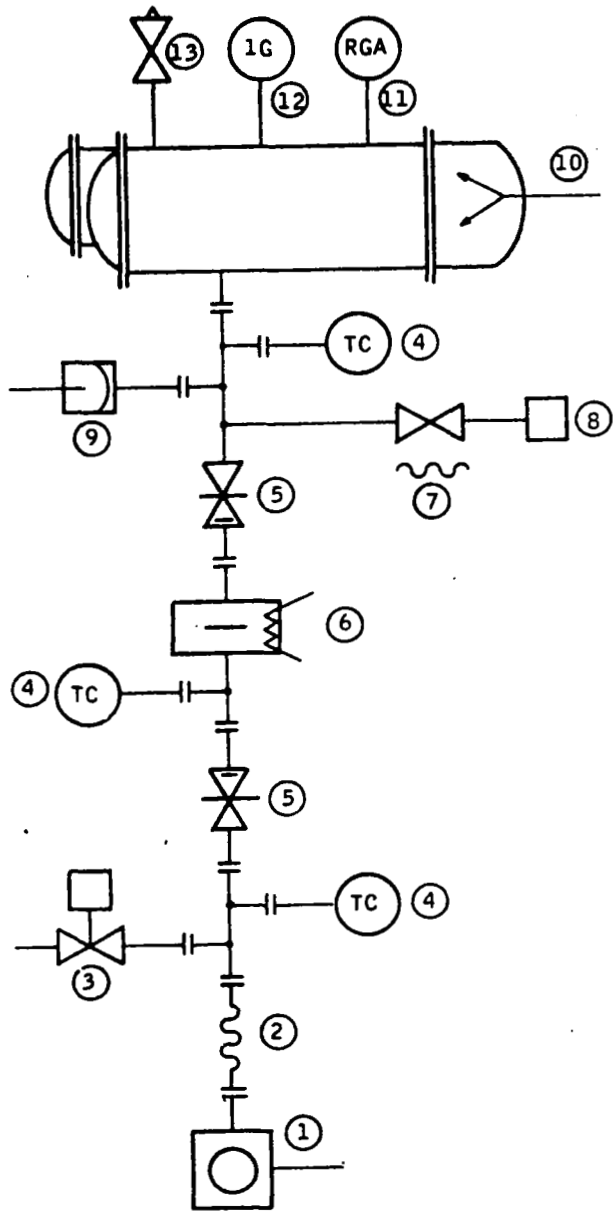

1. Mechanical pump
2. Vibration isolator
3. Solenoid valve
4. Thermocouple gauge
5. Slide valve
6. Liquid nitrogen baffle
7. Dry N_2 valve
8. Quick disconnect
9. Pressure switch
10. Ion pump
11. Gas analyzer
12. Ion gauge
13. Burst disc

Figure 15. PCS Vacuum System

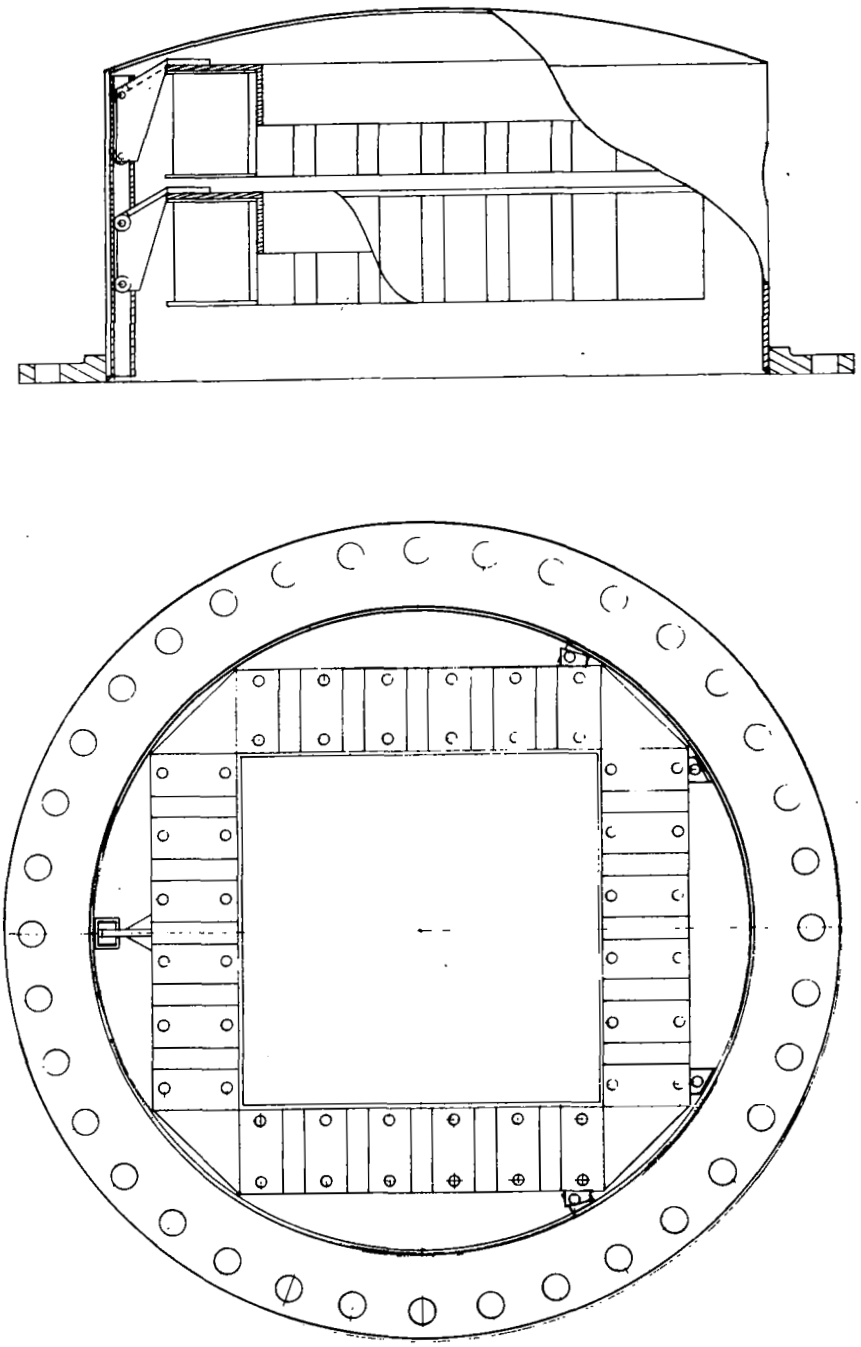

Figure 16. PCS Vac-Ion Pumps

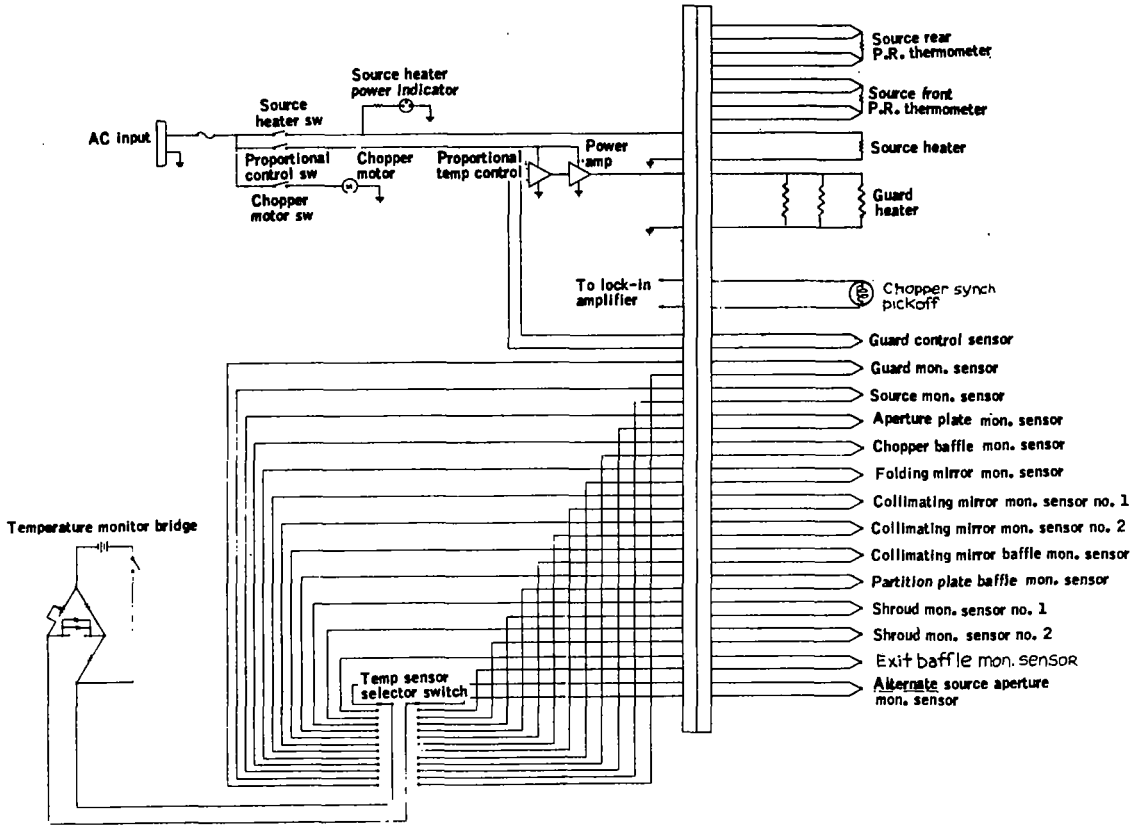

Figure 17. Primary Calibration Chamber Schematic

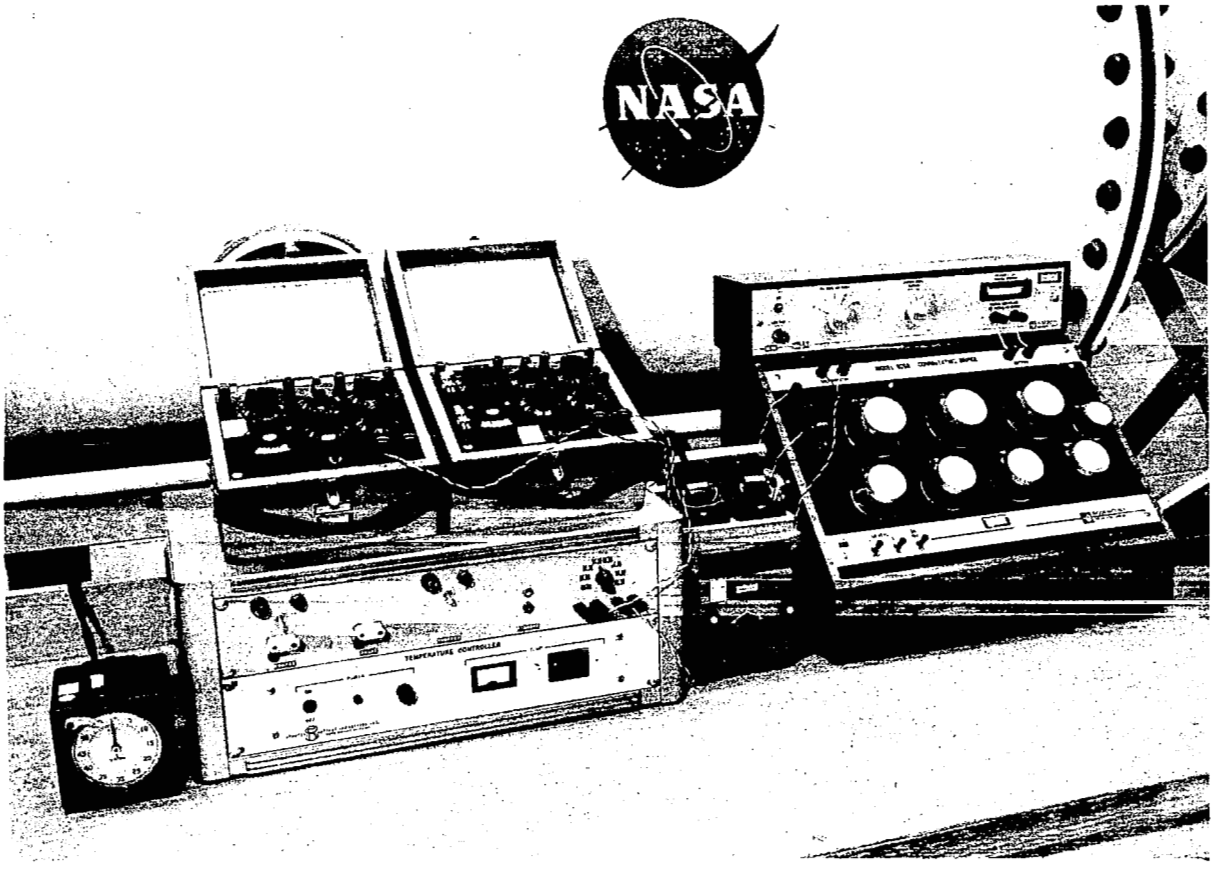

Figure 18. PCS Control Panel

Reflectometer

The reflectometer system used for performing in situ reflectance measurements of the PCS collimating mirror is contained within a separate uncooled vacuum chamber attached directly to the reducer end of the primary chamber. A description of the principal components of the reflectometer hardware and the reflectometer optics as well as an analysis of the reflectometer optical system is provided in the following paragraphs.

Reflectometer chamber. - The reflectometer chamber used to house the reflectometer optics is an ASME certified carbon steel cylindrical vacuum chamber made of SA-285-C carbon steel 4.7 mm thick. The chamber is 76 cm in diameter, 2.7 m long from end flange to end flange with 76 cm diameter concaved flanged end caps and one 51 cm diameter concaved flanged opening in the top. The end cap nearest the reflectometer optics mount is hinged to provide easy opening for adjustment of the reflectometer optics. The chamber is supported by a welded angle-iron frame on four 23 cm diameter full swivel wheels for ease of mating with the primary chamber. The inside of the chamber is painted with high-absorptivity black paint and the outside with rust resistant white enamel.

Optics. - The reflectometer optical system, shown schematically in Figure 19, uses an 875°K blackbody source capable of rotating 180°, a 300-Hz polished aluminum 150°K cooled chopper, a 25.4 cm diameter, 1.00 m focal length, 9° off-axis parabolic mirror stopped down to 17.7 cm for acceptance angle definition, three 10-cm diameter folding mirrors, and an Hg-Cd-Te infrared detector with a 14 to 16 micron bandpass filter attached.

The detector, located at the radius of curvature of the 25.4-cm auxiliary parabola, has its acceptance angle defined by the 17.7-cm diameter stop at the parabola. The detector is imaged by the auxiliary parabola and the collimator into the reflectometer blackbody cavity, located at the radius of curvature of the collimator, and rotated to position A of Figure 5. With the reflectometer blackbody rotated 180° to position B, the detector is then imaged directly by the auxiliary parabola into the blackbody cavity. The ratio of the detector signal at position A to that at position B is the reflectance of the collimating mirror. Since the detector field of view remains constant for both source positions A and B, the essential requirement for the source aperture position is that the detector be imaged completely within it (assuming a uniform source). The reflectometer field of view is such that the detector sees a full 53.3-cm diameter of the collimating mirror; hence, a true value of the near total average collimator reflectance is obtained.

Reflectometer ray trace analysis. - A geometric ray trace analysis was performed on the reflectometer optical system to determine blur circle sizes caused by geometric aberrations. A computer program was set up and run to establish energy distribution functions through the optical system shown in Figure 19. The results are given in Table 2.

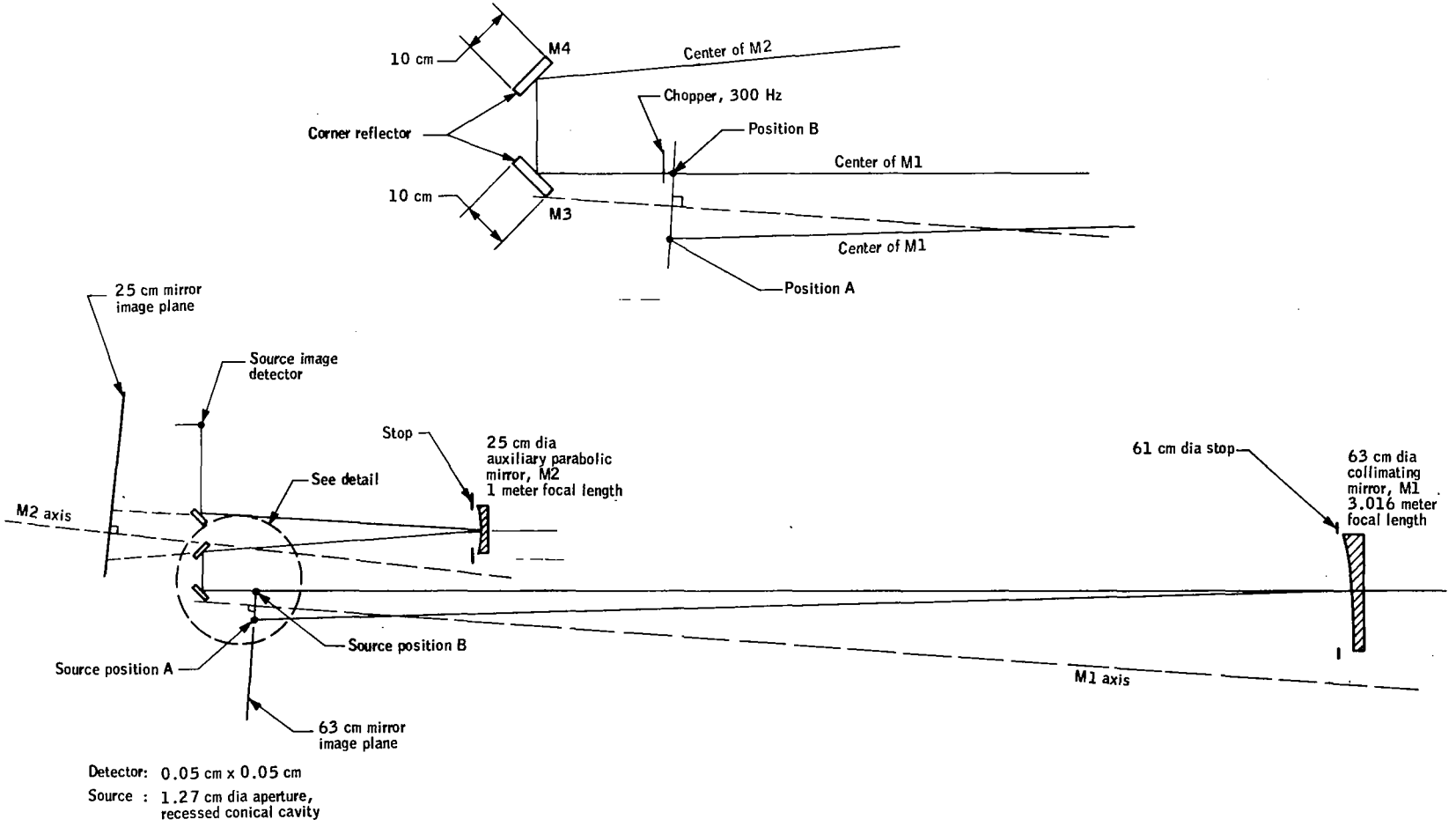

Figure 19. Reflectometer - Optical Layout

TABLE 2. - REFLECTOMETER BLUR CIRCLE SIZES

Reflectometer Position	Energy content within blur circle diameter, cm		
	80%	90%	100%
Position A to Position B			
Through PCS parabola, paraxial focus 6.03 m	0.761	1.066	1.546
Best focus shifted 10 cm away (circle of least confusion)	0.4506	0.5237	0.6162
Position B Only			
Through auxiliary parabola, paraxial focus 2.01 m	0.221	0.2967	0.4359
Best focus shifted 3.22 cm away	0.1234	0.1473	0.1707
Position A			
Through entire system, paraxial focus 2.02 m from auxiliary parabola	0.9718	1.3782	1.9807
Best focus shifted 14 cm away from auxiliary parabola or object 14 cm away from primary parabola or a combination	0.6172	0.7087	0.918

The blur circle sizes in Table 2 were calculated by assuming a point source, with the largest causes of the blur circle images due to spherical aberration and coma. The 100 percent energy blur circle image of 0.918 cm (operational case for position A) can be contained within the source diameter of 1.27 cm with proper attention to optical alignment and stability. This will ensure a uniform source image on the detector.

Analyses. - Detailed analyses were performed on the reflectometer to determine governing parameters of the system, including atmospheric absorption effects, signal-to-noise ratio, chopper location and internal reflection effects. These analyses are included in Appendices A through D, and their results are summarized as follows:

- Atmospheric absorption: The effects of atmospheric absorption in wavelength region of interest, 14 to 16.3 microns, are determined to be completely negligible, i.e., 0.46×10^{-6} absorption level at pressures of 75 microns or less.

- Signal-to-Noise: The reflectometer signal-to-noise ratio with a Hg-Cd-Te detector and a chopping speed of 300 Hz is 14,500 with a 14 to 16 micron bandpass filter in the optical path.

- Chopper location: It was determined that the optimum configuration for the chopper is to place it in the optical path directly in front of the source in position B and keep it fixed in this position. It was also determined that the chopper blade and associated radiation trap should be liquid-nitrogen cooled to make its own radiance negligible with respect to the source radiance output.

- Internal reflections: The internal chamber reflections were calculated to be less than 0.001 percent, a negligible amount.

Reflectometer rack. - The reflectometer rack (Figure 20) is of welded aluminum construction and serves as a single mounting frame for the chopper, source, folding mirrors, and miscellaneous baffling. The rack allows for easy removal of all reflectometer components from the chamber at once with the exception of the 25.4-cm diameter parabola which has its separate mounting to the chamber. The rack is baffled to prevent any off-axis radiation from the hot source can from radiating on the reflectometer mirrors.

Blackbody source. - The blackbody source used in the reflectometer consists of a modified inner can assembly and substituting two asbestos cavity support plates and concentric stainless steel radiation shields. The source cavity is a stainless steel, conically shaped block 2.54 cm in diameter and 10 cm long. The cavity is painted with a high-temperature black paint with a total emittance of 0.78 at 590° K to 0.90 at 1366° K. The stainless steel cavity is contained within a ceramic cylinder containing the heating element and control platinum resistance thermometer. An iron constantan thermocouple is located in the stainless steel block near the tip of the conical cavity for source temperature reference.

The source temperature is controlled by a full-wave-rectified SCR controller to within ±0.06°K of the 875°K set point.

Chopper assembly. - Because no acceptable rotary feedthrough devices could be obtained with speeds greater than 1000 rpm, the reflectometer chopper assembly was designed to utilize a hysteresis synchronous motor modified for vacuum operation by use of stainless steel bearings with teflon impregnated retainers. The motor is designed to operate from 115 vac, 60-Hz, power at 3600 rpm and is heat sinked to liquid-nitrogen-cooled baffles to prevent overheating. The 20.3-cm diameter, five-bladed, polished-aluminum cooled chopper blade is attached to the relatively hot motor shaft by a 4.44-cm long, 0.952-cm diameter hollow fiberglass shaft for thermal isolation. The chopping rate is synchronized at 300 Hz, which is as high as operational conditions would allow to minimize detector 1/f noise limitations. Chopper blade cooling is accomplished by placing liquid-nitrogen-cooled baffles on either side of the blade in close proximity to it. A black liquid-nitrogen-cooled cavity is included to provide a cold reference for the detector field of view when the chopper blade is closed.

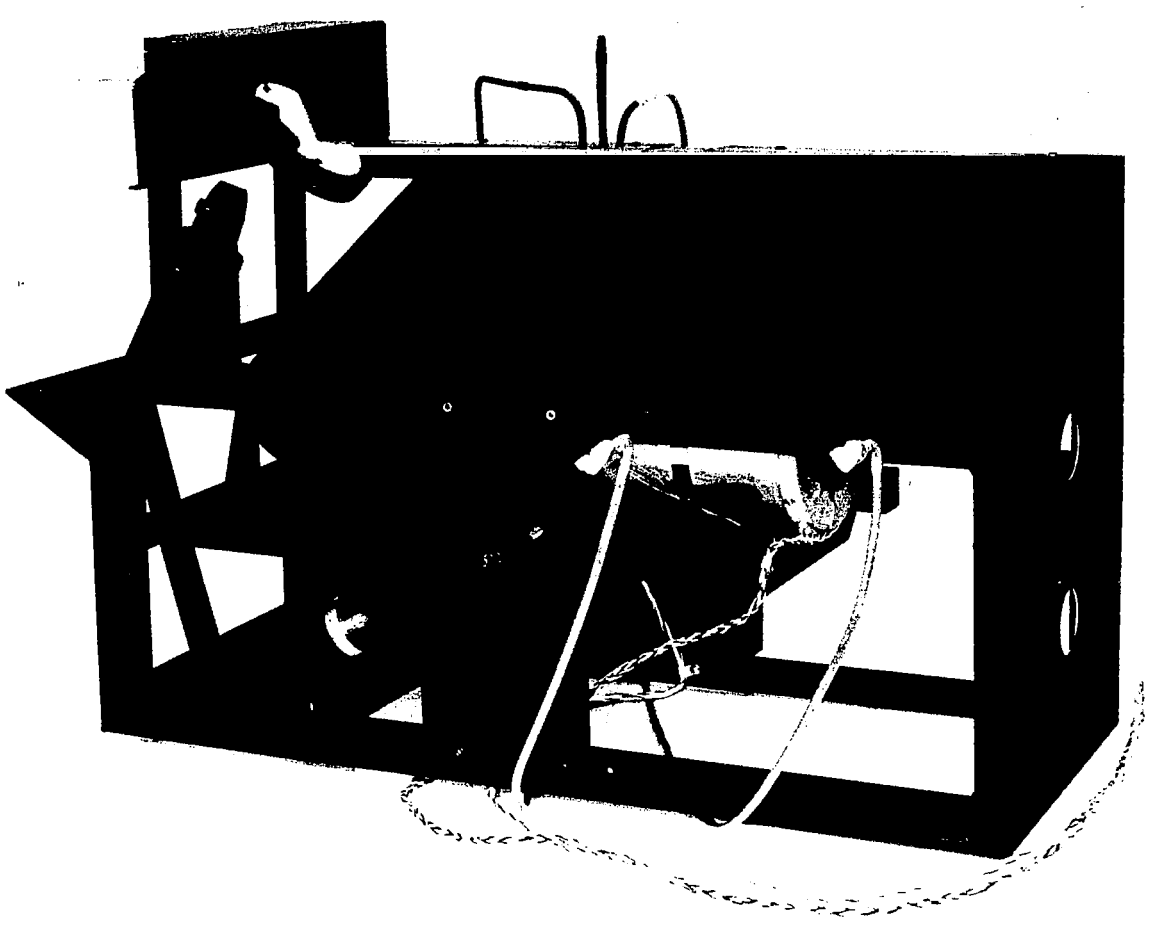

Figure 20. Reflectometer Rack Assembly

Folding mirrors. - Three 10-cm diameter, gold-over-chrome coated, pyrex mirrors with individual mounts are attached to the reflectometer rack and provide for the necessary folding of the reflectometer beam. Fine and coarse angular adjustment of each mirror is provided for in the mount.

Reflectometer parabolic mirror. - A 25.4-cm diameter off-axis parabolic mirror stopped down to 17.7 cm for reflectometer acceptance angle definition is attached with its separate mount in the 50.8-cm diameter opening of the reflectometer chamber. The mirror mount provides for angular mirror adjustment in all directions as well as focal length adjustment capability to position the mirror at its best focus within the optical system. The mirror is a 25.4-cm, 9-degree off-axis parabola made of CerVit material with a 0.355-mm diameter blur circle, and is coated with gold over chrome.

Hg-Cd-Te detector. - A 0.5 mm by 0.5 mm Hg-Cd-Te detector mounted in its own liquid nitrogen dewar is attached to the chamber through a flexible metal bellows mount which provides for detector motion adjustment of 0.254 cm in focal length. A 14 to 16 micron infrared bandpass filter is attached to the bottom of the detector dewar.

Source rotary feedthrough. - A 6.35-mm diameter shaft, 11.27×10^{-2} Newton meter (10-inch pound), maximum torque bellows rotary feedthrough is attached to the reflectometer chamber wall and provides 180-degree source rotation capability from outside the chamber.

Test Radiometer

The test radiometer was designed to experimentally determine the PCS output beam characteristics and is installed vertically in the reflectometer chamber in place of the reflectometer auxiliary parabola during radiometric testing. External control of the scanning mechanism of the radiometer is accomplished through a feedthrough flange at the bottom of the chamber.

Test radiometer chamber. - The test radiometer utilizes the reflectometer chamber with a 50.8-cm diameter by 45.7-cm long extension in place of the 50.8 cm diameter flanged cover. The test radiometer is inserted vertically into the reflectometer chamber through the 50.8-cm diameter opening in place of the reflectometer auxiliary parabola and mount. A 50° elliptical baffle is installed in the chamber behind the test radiometer and in front of the reflectometer rack to act as a trap for the unused portion of the collimated beam.

Optics. - The test radiometer optical system, shown schematically in Figure 6, uses a 25.4-cm diameter flat scanning mirror mounted at a 45-degree angle to the PCS collimated beam. This scanning mirror is used to fold a portion of the collimated beam up onto the 25.4-cm diameter, 20-degree off-axis parabolic mirror stopped down to 12.7 cm. The scanning mirror is capable of traversing up or down 22.8 cm from its center position to provide a complete traverse of the 61-cm diameter collimated beam with an effective 12.7-cm diameter scanner. The scanning mirror also has an angular or goniometric scanning capability of ±20 degrees with the mirror at the center traverse position. Very-small-angle goniometric scanning of the PCS

source aperture is provided through a micrometer adjustment. The off-axis parabolic mirror, with a 1-meter focal length, focusses the intercepted collimated energy from the scanning mirror at the detector. Figure 21 shows the basic optical configuration.

An 11.4-cm diameter flat folding mirror is used to fold the focussed energy again so the detector can be mounted in an upright vertical position at the top of the radiometer cover and allow gravity filling of the liquid nitrogen dewar. The detector and detector mount are the same as used for the reflectometer.

All optical components and the scanning mechanism are supported on a basic radiometer frame (Figure 22) consisting of four aluminum plates spaced various distances apart by four 1.9-cm diameter steel standoffs.

Analyses. - Analyses were performed on the test radiometer to quantitatively determine its performance characteristics. These analyses included determining the PCS output beam-radiometer interface characteristics, radiometer signal-to-noise ratio, and the internal baffling requirements. The analyses are included in Appendixes E through G, and their results are summarized below:

- PCS beam characteristics: It was calculated that the output beam from the PCS will be measured as constant across the entire 61-cm diameter aperture so long as the radiometer detector is smaller than the imaged source diameter. The flux density distribution of the collimated beam itself varies approximately 6 percent from top to bottom.

- Signal-to-noise ratio: The test radiometer signal-to-noise ratio is calculated to be 13,200 assuming a Hg-Cd-Te detector, 300° K source, and a chopping frequency of 66 Hz with a 1 Hz bandwidth.

- Baffling: The baffles included in the test radiometer will cause the stray radiation signal-to-noise ratio to be 220,000 to 1, making the stray radiation errors negligible.

Scanning mechanism. - The test radiometer scanning mechanism contains a 25.4-cm diameter mirror mount attached to the scanning mirror cradle by a shaft and bearing arrangement which allows the mirror to pivot ± 10 degrees about the horizontal axis perpendicular to the beam. The scanning cradle is attached to two 1.9-cm ground and hardened stainless shafts by four linear ball bushings, two in tandem on each shaft. The shafts act as vertical guides for the scanning cradle to traverse the 61-cm diameter collimated beam.

The lead screw used for traversing the mechanism up and down is attached directly to the scanning mirror mount with an extension arm and naval brass nut. The screw itself is carbon steel coated with a molydisulfide coating for lubrication in the vacuum environment.

A locking mechanism attached to the mirror pivot shaft and back of the cradle is used to lock the mirror in its 45-degree position for the traverse scan or to unlock the mirror and support the cradle in its midposition during angular scan.

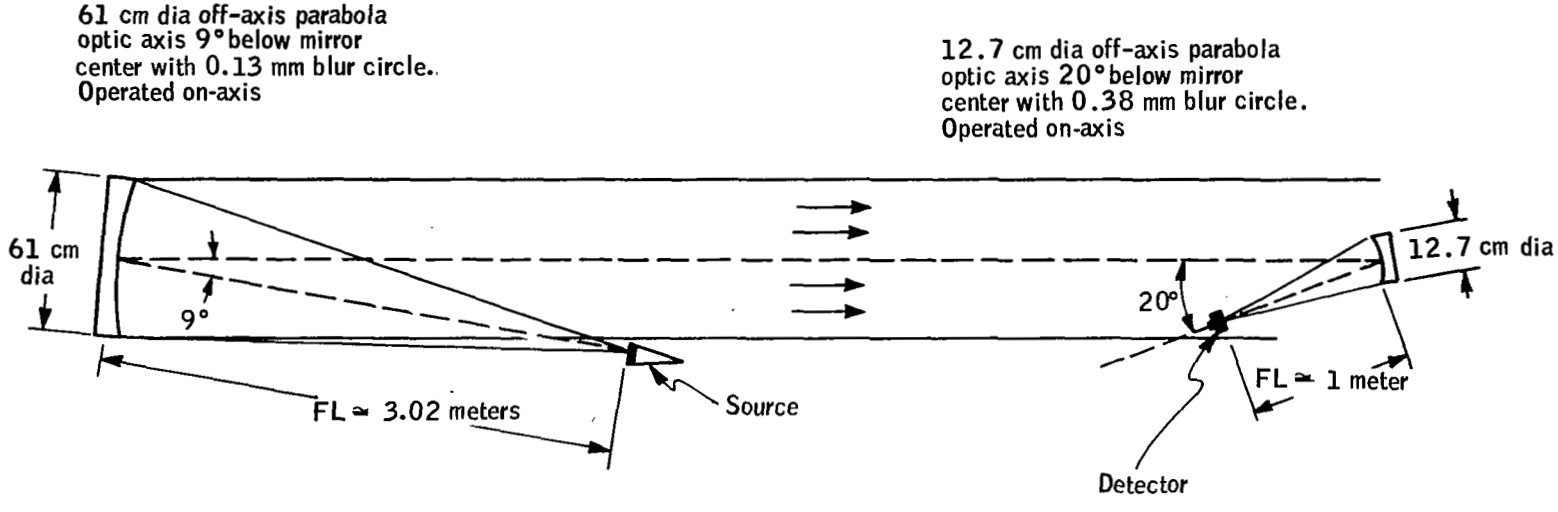

Figure 21. Test Radiometer Optical Configuration

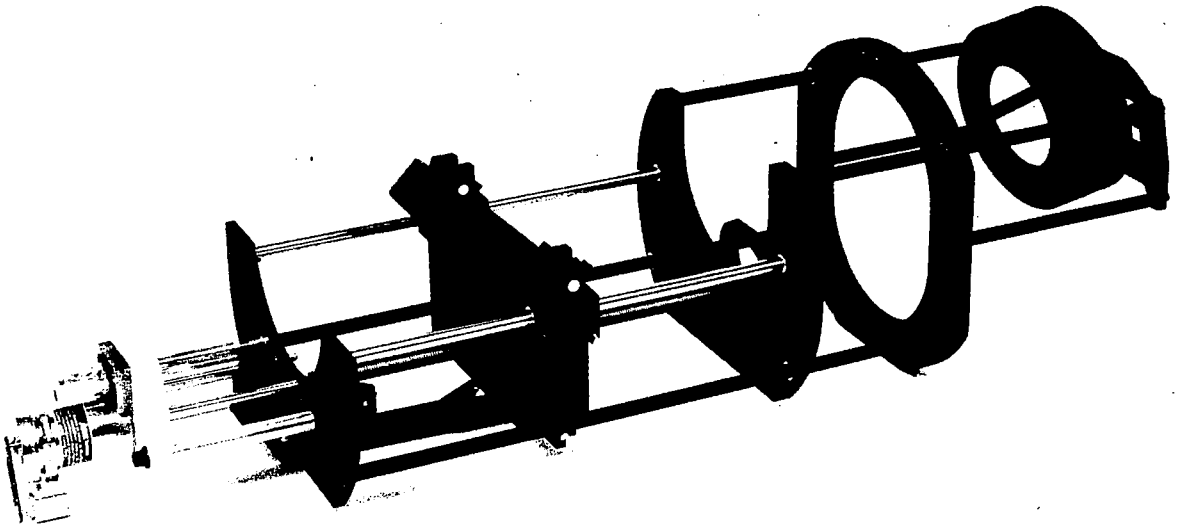

Figure 22. Test Radiometer Frame Assembly

The angular scan has a coarse control, by rotating the lead screw, or a fine adjustment, by raising or lowering the lead screw a small amount while fixing its rotation with a micrometer head and lever mechanism attached to the lower plate and feedthrough flange.

Bellows feedthrough flange. - The bellows feedthrough flange, located on the bottom of the reflectometer chamber directly below the test radiometer, has three bellows feedthroughs, two for linear motion and one for rotary motion. The large-diameter rotary feedthrough is used to rotate the radiometer lead screw. A four-digit counter is attached to this feedthrough to give translation position in 0.254-mm increments or angular position in 0.168-degree increments. One linear bellows feedthrough with an overcenter lever arrangement is used to lock and unlock the scanning mirror. The other linear bellows feedthrough with the micrometer head attached is used for fine angular adjustment. A 0.0254-mm increment on the micrometer head gives 0.028-cm movement of the detector image at the primary chamber source.

TEST RESULTS

Test Objectives

The Primary Calibration System was subjected to a series of functional and operational tests to establish its capability to provide an adjustable-temperature, extended-radiance source for testing IR radiometer characteristics. Specific objectives of the tests performed included the following:

- Checkout of the primary chamber peripheral equipment interface, including leak checking, vacuum pumping and monitoring, liquid-nitrogen-flow control and monitoring, chamber temperature monitoring, source temperature control and monitoring, and determination of thermal shock effects
- Determination of source thermal control characteristics
- Determination of source thermal gradients
- Determination of chamber gradient characteristics
- Performance of an *in situ* collimating mirror reflectance measurement
- Determination of the PCS output beam characteristics
- Determination of the adjustability of the source in the longitudinal direction

Test Parameters

The operational parameters measured during the series of tests included the following:

- LN_2 system seal integrity
- Vacuum system characteristics, including: vacuum system integrity, rough pumping, cryopumping, and ion pumping rates and levels
- Thermal characteristics of the system, including: operational characteristics of the source-guard control loop, source temperature drift, source thermal gradients, source-guard warmup rates, heater power versus temperature, LN_2 consumption rates, PCS cooldown rates and levels, and effects of temperature on alignment and adjustments.

- Collimator reflectance measurement <u>in situ</u>
- PCS output beam characteristics, including measurement of the beam uniformity across its defining aperture and measurement of the angular or goniometric characteristics characteristics of the beam.

Vacuum Characteristics

<u>Leak rate</u>. - The chamber is not readily capable of having its total leak rate measured directly. To do so would require enclosing the entire chamber in a leaktight shroud, injecting a known quantity of helium gas around the chamber and then measuring the leakage into the chamber with a mass spectrometer leak detector. An approximation can be made, however, by knowing the pressure levels attained and the pumping speeds of the ion pumps. The estimated leak rate is then calculated as follows:

Ion pumping rate = 40 x 25 liters/sec = 1000 liters/sec

Minimum measured pressure = 2.66×10^{-4} N/m^2 (2×10^{-6} torr)

System pumping flow rate = $10^3 \times 2.66 \times 10^{-4}$
= 2.66×10^{-1} N/m^2 liters/sec

Calculated chamber outgassing rate = 1.46×10^{-1} N/m^2 liters/sec

Leak rate = pumping flow rate-outgassing rate
= $2.66 \times 10^{-1} - 1.46 \times 10^{-1} = 1.2 \times 10^{-1}$ N/m^2 liters/sec

1 N/m^2 liter/sec = 5.66×10^{-3} std cc/sec

Leak rate = 6.8×10^{-4} std cc/sec

This compares with a design objective of 1×10^{-6} std cc/sec. The most probable cause for the higher-than-estimated leak rates is the liquid nitrogen circulatory system within the chamber. Considerable difficulty was experienced in achieving leaktight seals with the gyrolock fittings. This was traced to improper surface preparation of the tubes to which the gyrolock seal is made, i.e., tool and mill marks and minute surface scratches. The tubes were ground and polished down with some success. In addition, approximately 150 weld and braze joints were made in the LN_2 tubes and fittings with some probable residual leak rates. Also, several leaks in the shrouds and baffles had to be rewelded. The mirror plate and guard assembly presented additional problems with leaks in the aluminum welds. This was due primarily to the inherent difficulty of achieving leaktight joints with aluminum welds. Finally, the bellows couplings throughout the chamber in some cases evidenced problems in remaining sealed.

The primary chamber housing itself does not appear to be a problem with leakage. It was acceptance tested with a mass spectrometer leak detector and no evidence of leakage was observed at any time. Similarly, the aluminum flange seals appear to be performing properly. Continued operation of the system should result in lower pressure levels because the outgassing rates will decrease with time.

Pumpdown sequence. - A preferred pumpdown procedure has been established to prepare the system for normal operation. The step-by-step sequence is as follows:

1. Close upper rough pump gate valve.
2. Open pump bypass.
3. Turn on roughing pump; pull down line and trap to $\approx$100 microns.
4. Close bypass; pull trap down to 50 microns.
5. Open upper gate valve. Pull down chamber to 1000 microns. Cool down LN_2 trap. Pull down chamber to 20 microns. Close upper gate valve. Turn off roughing pump.
6. Start cryopumping by opening main shroud and baffle LN_2 valves approximately 1/4 turn. Cryopump down to 1.33×10^{-2} N/m^2 (10^{-4} torr).
7. Turn on ion pumps and operate in the start position. Switch to run position when current level drops below 200 ma.

Roughing pump rates and levels. - Figures 23 and 24 show the rough pumpdown rates of the primary chamber, by itself and with the reflectometer chamber attached. As shown, the times required to pump down to 50 microns are 21 and 34 minutes, respectively. This compares favorably with a requirement to pump down the primary chamber to 50 microns in 30 minutes.

It has been observed that the presence of water vapor in the chamber, trap, and pump line greatly influences the pumping rate and level. If the chamber has been exposed to a high humidity for some time, it has been necessary to pump down and backfill the chamber with dry nitrogen gas before the ultimate desired rough pumpdown pressure ($\approx$ 20 microns) is attained. Normal operation entails backfilling with dry nitrogen when a test is completed to ensure a dry internal ambient condition.

Cooldown Characteristics

Cooldown rates. - The cooldown rates of the primary chamber elements have been monitored and recorded. They are plotted in the following figures: source, guard, and aperture plate, Figure 25; chopper blade and baffle, Figure 26; folding mirror and triple-point cell aperture, Figure 27; collimating mirror, Figure 28; and shrouds and baffles, Figure 29. As shown, all

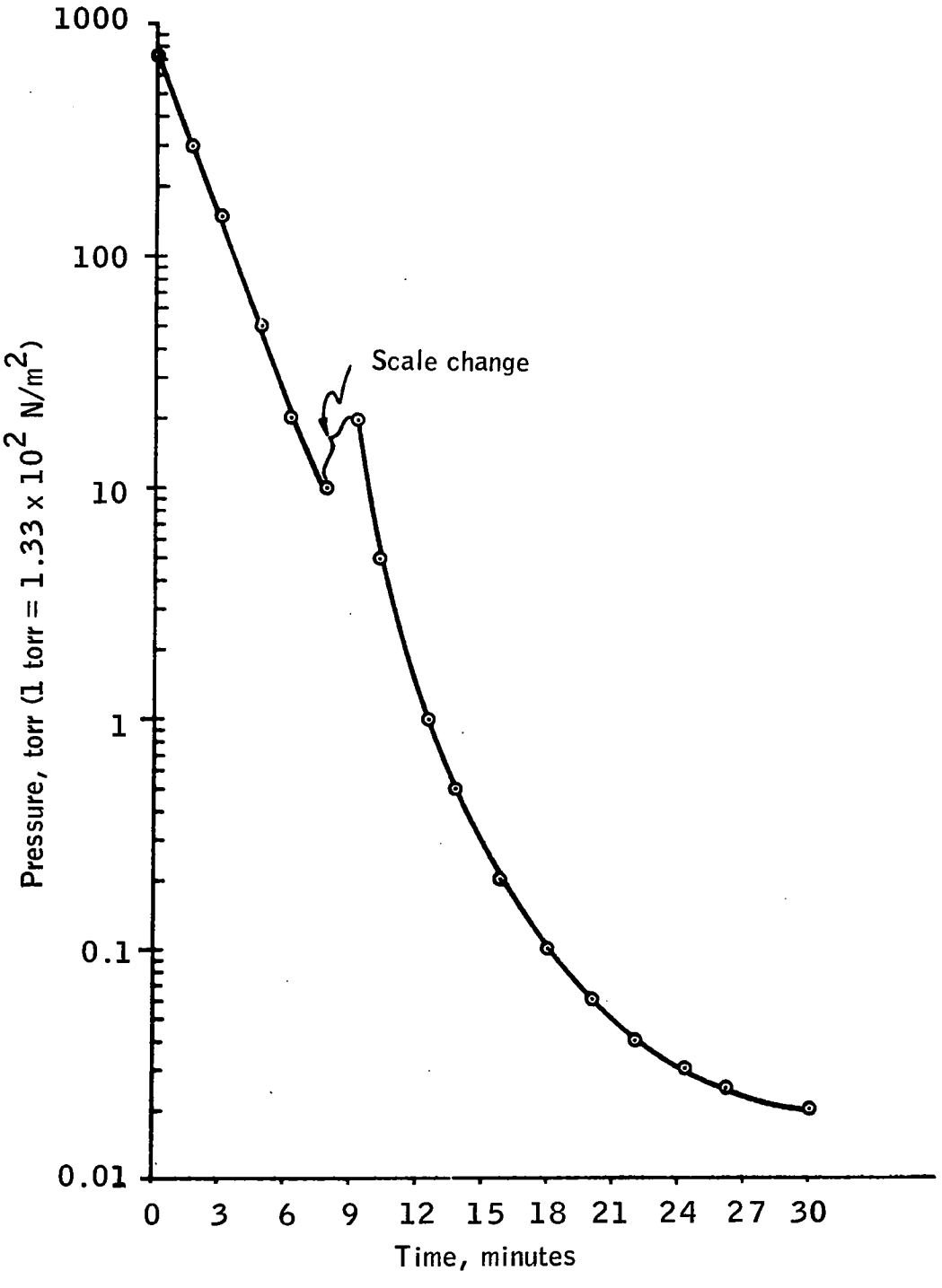

Figure 23. PCS Rough Pumping Rate

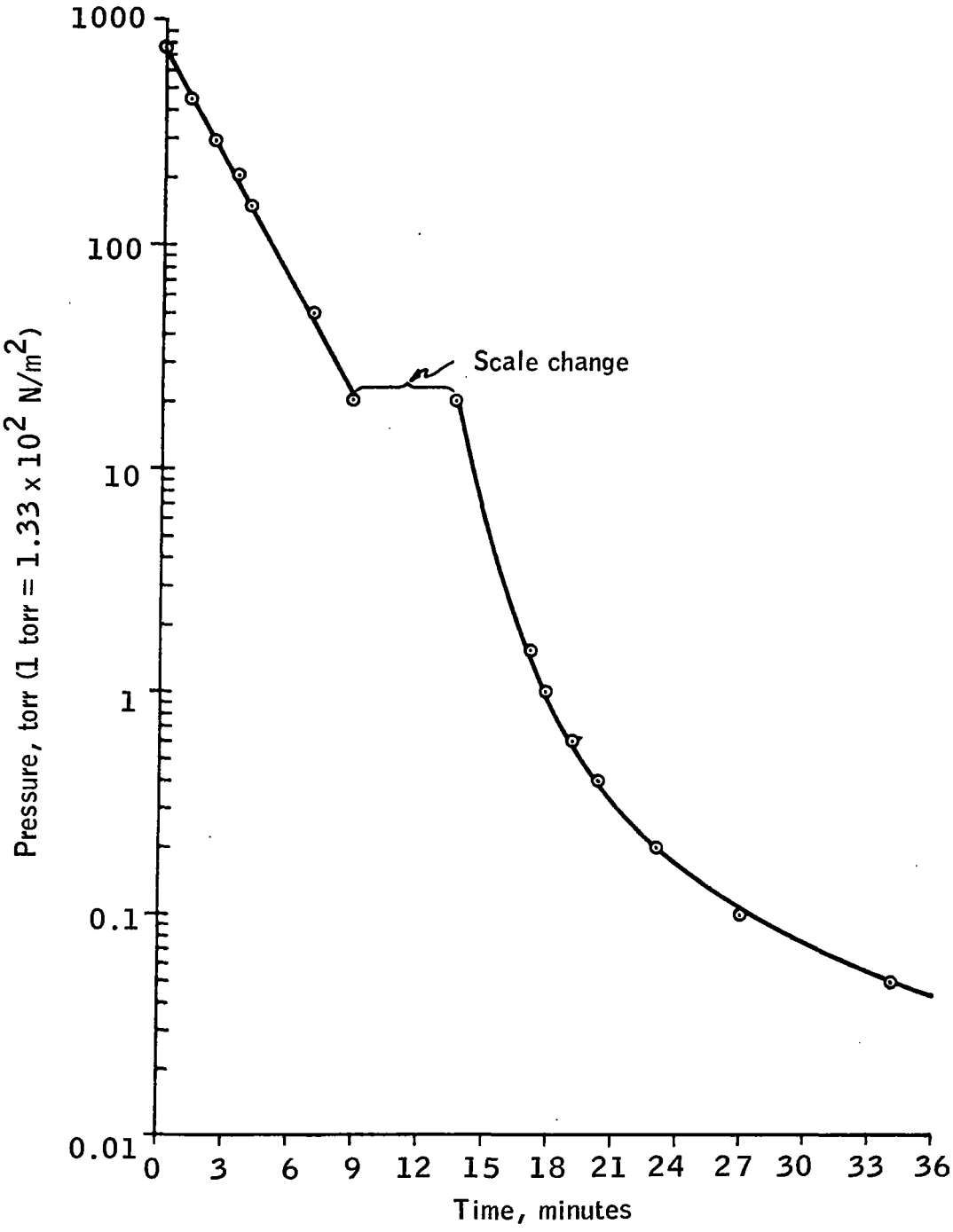

Figure 24. PCS Reflectometer Rough Pumping Rate

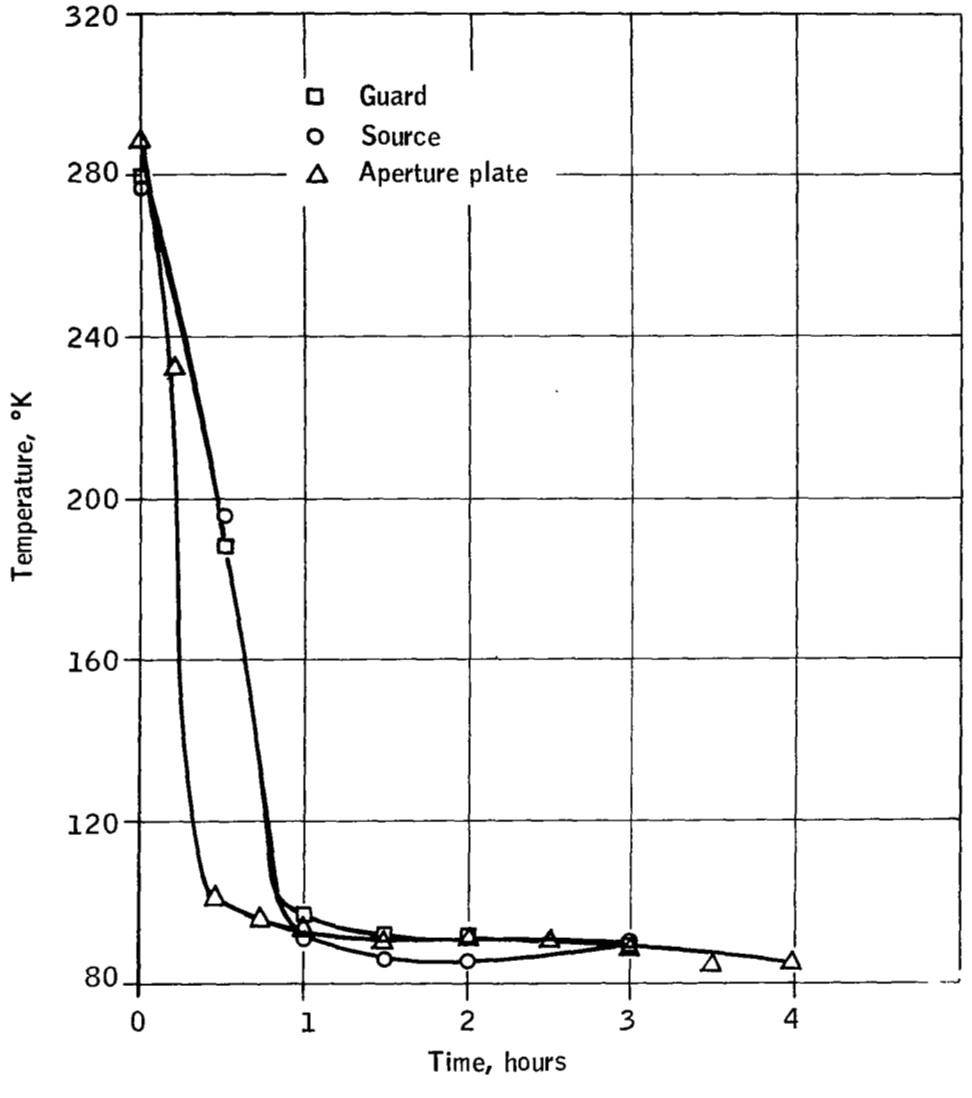

Figure 25. Source, Guard, Aperture Plate Cooldown Rates

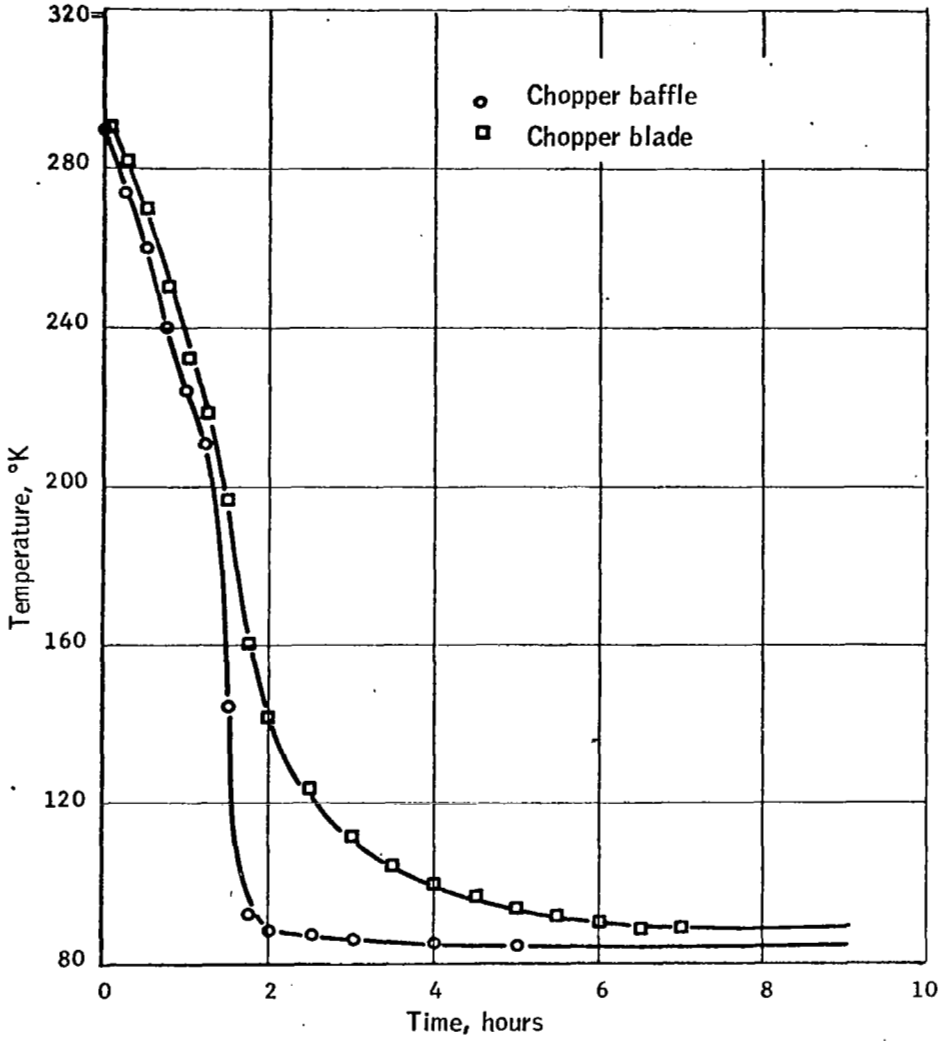

Figure 26. Chopper Blade Assembly Cooldown Rates

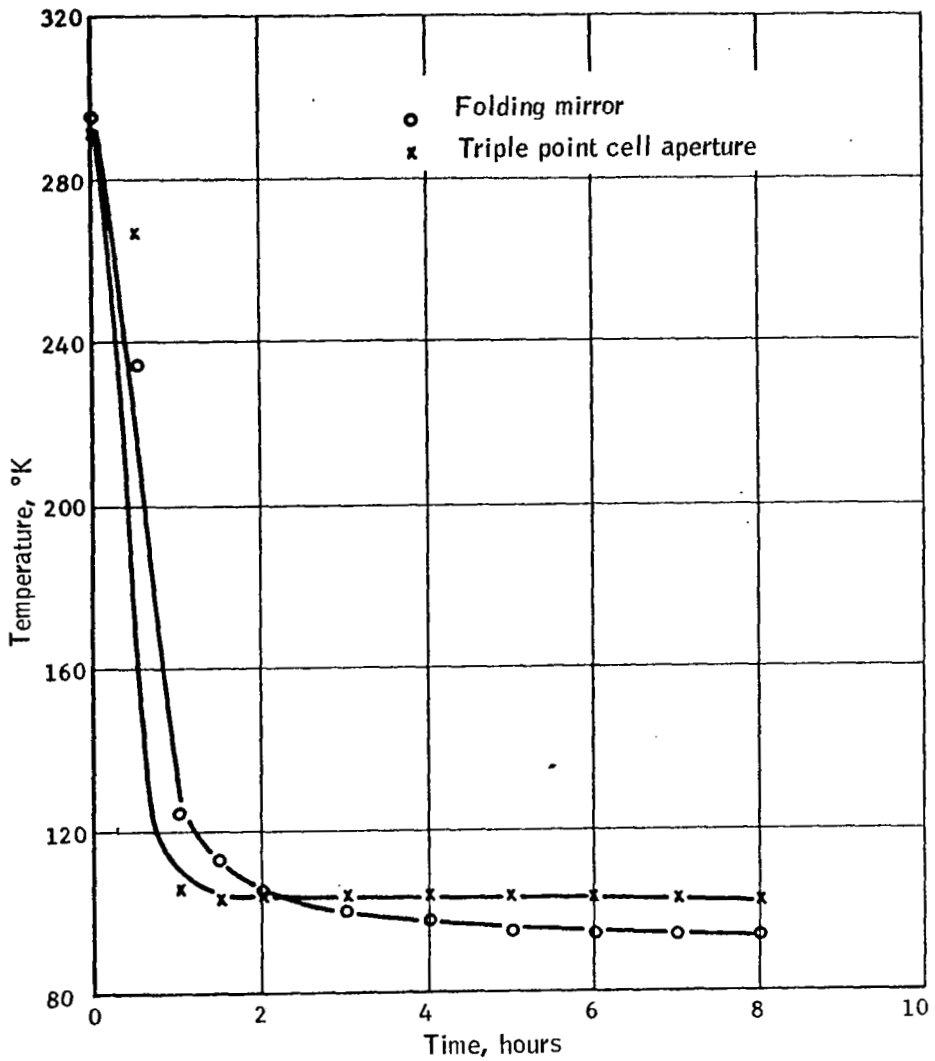

Figure 27. Folding Mirror, Triple-Point Cell Aperture Cooldown Rates

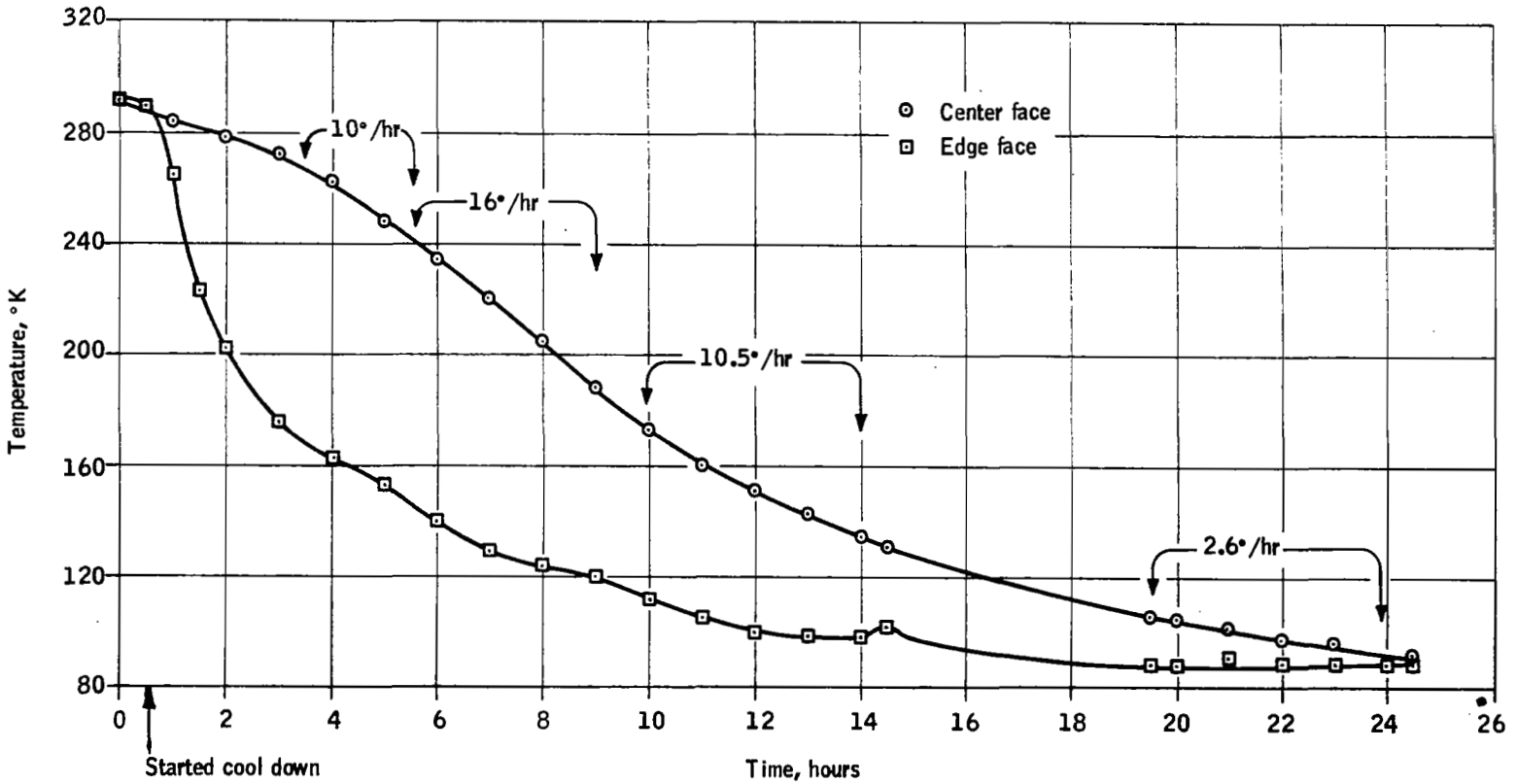

Figure 28. Mirror Cooldown Rates

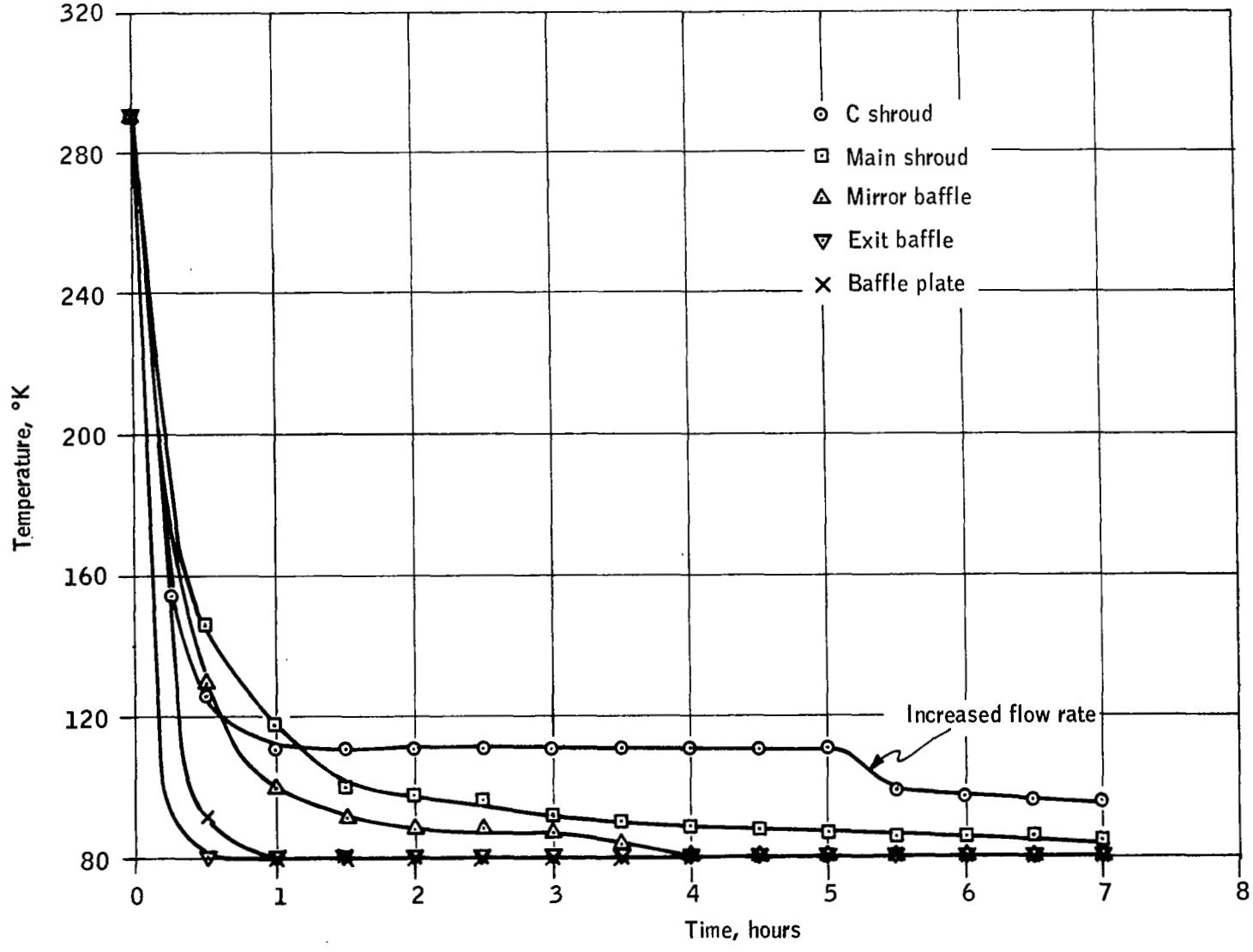

Figure 29. Shroud, Baffle Cooldown Rates

elements except the collimating mirror and chopper blade reach stabilized conditions below 100°K within 4 hours. The temperatures were measured with nickel-iron thermometers. A calibration curve for this type of thermometer is included in Appendix H.

As shown on Figure 28, the collimating mirror is cooled to 150°K after 12 hours of cooldown time. The primary problem with the mirror is its extremely low thermal conduction coefficient, 0.004 cal/cm/sec/°C. Numerous attempts were made to improve the thermal conduction condition between the mirror plate and the mirror. The configuration which was finally used incorporates a 0.15-cm-thick monel woven mesh between the mirror plate and the back of the mirror. Also, the mirror plate face and the back of the mirror are painted with a 0.9 emissivity black paint to maximize radiative coupling. In addition, a 0.15-cm-thick copper strap with LN_2 cooling lines soldered to it is attached around the mirror circumference. Nickel-iron thermometers were affixed to the mirror face to monitor the cooldown rates.

When cooling the mirror, caution must be exercized such that the main shrouds are first cooled down to at least 250°K before mirror cooldown is started. This is done to cause any water vapor present to be condensed out on the shrouds and not on the mirror, which could cause possible contamination and consequent reflectance degradation of the mirror surface. This initial cooldown of the shrouds normally occurs within 15 minutes.

The chopper blade temperature was monitored by temporarily affixing a nickel-iron thermometer to the blade with the blade rotated to a closed position looking at the 1-cm source aperture. No noticeable effect was seen on the blade temperature with various source temperatures. The chopper blade is both radiatively cooled from the chopper baffles and conductively cooled through the support bearings mounted on the chopper drive shaft. As seen in Figure 26, the chopper blade reaches an equilibrium temperature of 88°K within 7 hours of cooldown time.

LN_2 consumption. - Figure 30 shows the system LN_2 consumption rate during normal operation. The initial rate is 280 liters/hour for the first hour, 140 liters/hour during the cooling of most of the elements, and then a steady-state consumption of 90 liters/hour. In a 12-hour operating period, approximately 1500 liters are consumed. This consumption rate includes all losses, including the PCS itself, transfer lines and bulk tank boiloff. Little difference has been observed in LN_2 consumption rates with the reflectometer chamber attached.

Cryopumping. - Normally the chamber is rough pumped down to approximately 20 microns before starting LN_2 flow through the baffles and shrouds. The cryopumping action causes the chamber pressure to decrease to approximately 1.33×10^{-2} N/m^2 (10^{-4} torr), which occurs within 30 minutes after LN_2 flow is initiated. At this point, the ion pumps are energized to reach the ultimate pressure levels.

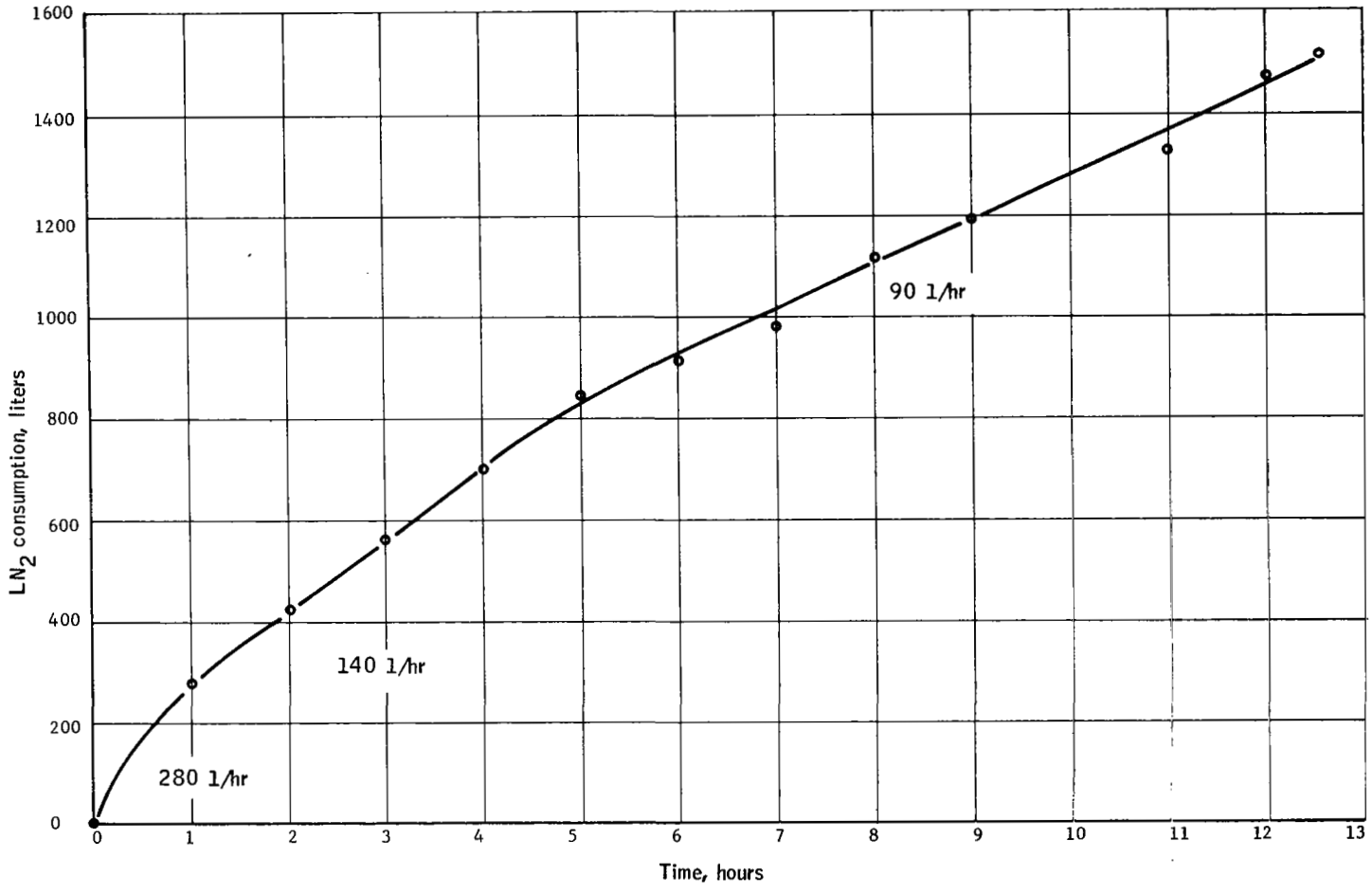

Figure 30. Cumulative LN_2 Consumption and Consumption Rate

Ion Pumping Characteristics

The observed pressure levels obtained with the ion pumps are well within the operational requirements of the system. As noted above, the primary chamber by itself has attained a pressure level of $\approx 2.66 \times 10^{-4}$ N/m^2 (2×10^{-6} torr). With the reflectometer chamber attached the pressure level is $\approx 3.99 \times 10^{-4}$ N/m^2 (3×10^{-6} torr). These pressure levels are normally attained within 30 minutes after the ion pumps are energized. The design requirement is 1.33×10^{-3} N/m^2 (1×10^{-5} torr), primarily to ensure that the ion pumps are not overloaded, with a consequent reduction in expected lifetime. In the pressure region of 1.33×10^{-3} - 1.33×10^{-4} N/m^2 (10^{-5} to 10^{-6} torr), the ion pumps are operating at maximum efficiency with current levels of 50 to 100 ma, a normal range of operation.

Source-Guard Temperature Characteristics

Source-guard warmup characteristics. - Figure 31 shows the source-guard warmup rates from various starting temperature conditions. The source and guard rates are nearly identical and track each other very closely, i.e., within 5°K. The average rate for each is 59°K/hour. The normal warmup procedure is to turn on the source and guard heater simultaneously, the source by turning on its power switch and the guard by setting the controller preset control (Figure 32) to approximately 2° below the desired temperature. The source switch is then turned off 2° below the desired temperature as monitored by the nickel-iron thermometer affixed to the source surface. The guard monitor sensor should also be observed to ensure that the guard temperature stabilizes at the proper preset point.

Thermal stability characteristics. - Figures 33 through 38 show the temperature stability characteristics of the source at 100°K, 150°K, 200°K, 240°K, 280°K, and 300°K. After the source power is turned off, the temperature of the front PRT is closely monitored and recorded every 15 minutes. The drift characteristics are noted from the previous reading, and the guard controller set point is adjusted accordingly to stabilize the drift condition of the PRT-measured temperature. When a continuous set of points are within 0.02°K for one hour without controller adjustment, the source is considered stable. Because the controller is a true proportional type, no significant oscillations in the source behavior are apparent. The guard temperature is set to just balance the heat losses of it and the source to the surrounding cold environment.

Gradient behavior. - The measured differential temperatures between the front and rear PRTs at 100°K, 200°K, and 300°K are shown on Figure 39. As shown, the maximum gradient occurs at 300°K, with the front PRT reading 0.03°K higher than the rear one. The gradient decreases linearly with temperature. The cause of the gradient is probably due primarily to conductive heat losses from the rear of the source through the LN_2 supply lines and electrical leadwires. Both have been well isolated from the surrounding cold baffes and shrouds; however, the losses are apparently still influencing the source temperature. When measuring the source gradients, it has been noted that the source drift must be minimal (less than 0.02°K/hour) in order

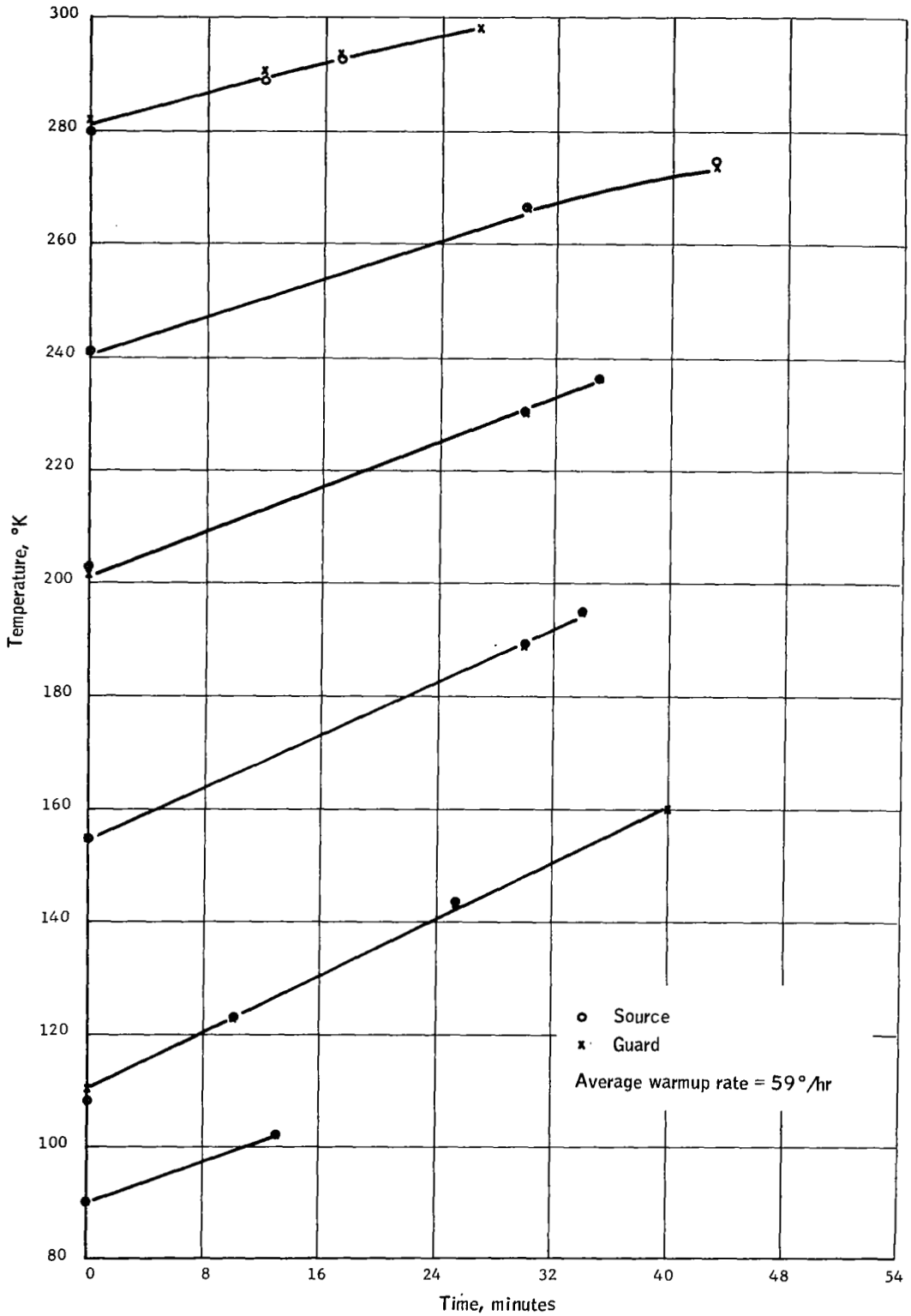

Figure 31. Source, Guard Warmup Rates

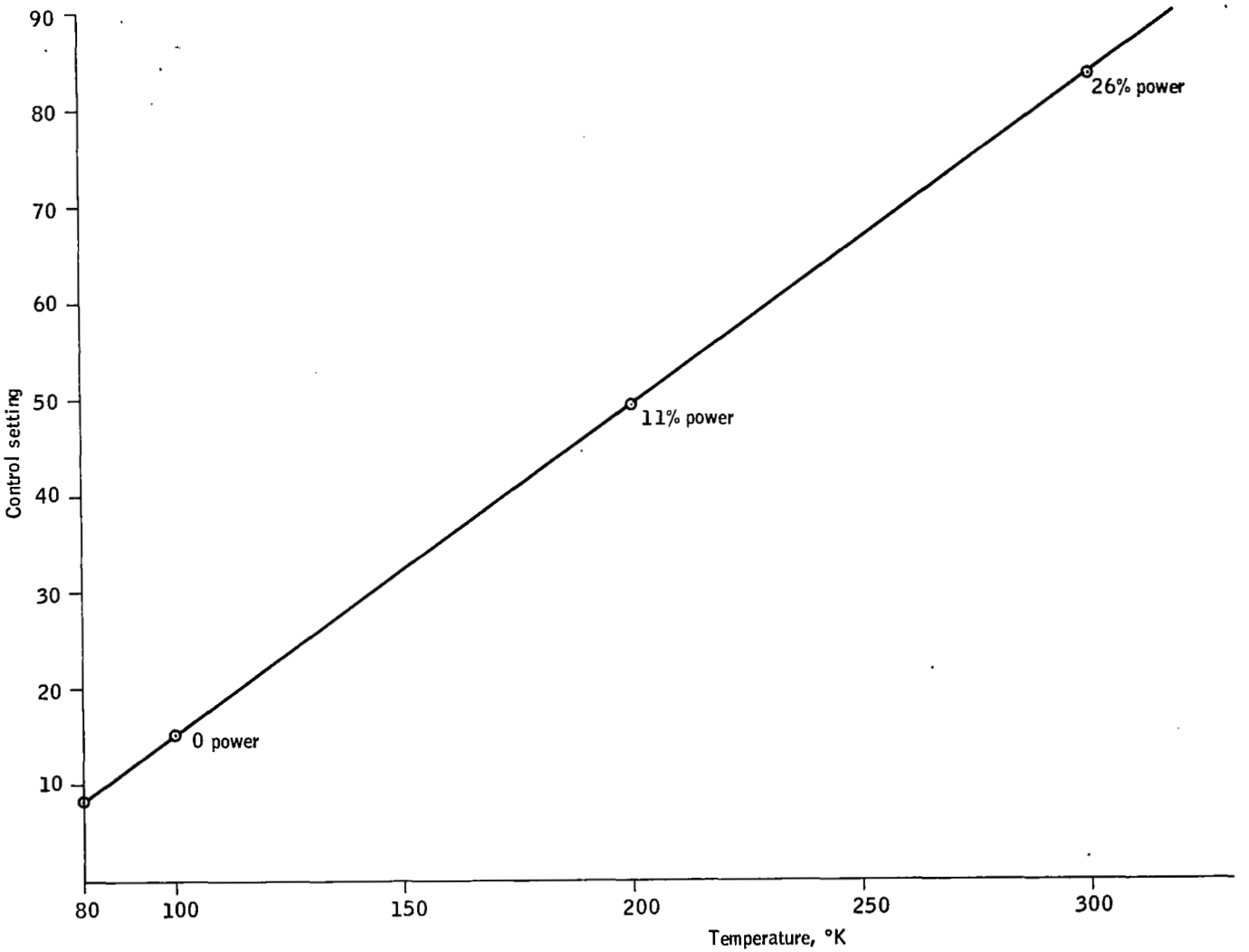

Figure 32. Guard Controller Set versus Temperature (stabilized conditions only)

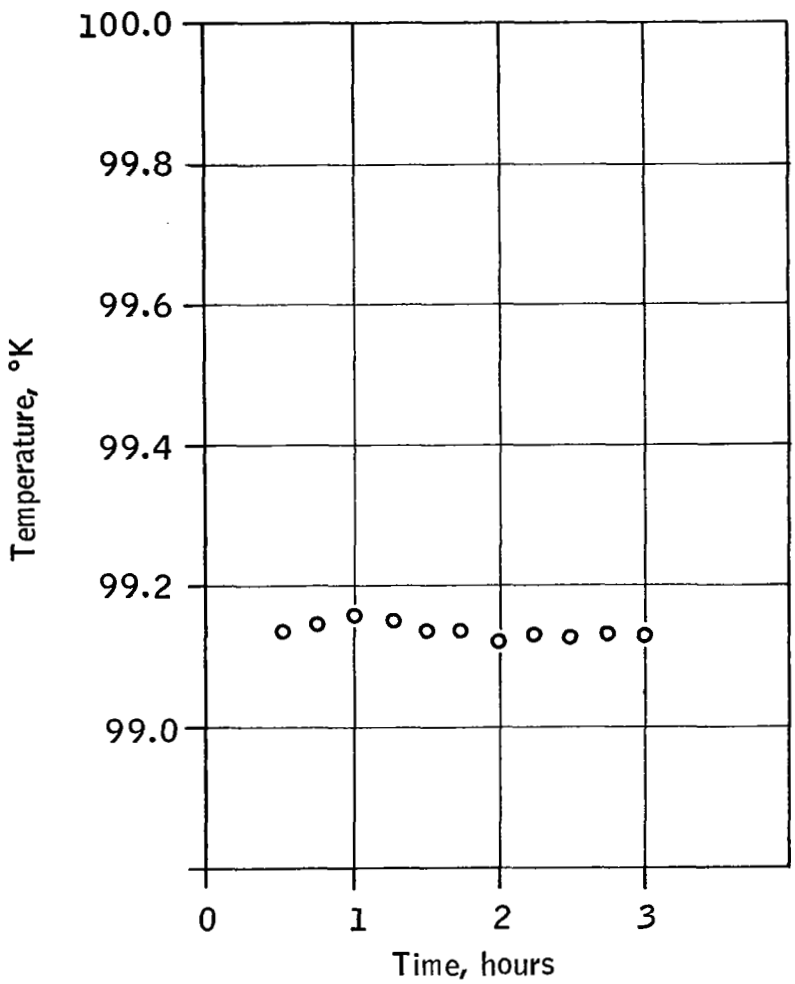

Figure 33. Source Temperature as a Function of Time, 100°K Temperature Stabilization Point

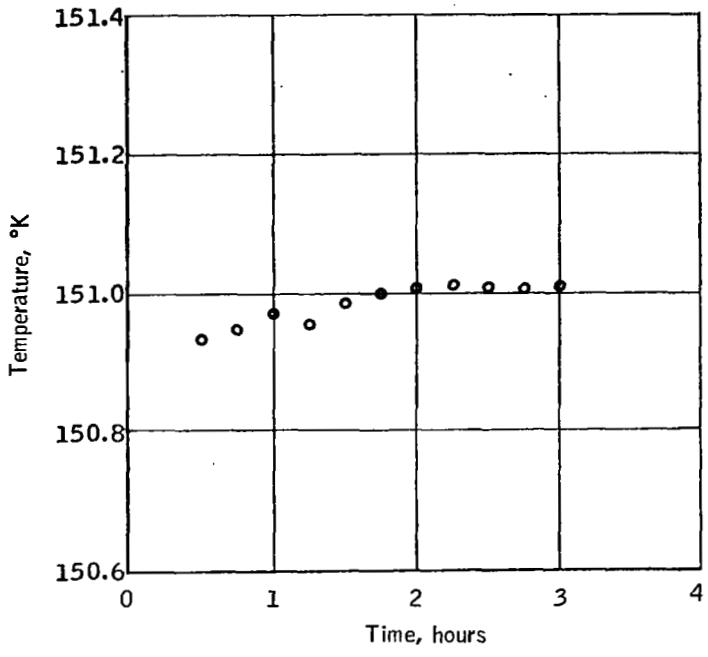

Figure 34. Source Temperature as a Function of Time, 150°K Temperature Stabilization Point

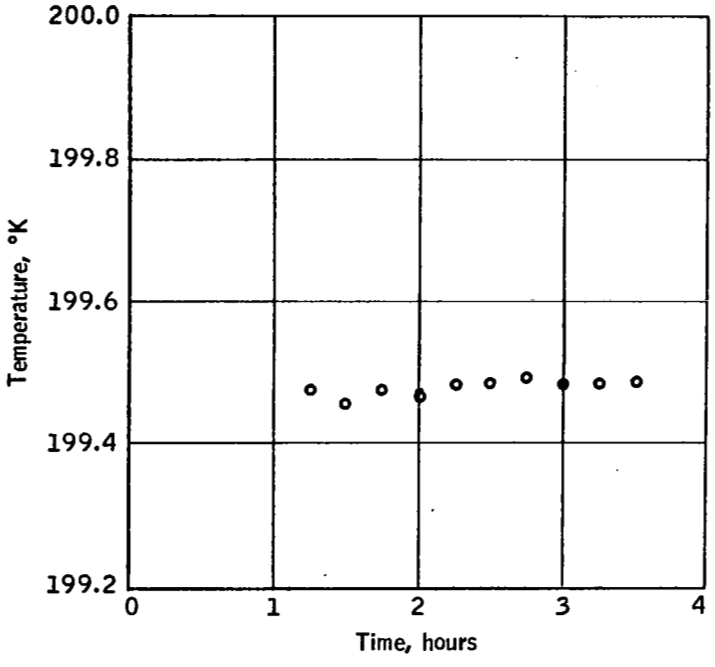

Figure 35. Source Temperature as a Function of Time, 200°K Temperature Stabilization Point

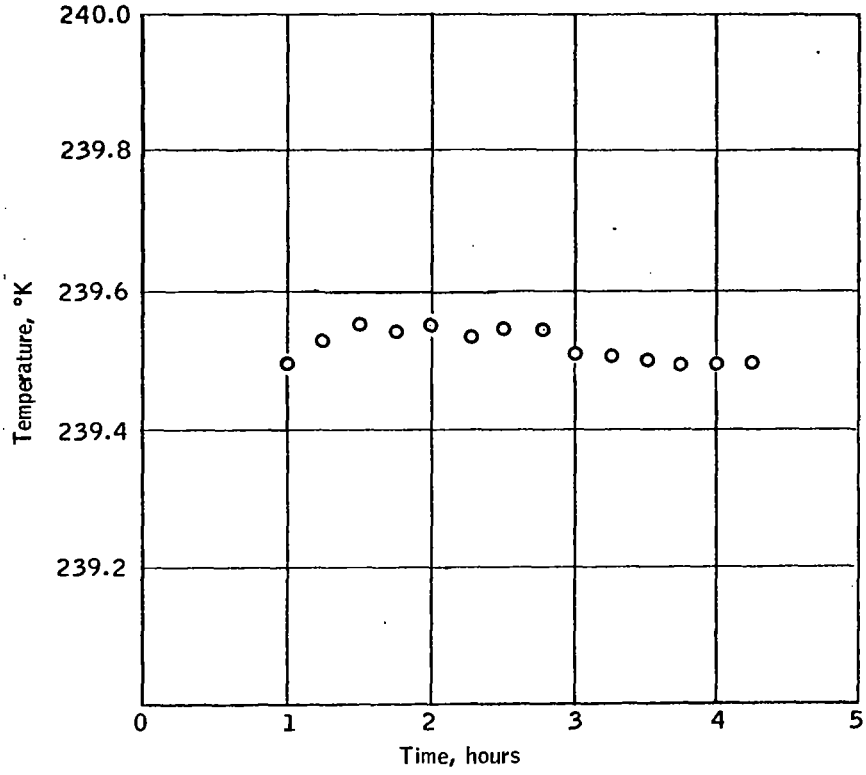

Figure 36. Source Temperature as a Function of Time, 240°K Temperature Stabilization Point

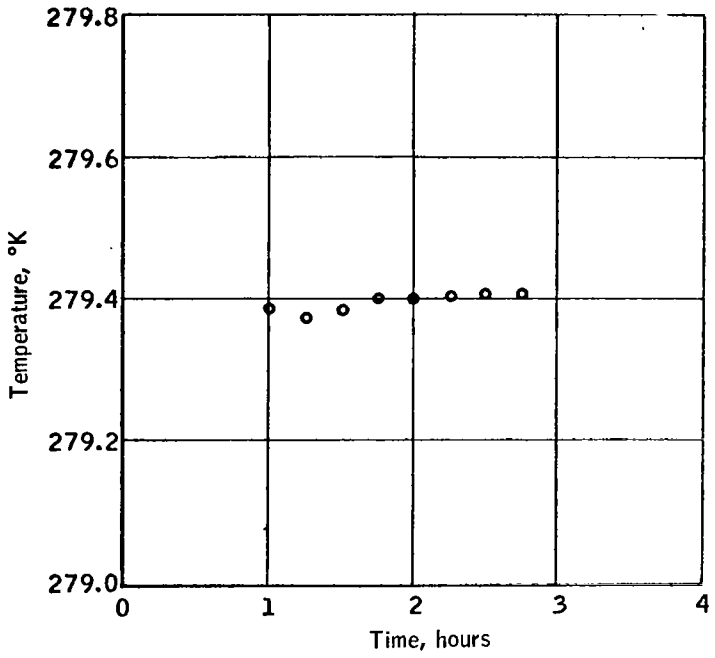

Figure 37. Source Temperature as a Function of Time, 280°K Temperature Stabilization Point

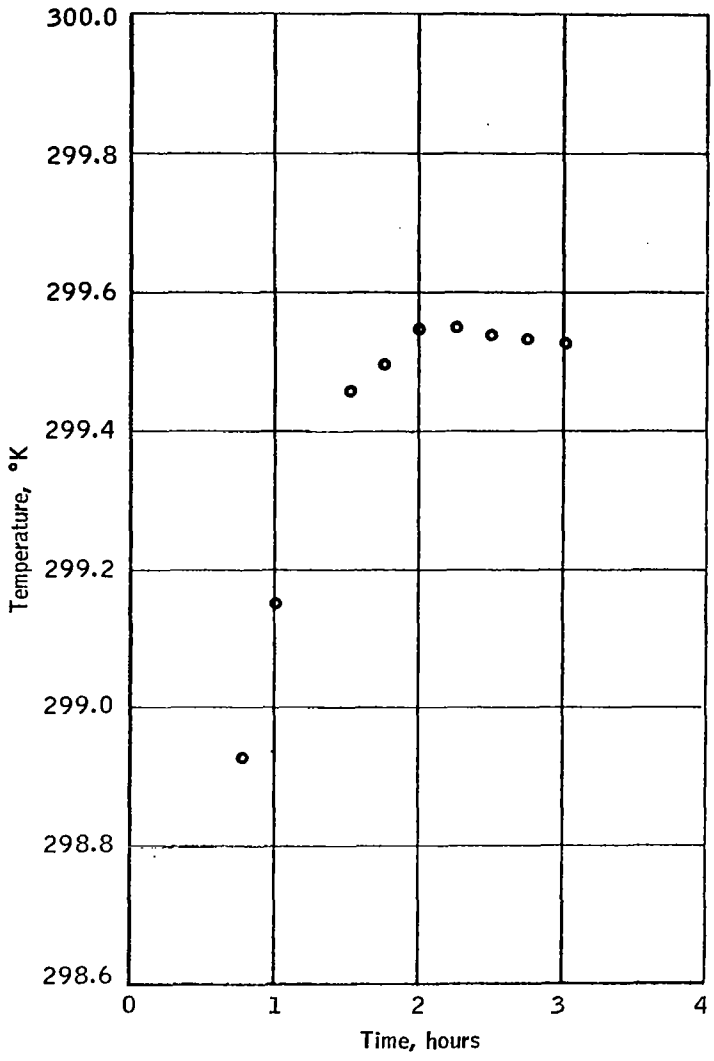

Figure 38. Source Temperature as a Function of Time, 300°K Temperature Stabilization Point

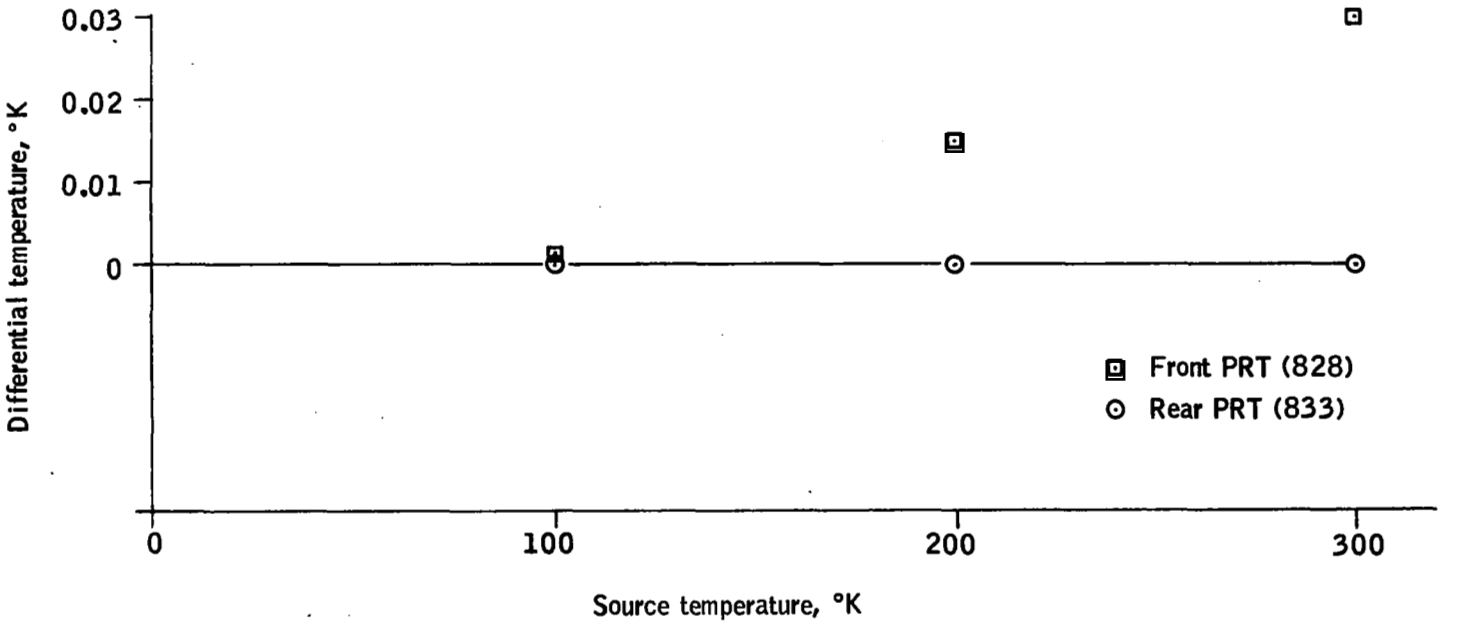

Figure 39. Source Gradient Characteristics as a Function of Temperature

to minimize the gradient characteristics. If the source temperature is changing, it apparently does so nonuniformly because of its mass disymmetry from front to rear. Significantly more thermal mass is present at the rear of the source with the emittance cone pointing forward and the rear PRT is located more nearly in the center of the copper block than the front one.

Platinum resistance thermometer calibration. - The two platinum resistance thermometers (No. 828 and No. 833) utilized in the blackbody source were calibrated to secondary standards traceable to the NBS. A third thermometer (No. 819) was built and calibrated the same way and sent to NBS for its independent calibration. The calibration tables, including the NBS calibration are included in Appendix H. The maximum difference between the manufacturer's calibration data and that from NBS is 0.00379°K, considered to be within normal tolerance limits of the PRT calibration.

The thermometers in the blackbody source consistently agree in measured temperature within 0.002°K at room-ambient stabilized conditions. The instrument used to read out the PRT resistances is a commutating Mueller bridge with a stated accuracy of 0.002 percent or 0.005°K. The resolution of the instrument is ± 0.0001 ohm or ± 0.001°K at 300°K.

Reflectance Measurements

Sample mirror coating test. - Prior to gold-coating of the collimator, a sample mirror coating test was conducted wherein seven small witness mirrors were used to establish confidence of obtaining uniformity of the reflectance coating of the collimator. The seven witness mirrors were placed in the locations shown in Figure 40 to represent several separate areas of the collimator. The mirrors were then gold-coated in the same manner as that planned for the collimator.

After coating, a precise reflectance measurement at wavelengths of 14, 15 and 16 microns was performed at the Naval Weapons Center, China Lake, California. The equipment at NWC has a stated accuracy of at least 0.001. The test results are shown in Table 3.

TABLE 3. - WITNESS MIRROR REFLECTANCES

λ (μ)	No. 1	No. 2	No. 3	No. 4	No. 5	No. 6	No. 7
14	0.9886	0.9883	0.9892	0.9886	0.9889	0.9877	0.9880
15	0.9889	0.9880	0.9895	0.9887	0.9893	0.9873	0.9885
16	0.9886	0.9885	0.9894	0.9888	0.9894	0.9873	0.9887
Avg	0.9887	0.9883	0.9894	0.9887	0.9892	0.9874	0.9884

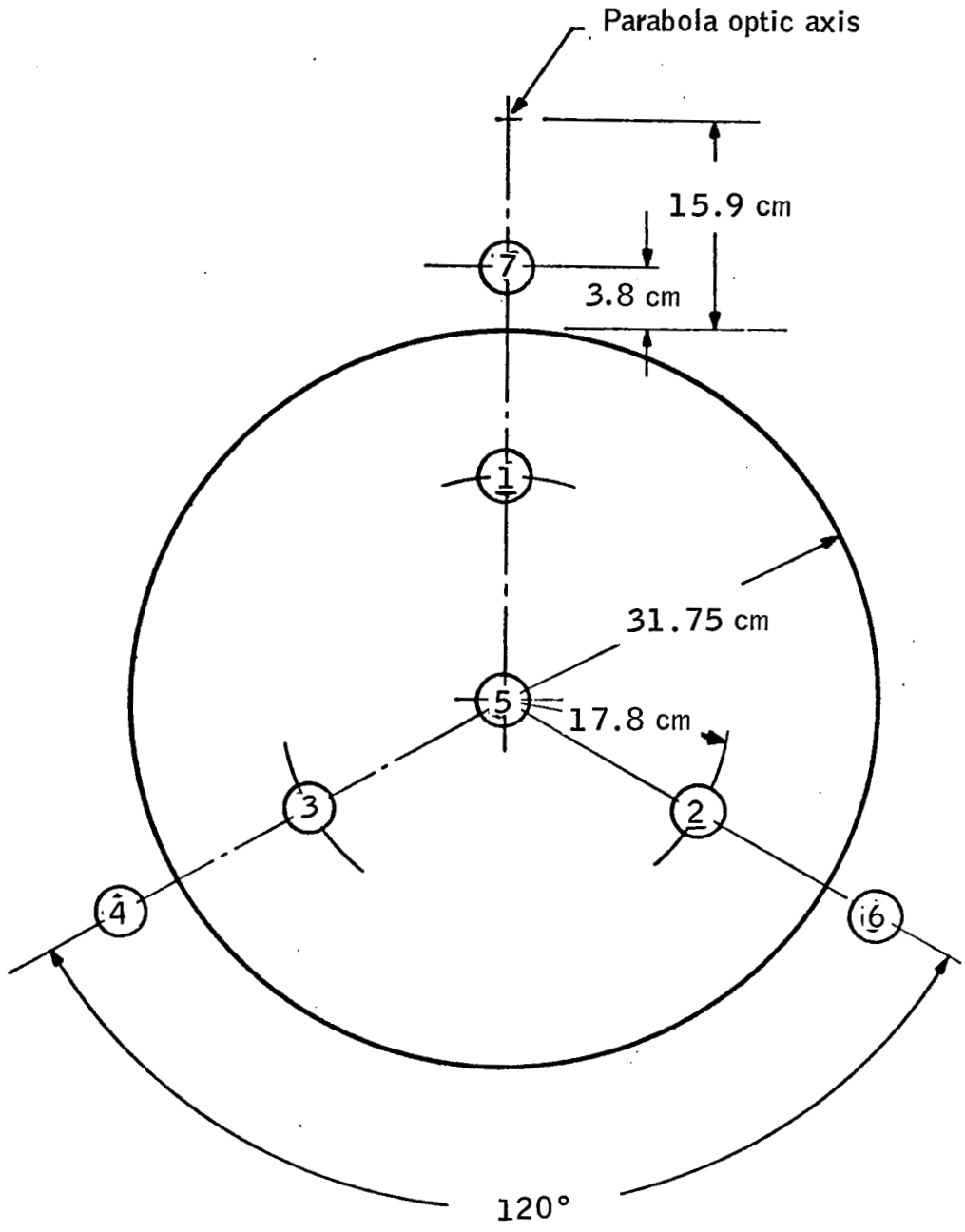

Figure 40. Sample Mirror Locations

As can be seen, the results indicated a total variation of ≈ 0.002 (mirrors 3 and 6), however this may have been due primarily to surface quality differences between mirrors. It can be expected to find a uniformity good to about 0.002 on a single mirror coating comparable to the above. The results, therefore, offered enough confidence to proceed with coating the collimator using the same techniques as were employed in the sample mirror coating.

Collimator witness flat reflectance measurements. - During the gold coating of the collimator, three witness flats were located 120° apart around the mirror and coated simultaneously with it. The witness flats were then sent to NWC for precision reflectance measurements. The results are shown in Table 4.

TABLE 4. - COLLIMATOR WITNESS FLAT REFLECTANCES

Item	Wavelength (μ)	ρ	Average
Mirror Vertex (No. 1)	14	0.9894	
	15	0.9897	0.98956
	16	0.9896	
120°CW (No. 2)	14	0.9888	
	15	0.9889	0.98893
	16	0.9891	
120°CCW (No. 3)	14	0.9869	
	15	0.9876	0.98719
	16	0.9871	

The average of each of the three mirrors reflectances varied 0.24 percent between mirrors No. 1 and No. 3. This was approximately the same spread as was noted on the seven witness samples measured previously. It is quite likely that this amount of spread in the reflectance uniformity cannot be improved upon using high-vacuum coating techniques which were employed.

Reflectance test setup. - The reflectometer electronic equipment was set up in the configuration shown in Figure 41. An Hg-Cd-Te detector with a measured D* of 3.18×10^9 cm $Hz^{1/2}$/watt (500, 1000, 1) was used. A germanium window was attached to the bottom of the detector dewar to cut off wavelengths below 2 microns. Readout electronics included a lock-in amplifier with a frequency programmer and preamplifier. The detector was coupled to the low-impedance input of the preamplifier with a 4.7-mfd coupling capacitor and bias supply. The lock-in amplifier received its sync signal from a magnetic pickoff attached to the constant-frequency 300-Hz chopper built into the reflectometer. The internal filter was set for a 0.33-Hz bandwidth. A signal processing block diagram is shown in Figure 42.

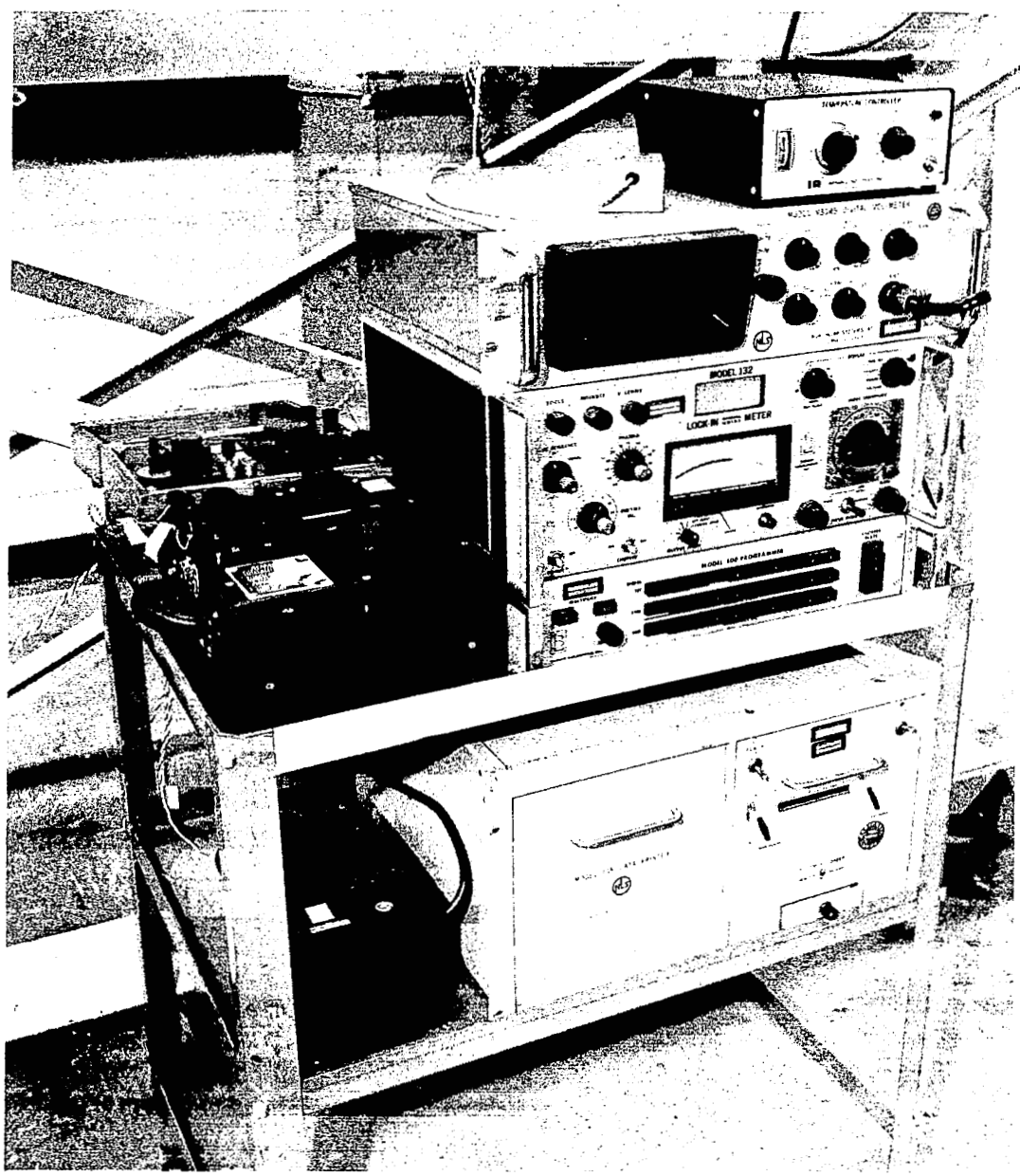

Figure 41. Reflectance Measurement Equipment

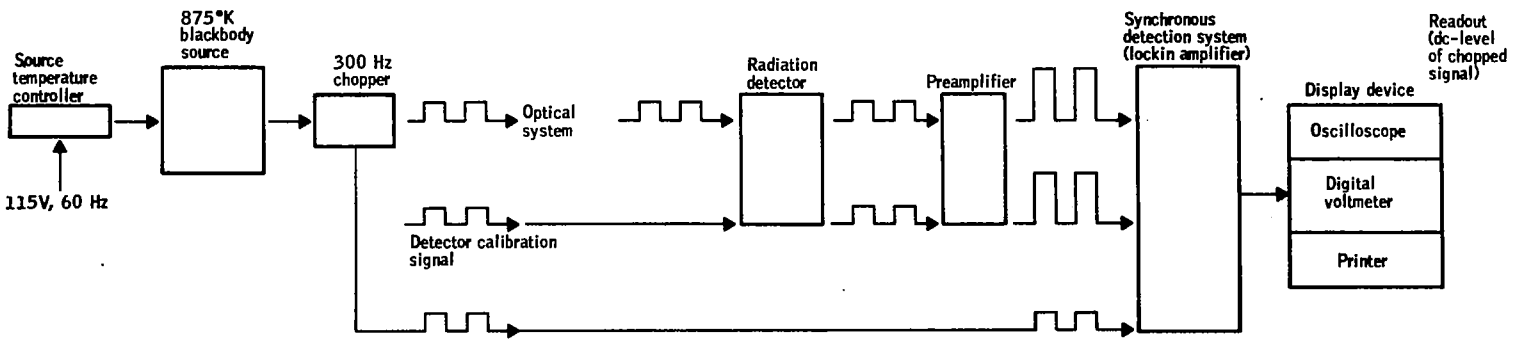

Figure 42. Reflectometer Signal Processing Diagram

Test procedure. - To prepare the system for a reflectance measurement, a visible light source with 0.254-cm diameter aperture was installed in place of the detector and a white screen was placed behind the reflectometer source aperture. With the reflectometer source in position B of Figure 5, the reflectometer optics was aligned to give the best image of the detector centered at the source aperture. The source was then rotated to position A, and the collimator was adjusted to give the best image of the detector centered at the source. Observations were made to ensure that the beam to the collimator was not vignetted. The white paper screen and detector light source were removed, the chamber was sealed and initially rough pumped down to about 20 microns pressure. The reflectometer source controller power was then applied, and about 2 hours was allowed for it to reach its stabilized temperature of $875^{\circ}K \pm 0.07^{\circ}$. Liquid nitrogen flow to the reflectometer chopper baffles and cold trap was started and as soon as the chopper baffle temperature reached $200^{\circ}K$, as measured by an attached copper constantan thermocouple, the chopper motor was started. Since the chopper motor was heat sinked to the chopper baffles, starting it at this point allowed the shortest stabilization time of motor, baffle, and cold trap temperature as measured by attached thermocouples. The baffle, motor, and cold trap temperatures stabilized in about 30 minutes. The electronics were also turned on and allowed to stabilize for about 1 hour. The detector dewar was filled with liquid nitrogen, the bias current was applied to the detector and detector output was monitored with the source in position B until the signal level stabilized, usually in about 15 minutes. Once the signal had stabilized, the source was rotated to position A, and the signal was peaked in this position by slightly changing the collimator position. Because of nonlinearities in the detector window the detector adjustment screws were not moved once the reflectometer optics was aligned visually in position B. Tilting of the detector by using the adjustment screws would give an erroneous signal peak in position B because of transmission through different areas of the dewar window.

Signal-level readings for reflectance measurements were taken as follows: with the source in position A the digital printer was turned on and allowed to print for 1 minute, printing 1 data point every time the voltage output changed enough to register a new value on the digital voltometer. The last digit on the voltometer read out millivolts with full-scale output of the lock-in amplifier scaled to 10 volts. The source was then rotated to position B with 30 seconds allowed for stabilization before beginning the one-minute data run for position B. This procedure was repeated 10 times to obtain 10 full sets of reflectance data. The detector dewar was refilled between data sets taking care not to disturb the reading by thermal transients from the refilling process. A reflectance value ρ_c was obtained by taking the average of each 1 minute of data for position A, V_a, and dividing it by the average for position B, V_b, i.e., $\rho_c = \frac{V_a}{V_b}$. The 10 values of reflectance were then averaged to obtain an average value of reflectance for the 30 minutes of data taken.

System stability tests. - Prior to making actual reflectance measurements, several tests were run to determine system stability and signal-to-noise ratio. The results are as follows:

To ensure that the electronic system was detector-noise limited, the electronics were warmed up and a 21-ohm resistor substituted for the detector. With bias current on and the lock-in amplifier in noise mode with 0.33-Hz bandwidth, the noise reading was less than 0.5 nv. With a detector in the system noise values of 5.0 to 10.0 nv were typical. Thus it was verified that the readout system was detector-noise limited.

To check the system for thermal stability, the reflectometer was placed in its normal operating mode in position B, and the source temperature was monitored with the iron-constantan thermocouple installed at the tip of the source cavity and a thermocouple potentiometer. Source stability was ±0.07°K at its 875°K setpoint. Other temperatures recorded during this test by installed copper-constantan thermocouples were: motor bearing temperature 311°K, chopper baffle temperature less than 144°K, source aperture plate 342°K, motor baffle 274°K, and source outer can 471°K. To determine the effect of these temperatures on detector output, the liquid-nitrogen cooling to the baffles and cold trap was turned off for about 10 minutes, producing greater than a 10°K rise at the chopper baffle with no change observed in detector output. Typical system output stability for both positions A and B was ±0.05 percent for the 1 minute readings with long-term drift for 30 minutes less than ±0.16 percent. Signal-to-noise values from 133,000:1 to 320,000:1 were obtained with the 0.33-Hz bandwidth utilized.

Room temperature measurement. - To gain confidence that the absolute accurace of the reflectometer is within 0.1 percent, a reflectance measurement was made with the reflectometer source and the collimator mirror at the same temperature, i.e., 295°K. The measured reflectance (V_a/V_b) should theoretically be 100 percent because the radiance from position A will be equal to $N_{(source)} \times \rho\,(mirror) + \epsilon\,(mirror)$, which will be the same as $N_{(source)}$ in position B if the source and mirror are at the same temperature. The measured value for this test was $V_a/V_b = 100.02$ percent. For this measurement, the chopper baffle and cold trap were cooled down to provide a low background reference level. The S/N of the measurement was 3,500:1, adequate to provide reasonable precision in the measurement.

Collimator blur circle measurement. - A measurement was made of the collimator blur circle with an incandescent light source, 1.27 cm in diameter, at position A by observing the source image at position B. The best image condition was at the ray-trace-analysis-calculated focal length, with an image size of $\approx$1.9 cm, which checks with the calculated value (1.27 cm + 0.6162 cm, Table 2).

Source scan. - The reflectometer source was scanned across the detector by rotating the collimator in elevation through the field of view of

the system. The results of the scan are shown in Figure 43. As shown, the energy level is down approximately 50 percent over the extremities of the source aperture diameter of 1.27 cm. As can be seen, the signal is very uniform over a total displacement of 0.26 cm. The predicted total diameter over which a uniform source image can be expected at the detector is determined as follows:

Blur circle diameter from ray trace analysis, Table 2	0.917 cm
Image quality of collimator	0.013
Image quality of auxiliary parabola (est.)	0.036
Detector diameter	0.050
Total	1.016 cm

The diameter of constant uniformity = 1.27 - 1.01 = 0.26 cm. This means that the detector image must be located within ±0.13 cm of the center source area to be receiving the total true source radiance. All reflectance measurements were made with this in mind, and care was exercised to ensure that the system was peaked out in position A to locate the detector within the area of constant uniformity of the source image.

Reflectance test results. - An initial room temperature reflectance measurement was made of the PCS collimator in a vacuum environment. The average value for reflectance for 17 sets of data was 0.9862 $\frac{+0.04}{-0.03}$ percent. An attempt was then made to cool down all PCS elements, including the mirror to cold operational temperatures; however, the test was suspended after 5 hours cooling due to LN_2 leaks in several cooling lines. The elements were then warmed up overnight and a reflectance reading taken the following day. Since the mirror and plate were still changing temperature, a stable reading of reflectance over a 30-minute period could not be obtained because the signal would not remain peaked in position A. A definite decrease in signal strength in position A was observed. The signal in position A was then peaked again, and 4 sets of data were taken with values from 0.9862 to 0.9865.

The chamber was then opened on both ends, the leaks in the cryogenic system were repaired, the optics were realigned and the chamber sealed and pumped down again. Another set of reflectance data was taken with a measured average reflectance of 0.9856 $\frac{+0.01}{-0.03}$ percent for 10 sets of data.

The PCS elements were next cooled down over a 26-hour continuous period. The mirror reflectance was then measured with the mirror temperature at 85°K with a measured reflectance of 0.9880 $\frac{+0.02}{-0.05}$ percent. The reflectance

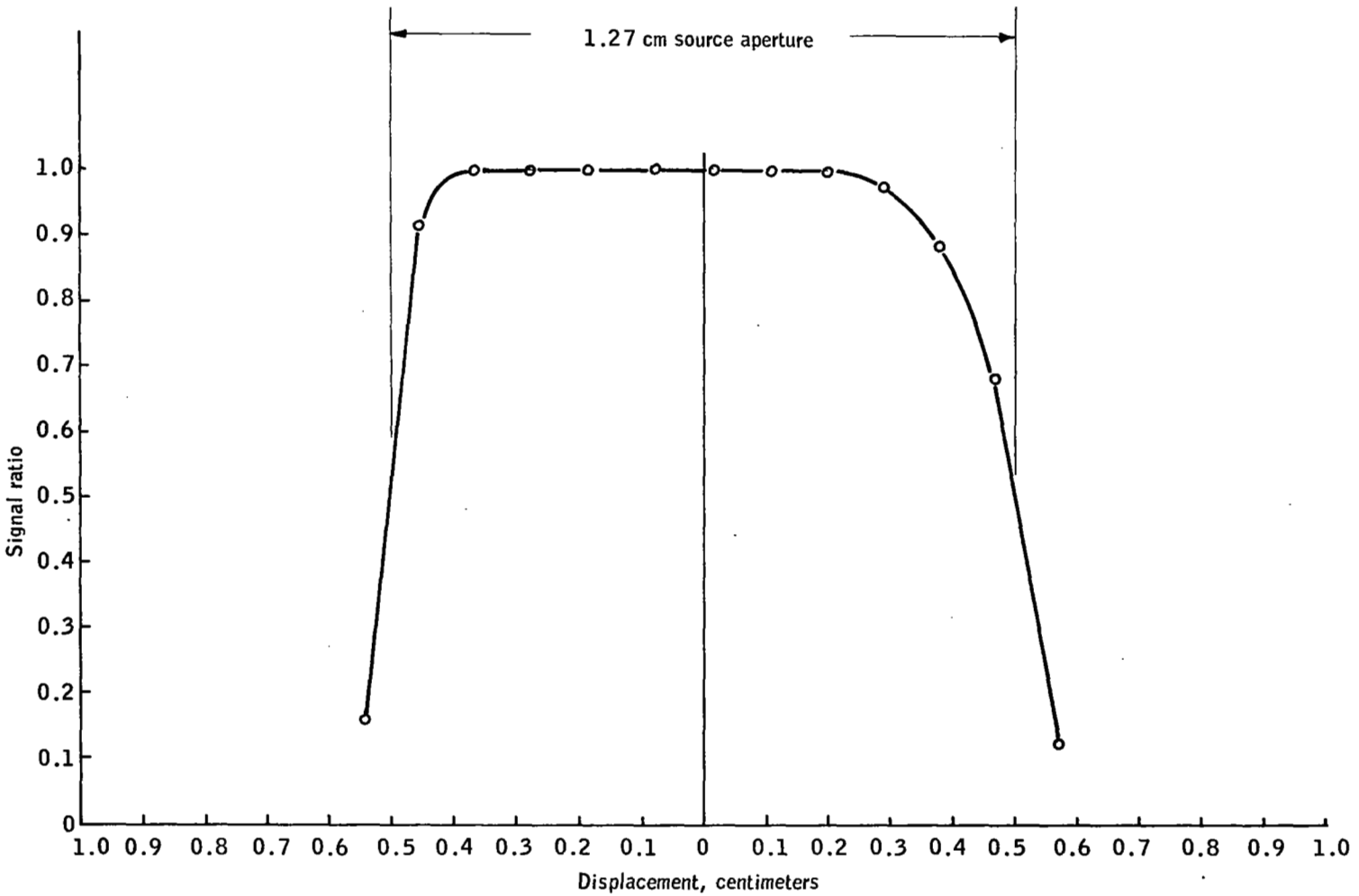

Figure 43. Reflectometer Source Scan

increased from room temperature by 0.24 percent which compares favorably with data obtained by Padalka and Shklyarevskii (Reference 5), who report a reflectance increase of 0.25 percent from 295°K to 82°K.

The system was then allowed to warm back to room ambient temperature conditions (295°K). The reflectance was again measured and found to be $0.9845 \frac{+ 0.02}{- 0.03}$ percent. Visual inspection of the mirror after testing revealed some additional contaminant on the mirror, which was deposited primarily near the mirror center.

The mirror was warmed by forcing 100°C air through the cryogenic plumbing to the mirror; however, due to a shortage of liquid nitrogen in the bulk tank the chamber was backfilled with dry nitrogen after 30 hours of warming. After the conclusion of the above test the chambers were again closed and evacuated to 5 to 10 microns. The mirror plate was warmed for about 16 hours, and the chambers were kept under room temperature vacuum for about 48 hours. Inspection of the mirror after opening the chambers showed that almost all traces of mirror contamination had disappeared. The above described series of tests and the pattern of the deposit on the mirror appear to correlate with the changing value of room temperature reflectance. It also points out that extreme care and patience is required when warming the mirror after cooling it to below room temperature.

Subsequent to the above tests and a series of radiance tests, the reflectometer was again installed, and a collimator room ambient temperature reflectance measurement was performed. The measured reflectance was $0.9806 \frac{+0.007}{-0.005}$. The net decrease in reflectance from previous measurements is indicative of surface degradation of the collimator with time, an important factor in the overall PCS operation. This indicates the necessity of performing the reflectance measurement periodically to determine precisely the collimator reflectance characteristics for inclusion in the PCS output radiance parameter definition.

Radiance Measurements

Test setup. - The test radiometer electronic equipment was set up as shown schematically in Figure 44. The Hg-Cd-Te detector with a measured D* of 3.18×10^9 (500, 1000, 1) cm $Hz^{1/2}$/watt was used, the same as for the reflectometer. Readout electronics included a lock-in amplifier with a frequency programmer and preamplifier. The detector was coupled to the low-impedance input of the preamplifier with a 4.7-μfd coupling capacitor and bias supply. The lock-in amplifier received its synch signal from a magnetic pick-off attached to the PCS chopper driven at 66 Hz by a chopper motor through a bellows feedthrough drive. The amplifier internal filter was set for a 1.0-Hz bandwidth. The amplifier output was monitored and recorded with a DVM-printer combination.

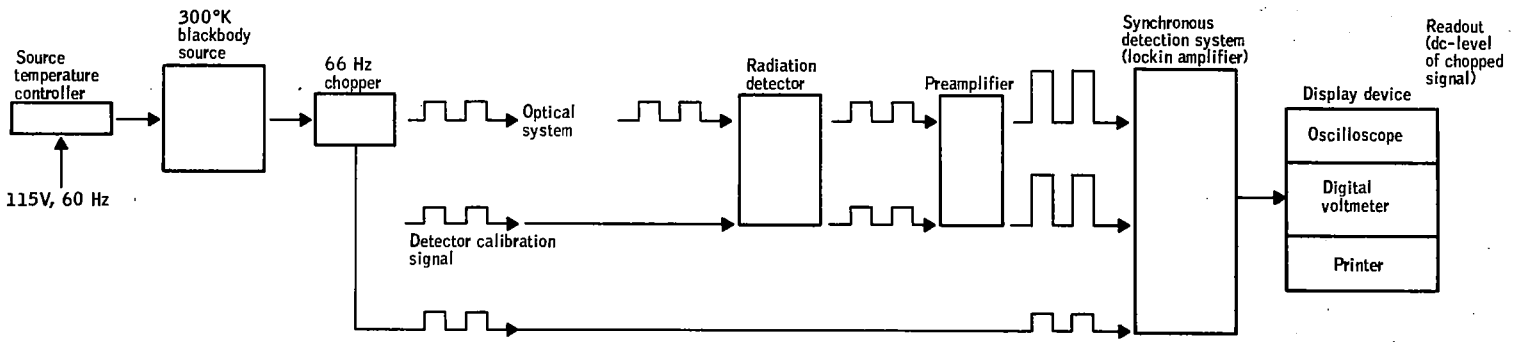

Figure 44. Test Radiometer Signal Processing Diagram

Test procedure. - To prepare the system for radiance measurements, the visible light source on the PCS aperture plate was rotated up and centered within the chopper and baffle apertures. The light was then autocollimated with a flat mirror and the PCS collimator back to the aperture plate, and the source assembly was moved longitudinally to obtain the circle of least confusion, thus positioning the aperture plate at the mirror focal point. The collimator was then finely adjusted in elevation and azimuth to center the output beam within the 76-cm-diameter radiometer chamber. The radiometer was then installed and the optics positioned to image the light source at the detector position. A dummy detector with a series of concentric rings on a frosted screen was used for ease of viewing. Adjustments were made to the radiometer mount to reduce the runout and misalignment of the assembly while translating the scanning mirror and observing the source-image movement. The effects on the source-image movement were also observed when changing the radiometer from the translation to goniometric scanning mode. Fine adjustments were made to the radiometer mechanism to reduce transient effects due to minor misalignments.

After the radiometer positioning adjustments were completed, the Hg-Cd-Te detector was installed, the 1.0-cm-diameter aperture was centered in front of the PCS source, the chambers were sealed, and the system was evacuated to approximately 10 microns pressure. All PCS baffles and shrouds were cooled down with liquid nitrogen, except for the collimator, which was operated at room ambient temperature because of the lengthy times required to cool it down. The source and guard temperatures were controlled at 320°K. After the source and baffle temperatures were stabilized, the chopper was turned on and the detector output was peaked by carefully adjusting its position in the source beam image.

Visual alignment. - Visual alignment of the system was measured with the translation mechanism moved through its entire traverse. The radiometer was initially aligned in the vertical position. The radiometer chamber was then rotated approximately 40 degrees, and the alignment was rechecked. Some sag was noted in this position; this was corrected by readjusting the radiometer mount attachments. The shift after readjustment was limited to ≈ 0.025 cm through the translation scan. The same results were obtained by rotating the chamber in the opposite direction from vertical.

System stability tests. - With the source, guard, and all baffle temperatures stabilized, signal stability and noise tests were performed. The signal-to-noise level was measured to be $\approx$20,000:1 with the PCS source temperature at 320°K. The system was verified to be detector-noise limited. Long-term signal stability was excellent, provided that several seconds were allowed after refilling the detector dewar.

Fine goniometric scan. - The source image was fine-scanned goniometrically in the vertical axis by the scanning mirror tilt mechanism, with the results as shown in Figure 45. The results shown in Figure 45 indicate the source image radiance to be down ≈ 1.0 percent over a 0.615 cm diameter. The response was flat over 0.523 cm. The predicted area of source image uniformity can be determined by adding the known contributions of nonuniformity, as follows:

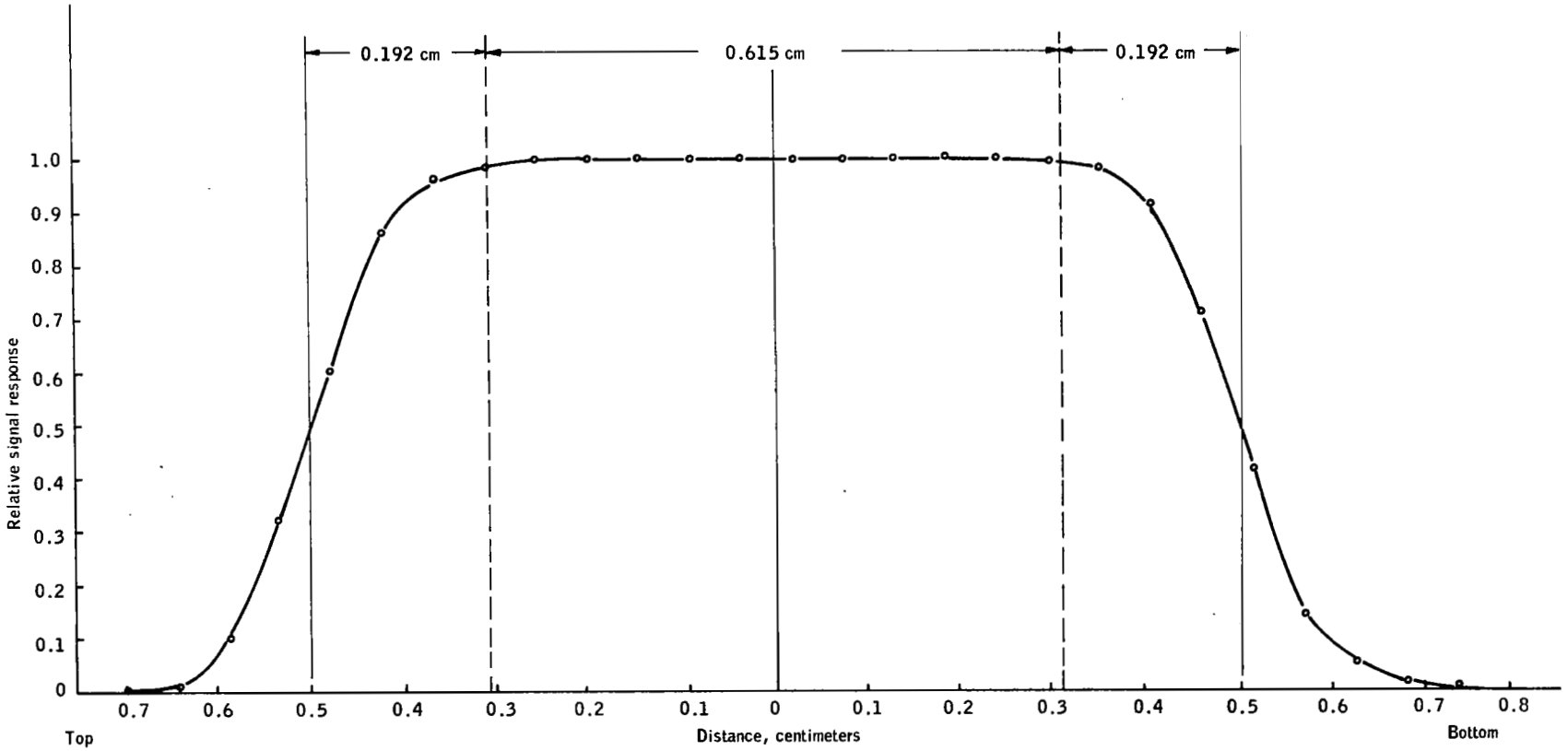

Figure 45. PCS Source Goniometric Scan with Test Radiometer

Radiometer mirror blur circle (translated to the source) = 0.038 cm x 3.2	= 0.120 cm
Detector diameter (translated to the source) = 0.05 x 1.4 x 3.2	= 0.225 cm
Collimator blur circle	= 0.013 cm
Diffraction (first order at 15μ) = 2.44 λ/d = 2.88×10^{-4} radians	= 0.027 cm
Total	0.385 cm

Source diameter = 1.0 cm. The predicted diameter of constant uniformity of the source image = 1.000 cm - 0.385 = 0.615 cm.

Coarse goniometric scan. - The coarse goniometric scan was performed in the vertical axis to determine off-axis rejection of the chamber radiation over a ±20-degree angle. The off/on axis signal level ratio over the entire scan was measured to be $\leq 7 \times 10^{-5}$ over the entire scan outside the source image location.

Translation scan. - A translational scan of the collimated output beam was performed in the vertical axis with the scanning mirror mechanism. Data points were taken at 5 cm intervals, with the results as shown in Figure 46. As can be seen, the beam image is uniform to within ±0.1 percent over 51 cm. The falloff in signal near the bottom edge of the collimator is probably due to chopper baffling obstructions near the bottom of the source beam. This will be corrected during the final reassembly of the system.

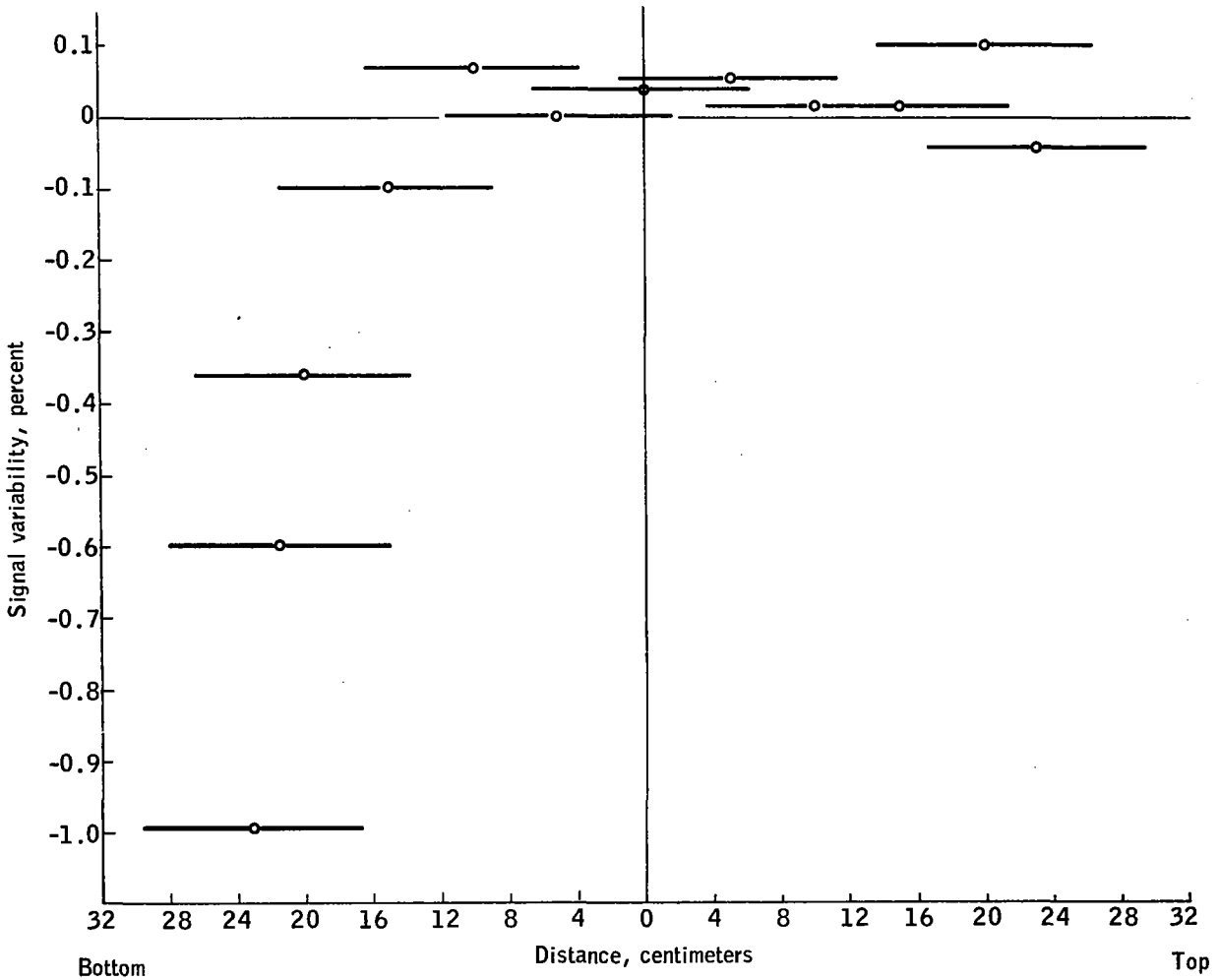

Figure 46. Radiometer Translation Scan

CONCLUSIONS

A Primary Calibration System has been developed, constructed, and evaluated to establish a capability to provide an adjustable temperature, extended-radiance source for testing infrared radiometer characteristics. A reflectometer for measuring the in situ collimator reflectance and a test radiometer to measure the output beam characteristics were also constructed as part of the operational system.

The system was developed and constructed, and functional tests were performed to experimentally verify the system operational characteristics, including vacuum pumping and monitoring, liquid-nitrogen flow control and monitoring, source temperature control and monitoring, and effects of thermal shock. External adjustments of the source, mirrors, and variable aperture were evaluated.

The source thermal control capability from 100°K to 300°K was verified, with a stability of 0.02°K and thermal gradients through it of less than 0.03°K. Shroud and mirror cooldown rates and stabilization times were determined to establish a 12-hour time period to attain an operational condition for all cooled elements within the system.

Measurements of the PCS collimator reflectance were made to accuracies within 0.1 percent over extremes of 295°K to 85°K collimator temperatures. The collimator reflectance at 295°K was measured to be between 0.9845 and 0.9865 to within an accuracy of 0.1 percent, depending on the mirror cleanliness condition. The mirror reflectance increased by 0.25 percent at 85°K.

The PCS output beam characteristics were measured, both goniometrically to determine source aperture angular beam characteristics and for uniformity across the collimated beam diameter. The goniometric scan indicated a uniform Lambertian characteristic over 0.523 cm and a beam uniformity to within ±0.1 percent over a 51 cm beam diameter. The experimental results verify the performance characteristics of the system and its capability of providing an order of magnitude improvement over previous methods of infrared radiometer calibration.

APPENDIX A
ABSORPTION ANALYSIS

The total path length in the configuration for the PCS-Reflectometer combination is 16.25 meters. This includes a 12.2-meter path length for the PCS collimator and a 4.05-meter path length for the source-auxiliary parabola-detector combination.

The atmospheric transmission effects can be determined by use of infrared transmission curves (Reference 6). The atmospheric absorption constituents in the wavelength region of interest (1 to 24 microns) are seen to be water vapor, carbon dioxide, and ozone. The contributions of absorption due to each was calculated as follows:

$\underline{H_2O}$ — Assumed 20°C, 50 percent relative humidity which gives 0.085 cm precipital water vapor/100 m or 0.14 cm H_2O /16.25 m. This value was extrapolated from curves of Reference 6.

$\underline{CO_2}$ — Interpolated 0.016-km path length from curves of Reference 6.

$\underline{O_3}$ — Extrapolated 0.008-mm ozone /16.25 m from curves of Reference 6.

The transmission factors due to each of the atmospheric constituents were determined for 1-micron wavelength intervals from 1 to 24 microns. The results are shown in Table A-1.

The effect of the atmospheric absorption on the blackbody radiance used in the reflectometer is next determined. The blackbody source operates at $\approx$ 900°K, which provides a total radiance, N, of 1.15 w/cm^2--sr. Table A-2 shows the incremental radiance over 1-micron intervals from 1 to 24, which includes $\approx$ 98 percent of the total blackbody radiance at 900°K. Also listed is the net radiance due to the effect of the atmospheric absorption constituents over the 16.25-meter path length.

The effect of the atmospheric absorption constituents at STP is significant; the percent transmission over 1 to 24 microns = $\frac{0.8411}{1.126} \times 100 = 75$ percent transmission, or 25 percent of the radiance is absorbed.

TABLE A-1. - ATMOSPHERIC TRANSMISSION, 16.3-METER PATH LENGTH

Wavelength, μ	H_2O	CO_2	O_3	Atm.
1.0 - 2.0	.925	1.00	1.00	.925
2.1 - 3.0	.643	.988	1.00	.635
3.1 - 4.0	.966	1.00	1.00	.966
4.1 - 5.0	.953	.895	.996	.849
5.1 - 6.0	.45	1.00	1.00	.450
6.1 - 7.0	.289	1.00	1.00	.289
7.1 - 8.0	.773	1.00	1.00	.773
8 - 9	.97	1.00	1.00	.970
9 - 10	.971	.996	.966	.934
10 - 11	.975	.998	1.00	.973
11 - 12	.975	1.00	1.00	.975
12 - 13	.971	.985	.998	.955
13 - 14	.965	.795	.994	.763
14 - 15	.955	.20	.997	.190
15 - 16	.935	.51	.999	.476
16 - 17	.909	.93	1.00	.846
17 - 18	.885	.994		.880
18 - 19	.85	1.00		.85
19 - 20	.81			.81
20 - 21	.765			.765
21 - 22	.715			.715
22 - 23	.665			.665
23 - 24	.61			.61

TABLE A-2. - BLACKBODY RADIANCE OUTPUT

$\Delta\lambda$ (μ)	N_{bb} (w/cm^2-sr)	16.25-m path length N Atm, (w/cm^2-sr) STP
1 - 2	.045	.042
2 - 3	.189	.120
3 - 4	.229	.220
4 - 5	.180	.153
5 - 6	.132	.060
6 - 7	.092	.027
7 - 8	.069	.053
8 - 9	.046	.045
9 - 10	.034	.032
10 - 11	.025	.024
11 - 12	.020	.019
12 - 13	.015	.014
13 - 14	.012	.0085
14 - 15	.008	.0015
15 - 16	.0069	.0033
16 - 17	.0058	.0049
17 - 18	.0046	.0041
18 - 19	.0035	.0030
19 - 20	.003	.0024
20 - 21	.0023	.0018
22 - 23	.002	.0014
23 - 24	.0018	.0012
Totals	1.126	.8411

In the wavelength region of 13 to 17 microns the effect is more significant:

λ	N_{bb}	N Atm
13 - 14	.012	.0085
14 - 15	.008	.0005
15 - 16	.0069	.0033
16 - 17	.0058	.0049
	.0337	.0182

$$\frac{.0182}{.0337} \times 100 = 54 \text{ percent transmission, } 46 \text{ percent absorption}$$

This clearly shows the necessity of operating the system in a vacuum to minimize atmospheric absorption effects.

The plans for operating the PCS reflectometer in combination are to evacuate the system with a vacuum roughing pump down to ≈ 75 microns. This amounts to approximately four orders of magnitude below atmospheric pressure.

$$1 \text{ Atm} - 760 \text{ torr} - 76 \times 10^4 \, \mu$$

$$\frac{75 \, \mu}{76 \times 10^4 \, \mu} \cong 10^{-4}$$

The following relationship exists between absorption and pressure

$$\frac{A1}{A2} \cong \left(\frac{P1}{P2}\right)^{3/2}$$

or, with a fourth order of magnitude reduction in pressure we will get a sixth order of magnitude reduction in absorption. Absorption will then be 0.46×10^{-6}, completely negligible.

APPENDIX B

REFLECTOMETER SIGNAL-TO-NOISE RATIO

The reflectometer design evolved to a configuration which utilizes a Hg-Cd-Te detector and a cooled chopper blade and field-of-view trap. The radiance seen by the detector with the chopper closed is then negligible compared to source radiance. The signal on the detector is

$$P_d = \frac{N_s A_d A_{ap} k}{F^2} = \frac{\pi N_s A_d k}{4F^2}$$

$$= \frac{\pi \times .016 \times .25 \times 10^{-2} \times .55}{4\,(11)^2} = 1.4 \times 10^{-7} \text{ w}$$

where N_s = source radiance = .016 w/cm^2-sr (600°C, 14-16 μ)

A_d = detector area = $(.05)^2$ cm^2

F = system F-number = F/11

k = optics efficiency = .55; .6 for filter, $(.98)^4$ for four reflectances

The filter bandpass curve is shown in Figure B1.

The detection D* for a chopping frequency above 200 Hz is 3×10^9, leading to an NEP of

$$NEP = \frac{\sqrt{A_d}\ \sqrt{f_n}}{D^*} = \frac{0.05 \times .58}{3 \times 10^9} = 9.7 \times 10^{-12} \text{ w}$$

for the reflectometer electronics noise bandwidth of 0.33 Hz.

The system signal-to-noise ratio, at the detector, is then

$$S/N = \frac{P_d}{NEP} = \frac{1.4 \times 10^{-7}}{9.7 \times 10^{-12}} = 14{,}500$$

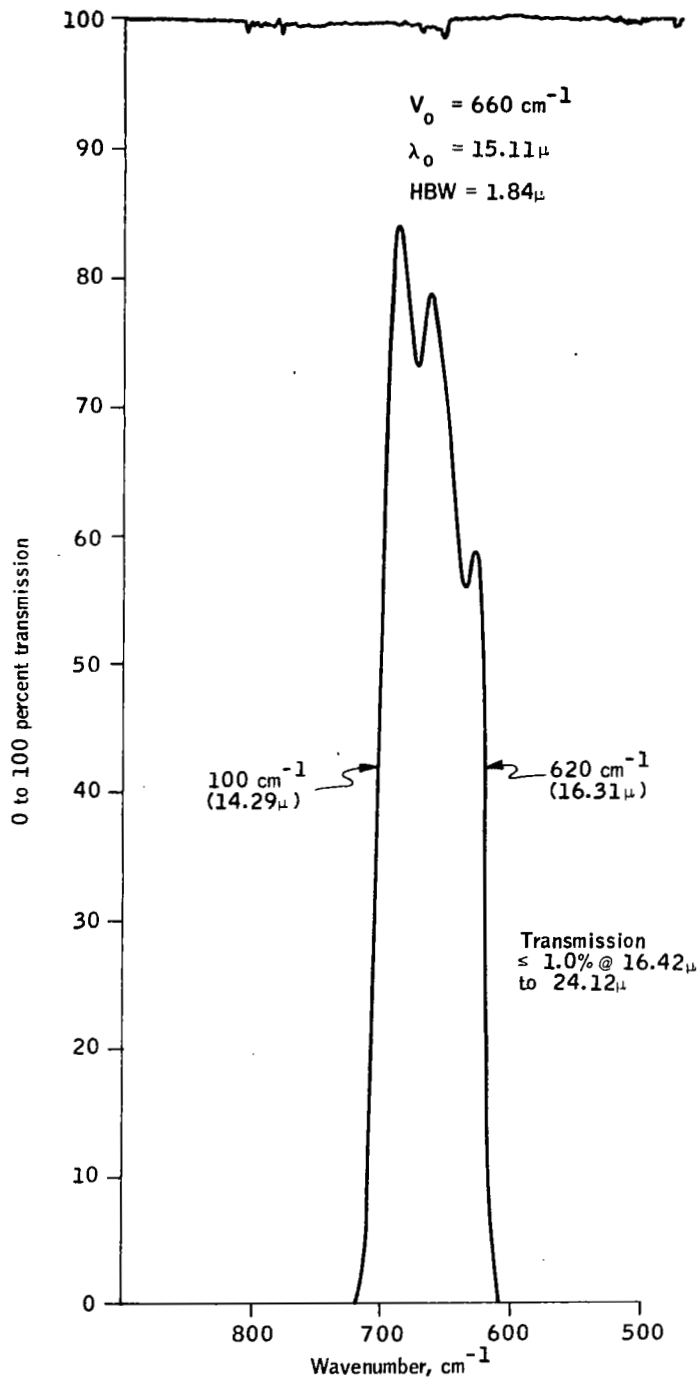

Figure B-1. Filter Bandpass Characteristics

APPENDIX C

CHOPPER LOCATION

The initial reflectometer configuration (i. e., baseline) had the chopper located outside the chamber directly in front of the detector-filter assembly. In this location, nearly all radiance incident on the detector, including both background radiance and blackbody source radiance, is modulated at the signal frequency. Any variations in the background temperature will thus show up in the signal as an indeterminate error. The detector output signal consists of a d-c signal produced by flux reaching the detector from sources between the detector and chopper plus an a-c signal proportional to the difference in flux seen by the detector with the chopper closed and with the chopper open. Since the detector is a-c coupled to the signal processing electronics, only the a-c portion of the detector signal is processed, assuming that the d-c background does not modulate itself at the signal frequency. Thus the signal of interest is proportional to the difference in that produced by the chopper and that produced by the combined background and blackbody source. For the source in position B of Figure C-1

$$e_{o_B} \propto P_b + P_s - P_c$$

where

P_b = flux on detector from the background with the chopper open

P_s = flux from the blackbody source, source in position B

P_c = flux on detector from the chopper, self emitted and reflected

The above neglects radiation interchange between the detector and chopper and between the detector and background; however, for a Hg-Cd-Te detector operating at $\approx 80^{\circ}K$, the radiation is essentially unidirectional toward the detector.

For the source in position A of Figure C-1, we assume that the background and chopper signals do not change (this assumption is later modified in considering background stability) so that only the signal from the source changes and only by the reflectance, ρ, of the PCS collimator; then

$$e_{o_A} \propto P_b + P_s - P_c$$

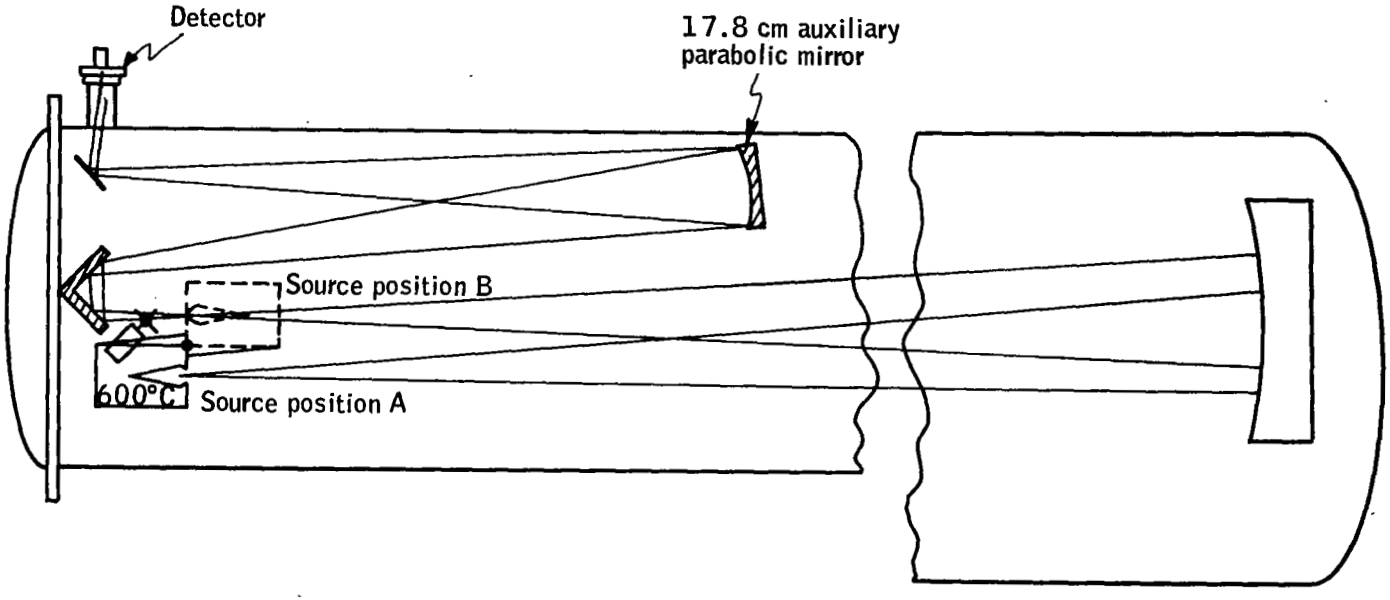

Figure C-1. PCS Reflectometer

The ratio of the two signals gives

$$\frac{e_{o_A}}{e_{o_B}} = \frac{P_b + \rho P_s - P_c}{P_b + P_s - P_c}$$

Note that the ratio does not give reflectance directly because of the additive terms from the background and chopper. Reflectance is given by

$$\rho = \left(\frac{e_{o_A}}{e_{o_B}}\right)\left(\frac{1 + P_b - P_c}{P_s}\right) - \left(\frac{P_b - P_c}{P_s}\right)$$

For high accuracy, the term $\frac{P_b - P_c}{P_s}$ must either be sufficiently small to

be negligible or must be known with a sufficiently small uncertainty.

If the term is sufficiently small, then the reflectance is calculated simply by taking the ratio of the two output signals

$$\rho_c = \frac{e_{o_A}}{e_{o_B}}$$

and the error is given by $\Delta\rho = \rho_c - \rho = \dfrac{(1-\rho)\dfrac{Pb - P_c}{P_s}}{1 + \dfrac{P_b - P_c}{P_s}}$

To achieve $\Delta\rho < 0.001$, we must have

$$(1 - \rho)\frac{P_b - P_c}{P_s} < 0.001\left(1 + \frac{P_b - P_{cc}}{P_s}\right)$$

The measured value of ρ is expected to be ≈ 0.985; then the above reduces to

$$\frac{P_b - P_c}{P_s} < 0.0715$$

Thus the difference between background signal and chopper signal must be less than about 7 percent of the blackbody source signal. Background and chopper signal are controlled by proper selection of temperatures, emissivities, fields of view, etc. The governing expressions for these signals are

$$P_b = \epsilon_b N_b \Omega_b A_d k_f$$

$$P_s = \frac{\pi N_s A_d k_o k_f}{4F^2}$$

$$P_c = \bar{N}_c \Omega_c A_d k_f$$

where

ϵ_b = emissivity of background

N_b = blackbody radiance of background temperature

Ω_b = background solid angle seen by detector

A_d = detector area

k_f = filter transmission

N_s = blackbody source radiance

k_o = optics efficiency, = 0.95

F = optics F-number = F/11

$\bar{N}_c$ = chopper radiance; self emitted and reflected

Ω_c = solid angle subtended by chopper

The governing inequality then becomes

$$\frac{P_b - P_c}{P_s} = \frac{\epsilon_b N_b \Omega_b - \bar{N}_c \Omega_c}{\pi N_s k_o / 4F^2} < 0.07$$

With the chopper in front of the detector, with the detector viewing a hemispherical background at ambient temperature, and with either a blackbody chopper or a reflective chopper, and a black, ambient temperature trap, the terms Ω_b and Ω_c are each the solid angle subtended by a diffuse hemisphere, or $\Omega_b = \Omega_c = \pi$. The term $\epsilon_b \approx 1.0$ since the detector is essentially viewing a cavity. Then

$$\frac{P_b - P_c}{P_s} \cong 500 \frac{N_b - \bar{N}_c}{N_s}$$

which leads to the requirement that

$$N_b - \bar{N}_c < \frac{0.07\ N_s}{500} = 1.4 \times 10^{-4} N_s$$

In the 14 to 16 micron region, source blackbody radiance (600°C) is ≈ 0.16 w/cm^2-sr. Thus the difference between background radiance and chopper radiance must be

$$N_b - \bar{N}_c < 1.4 \times 10^{-4} \times 1.6 \times 10^{-2} = 2.2 \times 10^{-6} \text{ w/cm}^2\text{-sr}$$

Assuming that both background and chopper are at approximately the same temperature the maximum allowable temperature difference can be computed from

$$\Delta T = \Delta N \div \frac{\partial N}{\partial T}$$

For 300°K chopper and background, the term $\partial N / \partial T$ is 1.4×10^{-5} w/cm^2-sr/deg for the 14 to 16 micron region. Then we must have

$$\Delta T < \frac{2.2 \times 10^{-6}}{1.5 \times 10^{-5}} = 0.16^{\circ}\text{K}$$

Thus satisfactory accuracy is achieved with a chopper-to-background temperature difference as large as 0.16°K. Temperature control of the chopper blade would be required to reduce conductive heating of the blade caused by chopper-motor-generated heat.

A more serious problem exists in the stability of the chopped background.

If the background changes as the source is alternately moved between positions A and B, then the ratio of output signal must be written as

$$\frac{e_{o_A}}{e_{o_B}} = \frac{\rho P_s + (P_b - P_{c_A})}{P_s + (P_b - P_{c_B})} = \frac{\rho + \frac{(P_b - P_{c_A})}{P_s}}{1 + \frac{(P_b - P_{c_B})}{P_s}}$$

For convenience, denote the difference, $P_b - P_c$ as P, understanding it to be the chopped background. Also let

$$(P_b - P_c)_B = P$$

$$(P_b - P_c)_A = P + \Delta P$$

where ΔP is the difference in background signal with the source in position A relative to position B.

$$\frac{e_{o_A}}{e_{o_B}} = \frac{\rho + \frac{P + \Delta P}{P_s}}{1 + \frac{P}{P_s}} = P_c$$

As before, the error in reflectivity is given by

$$\Delta\rho = \rho_c - \rho = \frac{\frac{P}{P_s}(1 - \rho) + \frac{\Delta P}{P_s}}{1 + \frac{P_b}{P_s}} \qquad < .001$$

Assume that ρ nominally is .985 and that the term P/P_s has been driven to $\approx .05$ by proper design in order to make it negligible in the reflectivity calculation. Then

$$\Delta\rho = \frac{.05 \times .015 + \frac{\Delta P}{P_s}}{1.05} \qquad < .001$$

This requires that

$$\frac{\Delta P}{P_s} < .001 \times 1.05 - .00075 = .0003$$

or that the background be stable to within 0.03 percent of the source signal. To obtain the required background-temperature stability we again use the ratio

$$\frac{P_b - P_c}{P_s} = 500 \frac{N_b - N_c}{N_s}$$

Since $\Delta P/P_s$ is given by

$$\frac{\Delta P}{P_s} = \frac{(P_b - P_c)_A}{Ps} - \frac{(P_B - P_C)_B}{P_s}$$

it is also expressible by

$$\frac{\Delta P}{P_s} = 500 \left(\frac{N_b - \bar{N}_c}{N_s}\right)_A - 500 \left(\frac{N_b - \bar{N}_c}{N_s}\right)_B$$

Define ΔN to be the difference between the relative background to chopper radiances; then

$$\frac{\Delta P}{P_s} = 500 \frac{\Delta N}{N_s} < .0003$$

or,

$$\Delta N < 6 \times 10^{-7} N_s = 10^{-8} \text{ w/cm}^2\text{-sr}$$

Allowable temperature difference, ΔT, is calculated as before for $300^{\circ}K$ background and chopper:

$$\Delta T = \frac{\Delta N}{dN/dT} = \frac{\Delta N}{1.4 \times 10^{-5}} = \frac{10^{-8}}{1.4 \times 10^{-5}} \approx 0.0007^{\circ}K$$

This means that the temperature stability between background and source must be $0.0007^{\circ}K$ or better over the time reflectance measurements are made, an impractical requirement. Corrective measures include baffling the detector, cooling the chopper and background (including the reflectometer chamber) or relocating the chopper in the focussed beam.

With the same expressions used above, it can be shown that even by baffling the detector with a F/5 baffle so that background is modulated only in an F/5 cone, the required temperature stability would be $0.022^{\circ}K$ with the chopper and background both at $300^{\circ}K$. That type of temperature stability is representative of laboratory blockbodies and could not be achieved without precise, active, temperature control. An unattractive alternative, because of cost considerations,

is to cool both chopper and background, including the reflectometer chamber. Thus it was decided to relocate the chopper in the chamber, chopping the focussed beam in the vicinity of the blackbody source.

With the chopper in the focussed beam, only that part of the detector field of view which is focussed into the blackbody source is modulated. The background is then a d-c background and is rejected by the electronics, thus having no effect on the reflectance signal. The detector signal is then proportional to the difference between chopper radiance, both self-emitted and reflected, and blackbody source radiance. Two quantities must be determined, the maximum allowable chopper radiance and its required stability. The equations used above in the background computation still hold with background flux, P_b, set to zero and with the detector field of view at the chopper being the same as at the blackbody source. The following relationships hold:

- $$\frac{e_{o_A}}{e_{o_B}} = \frac{\rho N_s - \bar{N}_c}{N_s - \bar{N}_c} = \rho_c$$

- $$\Delta\rho = \rho - \rho_c = \frac{(1-\rho)\frac{\bar{N}_c}{N_s}}{1 - \frac{\bar{N}_c}{N_s}} < .001$$

- $$\frac{\bar{N}_c}{N_s} < .0625$$

- $$\bar{N}_c < .0625\, N_s$$

The chopper radiance, self emitted and reflected, must therefore be less than 6.25 percent of the source radiance to permit 0.1 percent accuracy in using the ratio to represent reflectance. Source radiance in the 14- to 16-micron region is .016 w/cm^2-sr; chopper radiance must then be less than .0625 x .016 = .001 w/cm^2-sr. The temperature which produces that blackbody radiance level in the 14- to 16-micron region is ≈275°K, considerably below ambient temperature. Thus if the black chopper were used, it would have to be cooled; or if a reflective chopper and field-of-view trap were used, the trap would have to be cooled. Recommended practice is to use a reflective chopper with a field-of-view trap; this technique is utilized in the reflectometer. Since a LN_2 supply is readily available, the trap is LN_2 cooled making its signal contribution truly negligible. Chopper radiance is then effectively its own self-emitted radiation plus the diffusely reflected radiance from the remainder of the chamber.

In Reference 4 it was shown that the polished chopper blades could be expected to have a specular reflectivity of 0.9, a diffuse reflectivity of 0.05 and an emissivity of 0.05. The contribution to chopper radiance from diffuse reflection is calculated as follows. The chopper blade is receiving 300°K hemispherical irradiance from the uncooled chamber. Irradiance at the chopper is

$$H_c = \pi N_{300} \text{ w/cm}^2$$

Reflected radiance, $\text{w/cm}^2\text{-sr}$, is

$$N_r = \frac{\rho_d H_c}{\pi} = \rho_d N_{300}$$

where ρ_d = diffuse reflectivity = 0.05

Chopper self emitted radiance for a 300°K chopper, is

$$N_c = \epsilon N_{300}$$

Effective chopper radiance is then

$$\bar{N}_c = \rho_d N_{300} + \epsilon N_{300} = 0.1 N_{300}$$

Blackbody radiance at 300°K is $\approx .0013$ $\text{w/cm}^2\text{-sr}$ (14-16μ) giving a chopper radiance of

$$\bar{N}_c = 0.1 \times .0013 = .00013 \text{ w/cm}^2\text{-sr}$$

sufficiently smaller than the allowable maximum of 0.001 $\text{w/cm}^2\text{-sr}$. Thus an uncooled reflective chopper with a cooled trap will meet accuracy requirements.

The required stability of chopper radiance must also be determined. If chopper radiance differs from source positions A to B by an amount ΔN_c we have

$$\frac{e_{o_A}}{e_{o_B}} = \frac{\rho N_s - (\bar{N}_c + \Delta N_c)}{N_s - \bar{N}_c}$$

from which reflectivity error is

$$\Delta\rho \quad \frac{\frac{\bar{N}_c}{N_s}(1-\rho) + \frac{N_c}{\bar{N}_c}}{1 - \frac{\bar{N}_c}{N_s}} < .001$$

reducing to

$$\frac{\Delta N_c}{\bar{N}_c} < .107$$

with

$\bar{N}_c = .00013$ (reflective chopper)

$N_s = .016$ (600° C BB)

$\rho = .985$

This means that chopper radiance, both reflected and self emitted, must not vary by more than ≈10 percent for source positions A and B. Note that if the chopper moves with the source, it will be reflecting irradiance from different parts of the reflectometer in positions A and B. In position A, irradiance on the chopper is produced by the PCS chamber, the PCS/reflectometer interface, and by that part of the reflectometer closest to the PCS chamber. In position B, irradiance is produced by the opposite end of the reflectometer and the corner reflectors. The accuracy criterion requires that the difference in radiance of these two differing "scenes" be less than ≈10 percent. Because of structure, baffles, and temperature differences, especially for a cold PCS chamber, it is not possible to guarantee that the differing "scenes" are the same to within 10 percent or even that they could be made the same to within 10 percent. Also note that the 10 percent value completely consumes the total reflectometer error allocation of ±.001; to allow for other error sources, the requirement on differing scenes should be limited to ≈±2 percent complicating the problem still further. Solutions are to cool the complete reflectometer so that the reflected background is essentially "frozen out" or to fix the chopper location in the chamber.

The latter approach was selected as being more economical. By fixing the chopper location, diffusely reflected radiance is constant (except for reflected source radiance shown later to be negligible), but the heat load on the chopper varies because of the varying relative source - chopper geometry for source positions A and B. The changing heat load will cause a variation in chopper temperature which may produce an intolerable chopper radiance variation. The criterion is for chopper radiance to be stable by better than 10 percent. Required temperature stability is given by

$$\Delta T = \frac{\Delta N_c / \bar{N}_c}{\frac{\partial (\Delta N / N_c)}{\partial T}}$$

For a 300°K chopper, radiance variation is 1 percent/°K; for 10 percent radiance stability, the allowable ΔT is

$$\Delta T = \frac{0.1}{0.01/^{o}K} = 10^{o}K$$

Chopper temperature must therefore be held constant to within $10^{o}K$. A thermal analysis was performed showing that a suitably baffled chopper located 5 cm from source position B will exhibit a temperature change of $\approx 1.5°K$ as the source moves from position A to B. This represents a marginally acceptable condition since the $10^{o}K$ consumes the total error budget and thermal analysis represents an approximate to actual condition. The result produced, $1.5^{o}K$, is sufficiently close to the limiting value of 10^{o} K to be considered marginal. Higher confidence in the chopper radiance stability is obtained by either moving the chopper further from source position B to reduce the changing heat load caused by the source or by cooling the chopper wheel, as in the PCS, to a temperature such that chopper temperature stability is no longer critical.

Moving the chopper away from the source is unattractive since the beam diameter increases with increasing source-to-chopper distance, causing the detector output waveform to degrade significantly from a desired square wave. Quantitative assessment of the resulting effect was not made, however, in a 0.1 percent measurement, good practice must be exercised wherever possible. This consideration led to the decision to locate the chopper close to source position B and to cool the chopper blade. The cooling method used resulted in a chopper blade temperature of $117^{o}K$ with the source in position B. A reflective chopper with an emissivity of 0.05 (a practical value for polished aluminum; reference 4) at 117°K will exhibit a 14- to 16 micron radiance of $.5 \times 10^{-6}$ w/cm^2-sr, acceptable since it is well below the allowable maximum of 10^{-3} w/cm^2-sr and also well below the allowable chopper variation of 10^{-4} w/cm^2-sr. With the source rotated to position A, removing the source heat load from the chopper will result in a lower chopper temperature and a smaller value of self-emitted radiance. Since the position B radiance is already less than the tolerable radiance variation by a factor of 20, any reduction in radiance in position A is negligible.

APPENDIX D
INTERNAL REFLECTIONS

Source radiance chopped at the signal frequency which reflects off surfaces in the reflectometer and reaches the detector can cause an error in measured reflectance. Steps taken in the reflectometer design to minimize internal reflections included the placing of black baffles in key areas such that the detector can only see black, diffuse, baffle surfaces and the auxiliary parabola. The baffles were painted with 3M Black Velvet paint which has an emissivity of 0.975, or, a diffuse reflectivity of 0.025.

Quantitative determination of the modulated stray radiation reaching the detector requires a laborious analysis of a multitude of rays traced through the baffle system from the detector to the source. In lieu of this, an upper bound can be easily determined which can demonstrate adequacy of the design.

Consider that baffles are placed such that all modulated rays from the source undergo a minimum of two diffuse reflections before reaching the source. Then the upper bound is determined by letting all modulated source radiance reach the detector after only two diffuse reflections. The magnitude of reflected radiance at each of the two diffusely reflecting surfaces must be determined. Flux incident on the first reflecting surfaces is given by

$$P_1 = \frac{N_s A_s A_{r_1}}{L_1^2}$$

where

N_s = source radiance

A_s = source area

A_{r_1} = reflecting surface area

L_1 = distance between source and reflecting area

Diffusely reflected radiance at the first reflecting surface is

$$N_{r_1} = \frac{\rho_b P_1}{\pi A_{r_1}} = \frac{\rho_b N_s A_s}{\pi L_1^2}$$

This radiance is incident on a second reflecting surface, A_{r_2}, located L_2 units from the first. Incident flux on A_{r_2} is

$$P_2 = \frac{N_{r_1} A_{r_1} A_{r_2}}{L_2^2}$$

Diffusely reflected radiance at the second surface is given by

$$N_{r_2} = \frac{\rho_b P_2}{\pi A_{r_2}} = \frac{\rho_b N_{r_1} A_{r_1}}{\pi L_2^2} = \left(\frac{\rho_b}{\pi}\right)^2 \frac{N_s A_s A_{r_1}}{L_1^2 L_2^2}$$

The detector is assumed to see the second reflecting surface directly, and the detector area, A_d, is L_3 units from A_{r_2}. Flux on the detector is

$$P_{d_r} = \frac{N_{r_2} A_{r_2} A_d}{L_3^2} = \left(\frac{\rho_b}{\pi}\right)^2 N_s A_s \left(\frac{A_{r_1}}{L_1^2}\right)\left(\frac{A_{r_2}}{L_3^2}\right) A_d \frac{1}{L_2^2}$$

The term A_{r_1}/L_2 is the solid angle into which modulated radiance is propagated. The chopper is baffled with a 1-inch aperture in the baffle to permit passage of the focussed beam, the blade and aperture being 2 inches from the source in position B. The 1-inch aperture 2 inches away defines the solid angle into which the modulated source radiance propagates.

Therefore

$$\frac{A_{r_1}}{L_1^2} = \frac{\pi}{4}\left(\frac{1^2}{2^2}\right) = \frac{\pi}{16}$$

The term A_{r_2}/L_3^2 in the solid-angle field of view of the detector into the reflectometer chamber. We assume the use of sufficient baffles near the detector to confine its field of view into the chamber into an F/5 cone. Thus

$$\frac{A_{r_2}}{L_3^2} = \frac{\pi}{4}\left(\frac{1}{5^2}\right) = \frac{\pi}{100}$$

Flux on the detector is then given by

$$P_{d_r} = \left(\frac{\rho_b}{\pi}\right)^2 N_s A_s A_d \times \frac{\pi}{16} \times \frac{\pi}{100} \times \frac{1}{L_2^2}$$

The only unknown in the above equation is the term L_2, the distance between the two reflective surfaces. Examination of the system configuration shows that diffuse surfaces are separated by distances ranging from a minimum of several inches up to a maximum of many feet. For this analysis, a conservative assumption will be made that the distance is constant at 10 cm. Then, with diffuse reflectivity, ρ_b, of 0.025, a source radiance of 0.16 w/cm^2-sr, detector area of 0.05 x 0.05 cm^2 and 0.5-inch source diameter, detector signal is

$$P_{d_r} = \frac{(0.025)^2}{\pi^2} \times 0.016 \times 1.22 \times 0.25 \times 10^{-2} \times \frac{\pi}{16} \times \frac{\pi}{100} \times \frac{1}{100}$$

$$= 1.25 \times 10^{-13} \text{ watts}$$

From Appendix B, the desired blackbody signal on the detector is 1.4×10^{-7} watt. The chopped background then produces a ratio of

$$\frac{P_{d_r}}{P_d} = \frac{1.25 \times 10^{-13}}{1.4 \times 10^{-7}} = 0.9 \times 10^{-6}$$

of desired signal, or, 0.00009 percent, a negligible amount.

When the source is rotated to position A, the chopper remains near position B and the only radiation that is chopped is the desired focussed beam plus radiation diffusely reflected from the PCS and reflectometer walls which passes through the aperture of the chopper baffle. This reflected radiation will be smaller in magnitude than that calculated above.

Thus both the magnitude of the chopped internal reflections and the variation in magnitude between source positions A and B will be negligible.

APPENDIX E
PCS BEAM CHARACTERISTICS

One of the ARRS PCS specifications is that the output beam be uniform or calibrated over its clear aperture to within ± 0.1 percent. The analysis below shows that the beam will not be uniform to within ± 0.1 percent but that the vertical flux density distribution varies by ≈ 6 percent from bottom to top of the aperture, due only to the contribution of standard geometric optics. It is also shown that the signal on the detector of an imaging system (e.g., a radiometer) placed in the PCS beam is independent of beam position, in spite of the beam nonuniformity, for the case where the imaging system detector is smaller than the image of the projected PCS source, which is the intended modus operandi for calibrating a radiometer. If the detector is larger than the source image, then the beam flux density variation will be sensed.

Relative to the ARRS PCS, output beam interface characteristics can only be stated in conjunction with the intended use of the PCS. Nonuniformities from geometric optics considerations disappear under the proper conditions but not under others.

Governing equations are summarized below:

Flux density distribution: $H(y) \cong N_s A_s \left(1 - \frac{y^2}{p^2}\right)$

Signal on detector:

Small detector large source: $P_d = N_s \frac{A_d A_c}{f_i^2}$

Large detector small source: $P_d \cong N_s A_s A_c \left(1 - \frac{Y^2}{P^2}\right)$

$H(y)$ = vertical flux density distribution
N_s = source radiance
A_s = source area
y = vertical axis
p = parabola focus ($y^2 = 4px$)
P_d = signal on detector
A_d = detector area
A_c = imaging system collecting area
f_i = imaging system focal length

Flux Density Distribution

From the standard equation for radiative transfer, the flux collected and transmitted by the element of mirror area, dA_m, in Figures E-1 and E-2 is (neglecting reflection losses, which are not pertinent)

$$P = \frac{P_s A_s \cos \theta_s \, dA_m \cos \theta_i}{L^2}$$

Flux density, H, is the transmitted flux divided by the transmitted beam area:

$$H = \frac{P}{dA_m \cos \theta_i}$$

But angle of reflection, θ_r is equal to angle of incidence, θ_i, so that

$$H = \frac{P}{dA_m \cos \theta_i} = \frac{N_s A_s \cos \theta_s}{L^2}$$

The distance L is related to mirror position, y, by

$$L^2 = y^2 + (p - x)^2$$

Parabola function gives $y^2 = 4px$ so that

$$L^2 = y^2 + (p - \frac{y^2}{4p})^2 = \left(\frac{4p^2 + y^2}{4p}\right)^2$$

Angle θ_s is given by

$$\theta_s = \theta - \theta_o$$

$$\cos \theta_s = \cos \theta \cos \theta_o + \sin \theta \sin \theta_o$$

from Figure E-1 and the equation for L, above,

$$\cos \theta = \frac{p - x}{1} = p - \frac{y^2}{4P} = \frac{4p^2 - y^2}{4pL} = \frac{4p^2 - y^2}{4p^2 + y^2}$$

$$\sin \theta = \frac{y}{L} = \frac{4py}{4p^2 + y^2}$$

Then

$$\cos \theta_s = \frac{4p^2 - y^2}{4p^2 + y^2} \cos \theta_o + \frac{4py}{4p^2 + y^2} \sin \theta_o$$

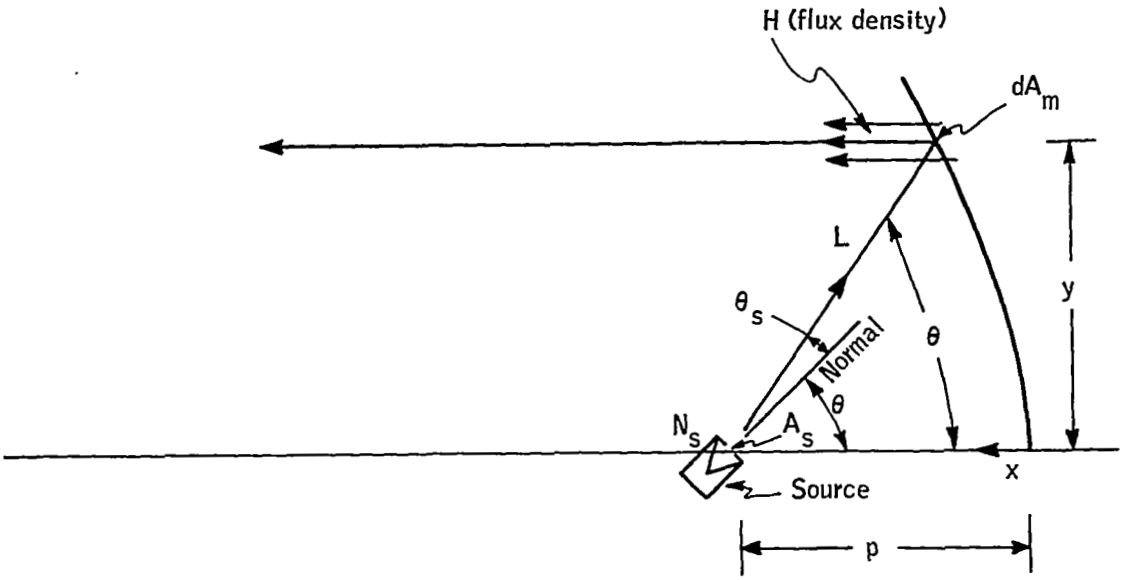

Figure E-1. PCS Beam Angular Relationships

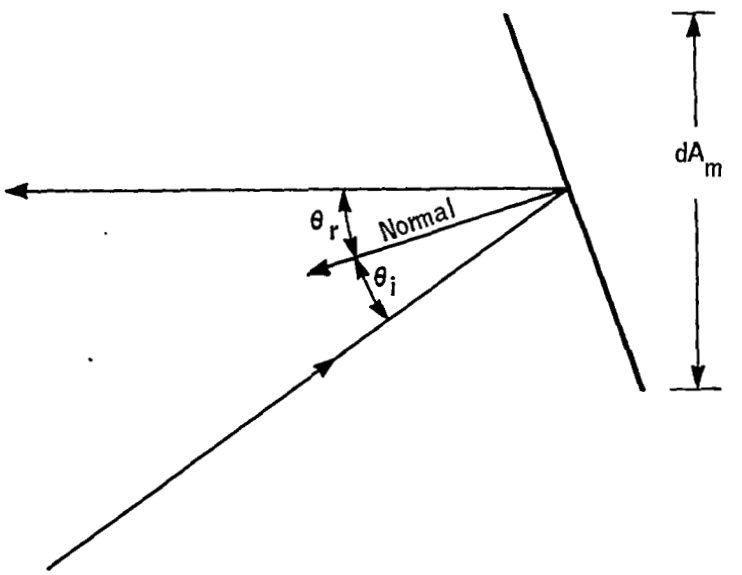

Figure E-2. Incident and Reflected Beams

The complete equation for flux density is then

$$H = N_s A_s \left[\frac{(4p^2 - y^2)\cos\theta_o + 4py \sin\theta_o}{(4p^2 + y^2)^3} \right] (4p)^2$$

For the PCS, $p \approx 120$, $\theta_o \approx 9$ degrees $6 \leq y \leq 30$.

One sees that $4p^2 >> y^2$ and using proper approximations on $\left(1 + \frac{y^2}{4p^2}\right)^n$ the vertical flux density distribution is given by:

$$H = \frac{N_s A_s}{p^2} \left(1 - 3/4 \frac{y^2}{p^2}\right) \left[\left(1 - \frac{y^2}{4p^2}\right) \cos\theta_o + \frac{y}{p} \sin\theta_o\right]$$

For further simplification, note that

$$\frac{y}{p} \sin\theta_o << \left(1 - \frac{y^2}{4p^2}\right) \cos\theta_o$$

resulting in

$$H \approx \frac{N_s A_s}{p^2} \left(1 - \frac{y^2}{p^2}\right) \cos\theta_o$$

Vertical distribution, normalized to $\frac{N_s A_s \cos\theta_o}{p^2} = 1.0$ is tabulated below:

y	H (y)
5	.99827
10	.99307
15	.9844
20	.9723
25	.9567
30	.9375

This shows that the flux density distribution across the aperture of the PCS is not uniform and that it varies by about 6 percent from bottom to top of the aperture. This is the variation which would be measured by moving a detector vertically across the aperture. However, this poses no problem in calibration accuracy when calibrating an imaging system with a field of view (detector) smaller than the projected PCS source, as shown below.

Imaging System Distribution

Consider the output flux density, H, of Figure E-1 being incident on and collected by an imaging system with an aperture smaller than dA_m. It collects flux of $P_c = HA_c$ where A_c is the optics collecting area. Signal on the detector is given by

$$P_d = H_i A_d$$

where H_i = image flux density = $\frac{P_i}{A_i}$

A_d = detector area

P_i is image flux and is equal to P_c; A_i is image area and is given by:

$$A_i = \Omega_s f_i^2$$

Where Ω_s is the solid angle field of the source projected by the collimator and f_i is the focal length of the imaging system.

From Figure E-1, $\Omega_s = \frac{A_s}{L^2} \cos \theta_s$

Recalling that $H = \frac{N_s A_s \cos \theta_s}{L^2}$, we get

$$P_d = \frac{N_s A_s \cos \theta_s}{L^2} \times A_d \times \frac{A_c L^2}{A_s \cos \theta f_i^2} = \frac{N_s A_d A_s}{f_i^2}$$

Thus the signal on the detector is independent of the imaging system in the PCS beam. Implied above is that the detector area is smaller than the image of the projected source. If the reverse is true, conditions change and detector signal can be shown to be

$$P_d = H A_c = \frac{N_s A_s \cos \theta_s}{L^2} A_c$$

$$* N_s A_s A_c \frac{\cos \theta_s}{L^2}$$

which exhibits the same vertical distribution as determined before, namely varying as

$$\frac{\cos \theta_s}{L^2} \approx 1 - \left(\frac{y}{p}\right)^2$$

APPENDIX F
TEST RADIOMETER SIGNAL-TO-NOISE RATIO

A primary objective of the test radiometer is to measure the geometric characteristics of the PCS output beam, especially the relative uniformity across the PCS output aperture. The governing performance parameter is measurement signal-to-noise ratio which determines the accuracy with which the relative uniformity measurements can be made. Required accuracy is implied by the PCS specification that the output beam be uniform or calibrated to within ± 0.1 percent. This requires a minimum signal-to-noise ratio of 1000. The test radiometer will produce a signal-to-noise ratio considerably better than 1000 as shown below.

Signal on the detector is calculated from

$$P_d = N \Omega A_{tr} k = 0.008 \times 0.25 \times 10^{-6} \times 177 \times 0.94 = 0.33 \times 10^{-6} \text{ w}$$

where N = source radiance in the detector response region $\cong$ 0.008 w/cm^2-sr for the source at 300°K

Ω = solid-angle field of view of the detector = 0.5 mr^2 for the Hg-Cd-Te detector (0.05 cm^2) and the test radiometer parabola (focal length = 100 cm)

A_{tr} = test radiometer parabola clear aperture area = 177 cm^2 for 15 cm aperture diameter

k = optics efficiency = 0.94 for four reflections, each with reflectivity of 0.985.

Noise is determined from measured detector parameters. Ata chopping frequency of 66 Hz, detectivity is 2 x 10^9 (cm Hz) 1/2/watt. This produces a NEP of

$$\text{NEP} = \frac{\sqrt{A_d}\sqrt{\Delta f_n}}{D^*} = \frac{0.05 \times 1}{2 \times 10^9} = 2.5 \times 10^{-11} \text{ w}$$

where A_d = detector area = 0.05 cm x 0.05 cm

f_n = noise bandwidth = 1 Hz

D* = detectivity = 2 x 10^9 cm Hz$^{1/2}$/watt

Signal-to-noise ratio, at the detector, is then

$$\frac{P_d}{NEP} = \frac{0.33 \times 10^{-6}}{2.5 \times 10^{-11}} = 13,200$$

APPENDIX G

TEST RADIOMETER BAFFLING

Stray light at the PCS signal frequency is caused by reflections from within the primary chamber and test radiometer chamber. Stray light from within the primary chamber does not cause a measurement error; rather is part of the PCS output beam and should be measured. Reflections reaching the test radiometer detector from any part of the test gear are measurement errors and should be eliminated. This is done by baffling at the detector, at the second folding mirror, and at the auxiliary parabola.

Figure G-1 shows the baffling for the test radiometer. The two baffles nearest the detector limit its operating field of view through their openings such that it will see either only the desired incoming radiation or a diffuse black surface which serves as the aperture stop for the system and is located at the surface of the 5-inch flat folding mirror. A second aperture stop is located at the surface of the parabola and is sized to the same F-number diameter as the folding mirror stop. A large diffuse black plate located in the reflectometer chamber at least 45 degrees to the incoming beam serves as an absorber for the unwanted incoming collimated radiance from the PCS source. The resultant incoming radiation will then reach the detector only if it is through the desired optical path or by at least two diffuse reflections. The maximum stray radiation reaching the detector is in the bundle of collimated output which specularly reflects off the first (scanning) folding mirror, then diffusely off the auxiliary parabola stop, then diffusely off the second folding mirror stop.

Figure G-2 shows the specular and diffuse reflections from the test radiometer optics. M_1 is the radiometer parabola and M_2 is the folding mirror which reflects the converging beam to the detector.

The input beam flux density is

$$H_{in} = \frac{N_s A_s k A_m}{F^2} \times \frac{1}{A_m} = N_s \Omega_s k$$

The output radiance from stop at M_1 is

$$N_1 = \frac{H_{in} \rho}{\pi}$$

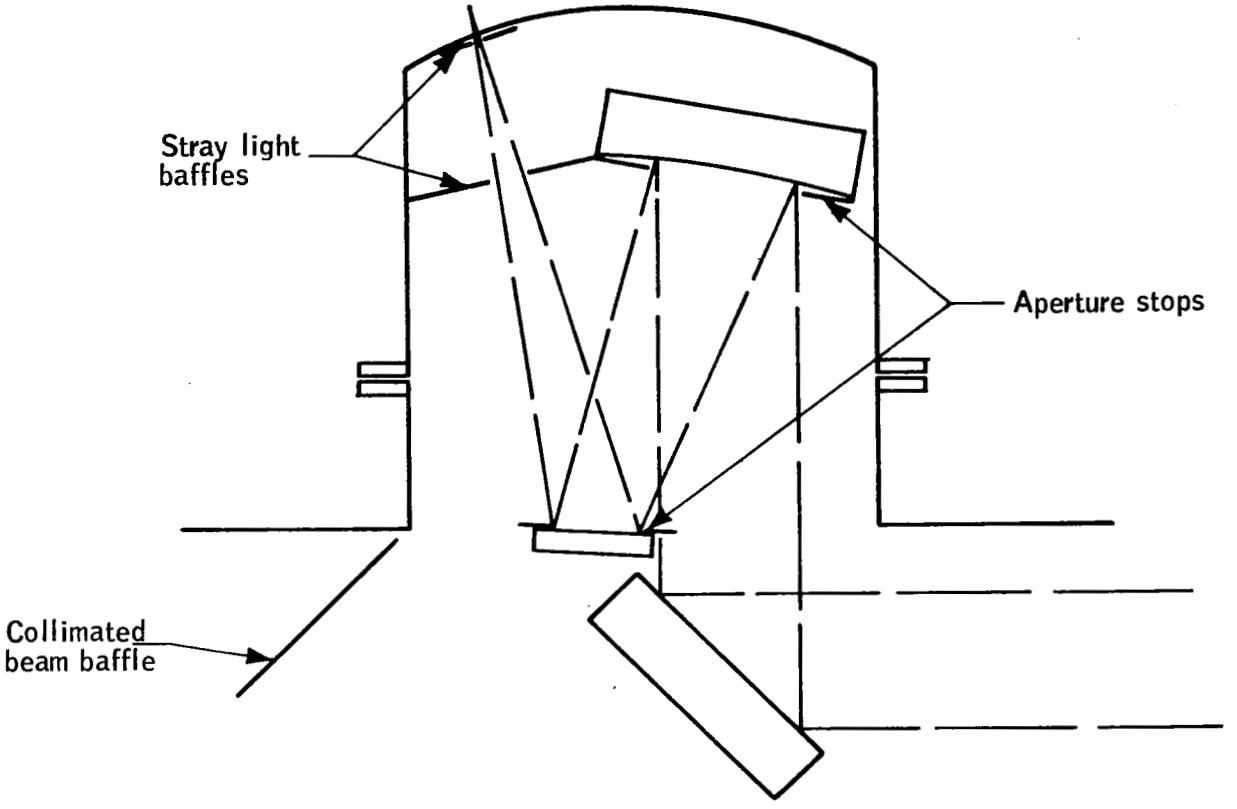

Figure G-1. Test Radiometer Baffles

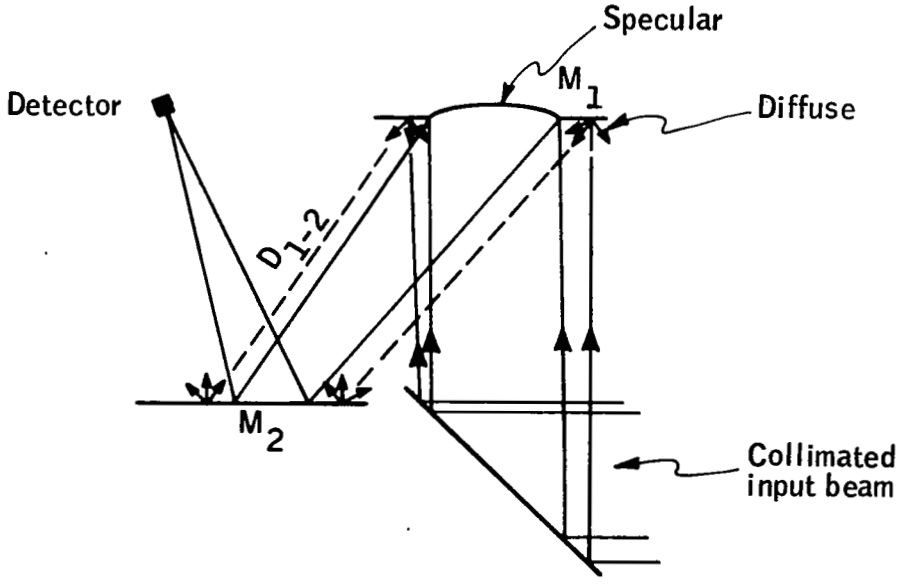

Figure G-2. Input Beam Reflections

The input flux to M_2 stop is

$$P_2 = \frac{N_1 A_1 A_2}{D_{1-2}^2}$$

The output radiance from M_2 is

$$N_2 = \frac{\rho P_2}{\pi A_2}$$

The detector signal $P_d = \frac{N_2 A_d A_2}{D_{2-d}^2} = \frac{\rho P_2 A_d A_2}{\pi A_2 D_2}$.

$$P_d = \frac{\rho N_1 A_1 A_2 A_d}{\pi D_2^2 D_{1-2}^2} = \frac{\rho H_{in} \rho A_1 A_2 A_d}{\pi\pi D_2^2 D_{1-2}^2} = \frac{\rho^2}{\pi^2} \frac{N_s \Omega_s k A_1 A_2 A_d}{D_2^2 D_{1-2}^2}$$

A_1 = 20-cm diameter input beam, 15-cm diameter stop

$$= \frac{\pi}{4} (20^2 - 15^2) = \frac{\pi}{4} (400-225) = 44\pi$$

$D_{1-2}^2 = 7500 \text{ cm}^2$

A_2 = 12.7-cm area seen by detector, stopped down to 8.9 cm

$A_2 = \frac{\pi}{4} (12.7^2 - 8.9^2) = \frac{\pi}{4} (161 - 79) = 20\pi \text{ cm}^2$

$D_{2-d} = 3560 \text{ cm}^2$

$\rho = 0.05$

$N_s = 0.008 \text{ w/cm}^2\text{-sr}$

$\Omega_s = \frac{\pi}{4} (3.3 \times 10^{-3})^2 = \frac{\pi}{4} \times 10^{-7}$

$k \cong 1.0$

$A_d = 0.05 \times 0.05 \text{ cm}^2$

$$P_d = \frac{0.05 \times 0.05 \times 0.008 \times 44\pi \times 20\pi \times 0.05 \times 0.05}{\pi^2 \times 7500 \times 3560}$$

$$= 1.5 \times 10^{-12} \text{ watts}$$

Normal signal on the detector

$$S = N\Omega A_{ap}\, k = 0.008 \times 0.25 \times 10^{-6} \times 177 \times 0.94$$

$$= 0.33 \times 10^{-6} \text{ watts}$$

The stray radiation $S/N = \dfrac{0.33 \times 10^{-6}}{1.5 \times 10^{-12}} = 220,000.$

Thus stray radiation errors are seen to be negligible.

APPENDIX H

THERMOMETER CALIBRATION DATA

This appendix contains the resistance-temperature data for the PCS thermometers. Figure H-1 is a resistance-temperature curve of the nickel-iron thermometers used throughout the chambers to measure temperatures of interest. Calibration reports of the source platinum resistance thermometers, Nos. 819, 828, and 833 are also included. Calibration data for thermometer No. 819 includes that from the National Bureau of Standards with a comparison in temperature, at 10°K intervals, to the manufacturer's data.

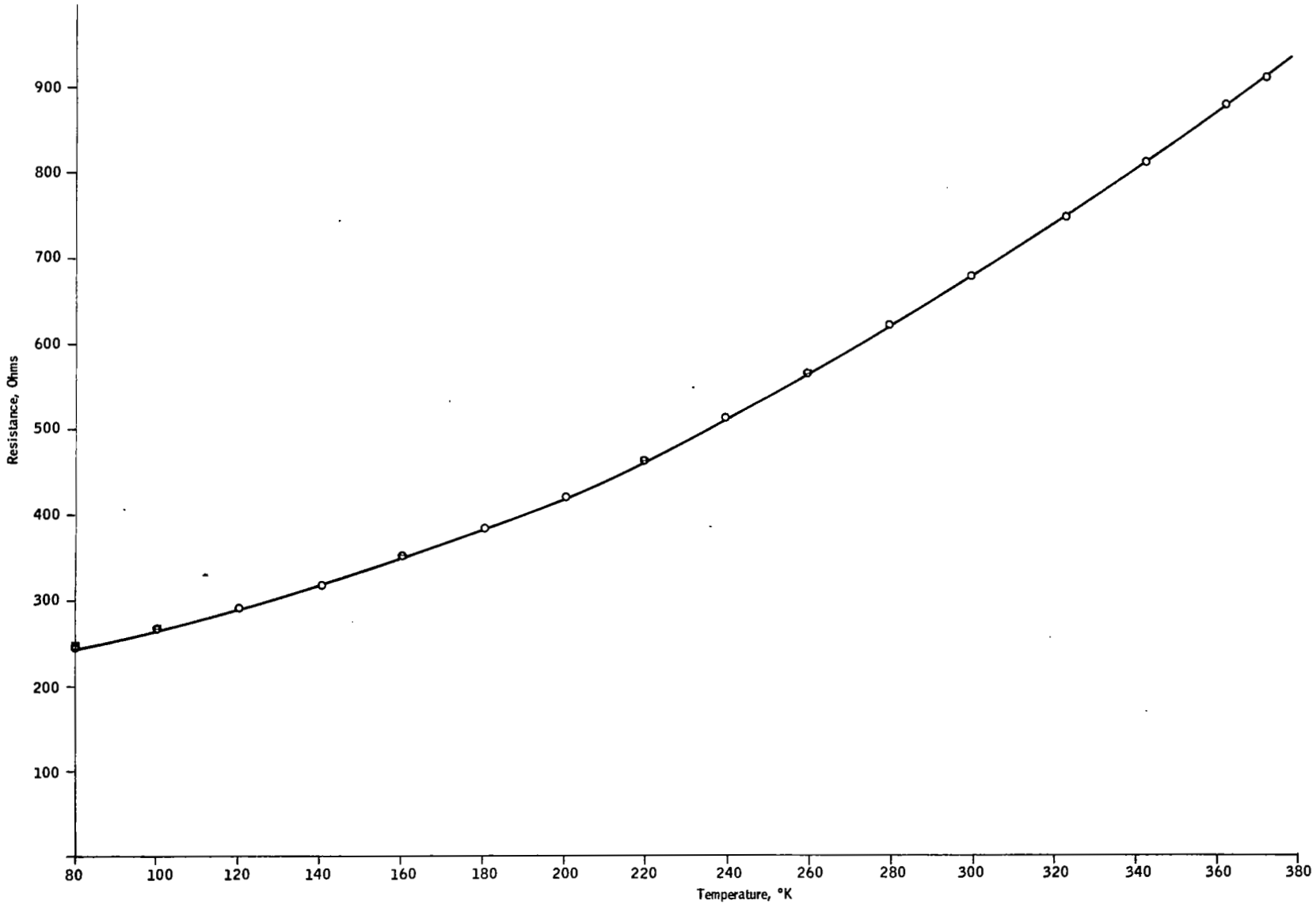

Figure H-1. Nickle-Iron Thermometer Resistence - Temperature Curve

National Bureau of Standards Calibration Data
Platinum Resistance Thermometer No. 819

The data on the following three pages are the calibration results performed by the NBS on thermometer No. 819 per the procedures described in Reference 7.

The thermometer was calibrated for use with continuous current of 1.0 ma. through the thermometer.

The following values were found for the constants in the International Practical Temperature Scale (1968) formulas:

Alpha = 3.926206-03	A4 = 2.389-07
Delta = 1.496493	C4 = 2.189-15

The resistance at 0 degrees C was found to be 25.6169 absolute ohms. During calibration, this resistance changed by the equivalent of 0.0003 degrees C.

JUNE 1970 IPTS-68 TABLE FOR RESISTANCE THERMOMETER 819

TEMP. KELVIN	RESISTANCE ABS. OHMS	INVERSE DIFF.		TEMP. KELVIN	RESISTANCE ABS. OHMS	INVERSE DIFF.	REC diff.
				100	7.33319	9.031	
				101	7.44384	9.037	
				102	7.55443	9.043	
				103	7.66495	9.048	
				104	7.77539	9.054	
				105	7.88576	9.061	
				106	7.99605	9.067	
				107	8.10627	9.073	
				108	8.21641	9.080	
				109	8.32646	9.086	
				110	8.43644	9.093	-.00272
				111	8.54634	9.099	
				112	8.65615	9.106	
				113	8.76589	9.113	
				114	8.87554	9.120	
				115	8.98511	9.126	
				116	9.09460	9.133	
				117	9.20401	9.140	
				118	9.31334	9.147	
				119	9.42259	9.154	
				120	9.53176	9.160	-.00302
				121	9.64084	9.167	
				122	9.74985	9.174	
				123	9.85877	9.180	
				124	9.96762	9.187	
				125	10.07639	9.194	
				126	10.18508	9.200	
				127	10.29370	9.207	
			REC diff.	128	10.40224	9.213	
				129	10.51070	9.220	
80	5.11101	9.011	+.0027	130	10.61908	9.226	-.00322
81	5.22266	9.005		131	10.72740	9.233	
82	5.33377	9.000		132	10.83563	9.239	
83	5.44493	8.996		133	10.94380	9.245	
84	5.55612	8.993		134	11.05189	9.251	
85	5.66734	8.992		135	11.15991	9.257	
86	5.77857	8.990		136	11.26786	9.264	
87	5.88980	8.990		137	11.37574	9.270	
88	6.00103	8.990		138	11.48355	9.276	
89	6.11225	8.991		139	11.59130	9.281	
90	6.22345	8.993	-.00206	140	11.69897	9.287	-.00343
91	6.33462	8.995		141	11.80658	9.293	
92	6.44577	8.997		142	11.91412	9.299	
93	6.55687	9.000		143	12.02159	9.304	
94	6.66793	9.004		144	12.12900	9.310	
95	6.77895	9.008		145	12.23635	9.316	
96	6.88991	9.012		146	12.34363	9.321	
97	7.00082	9.016		147	12.45085	9.327	
98	7.11167	9.021		148	12.55801	9.332	
99	7.22246	9.026		149	12.66511	9.337	
100	7.33319	9.031	-.00244	150	12.77214	9.343	-.00355

JUNE 1970 IPTS-68 TABLE FOR RESISTANCE THERMOMETER 819

TEMP. KELVIN	RESISTANCE ABS. OHMS	INVERSE DIFF.	REC diff.	TEMP. KELVIN	RESISTANCE ABS. OHMS	INVERSE DIFF.	REC diff.
150	12.77214	9.343		200	18.05862	9.556	
151	12.87912	9.348		201	18.16322	9.560	
152	12.98605	9.353		202	18.26778	9.564	
153	13.09289	9.358		203	18.37231	9.567	
154	13.19969	9.363		204	18.47679	9.571	
155	13.30643	9.368		205	18.58124	9.574	
156	13.41312	9.373		206	18.68565	9.578	
157	13.51975	9.378		207	18.79002	9.581	
158	13.62632	9.383		208	18.89435	9.585	
159	13.73284	9.388		209	18.99865	9.588	
160	13.83931	9.393	-.00357	210	19.10291	9.592	-.00374
161	13.94572	9.397		211	19.20713	9.595	
162	14.05208	9.402		212	19.31131	9.598	
163	14.15838	9.407		213	19.41546	9.602	
164	14.26464	9.411		214	19.51956	9.605	
165	14.37084	9.416		215	19.62364	9.609	
166	14.47699	9.421		216	19.72767	9.612	
167	14.58309	9.425		217	19.83167	9.615	
168	14.68914	9.430		218	19.93564	9.619	
169	14.79514	9.434		219	20.03956	9.622	
170	14.90109	9.438	-.00368	220	20.14345	9.625	-.00356
171	15.00699	9.443		221	20.24731	9.629	
172	15.11285	9.447		222	20.35113	9.632	
173	15.21865	9.451		223	20.45492	9.635	
174	15.32441	9.455		224	20.55866	9.639	
175	15.43012	9.460		225	20.66238	9.642	
176	15.53579	9.464		226	20.76606	9.645	
177	15.64140	9.468		227	20.86970	9.648	
178	15.74698	9.472		228	20.97331	9.652	
179	15.85250	9.476		229	21.07689	9.655	
180	15.95799	9.480	-.00379	230	21.18043	9.658	-.00358
181	16.06342	9.484		231	21.28394	9.661	
182	16.16881	9.488		232	21.38741	9.664	
183	16.27416	9.492		233	21.49085	9.668	
184	16.37947	9.496		234	21.59425	9.671	
185	16.48473	9.500		235	21.69762	9.674	
186	16.58995	9.504		236	21.80096	9.677	
187	16.69512	9.508		237	21.90426	9.680	
188	16.80025	9.512		238	22.00753	9.683	
189	16.90534	9.516		239	22.11077	9.687	
190	17.01039	9.519	-.00372	240	22.21397	9.690	-.00329
191	17.11540	9.523		241	22.31714	9.693	
192	17.22036	9.527		242	22.42028	9.696	
193	17.32529	9.531		243	22.52338	9.699	
194	17.43017	9.534		244	22.62645	9.702	
195	17.53501	9.538		245	22.72949	9.705	
196	17.63981	9.542		246	22.83249	9.708	
197	17.74457	9.546		247	22.93547	9.711	
198	17.84929	9.549		248	23.03841	9.714	
199	17.95398	9.553		249	23.14132	9.717	
200	18.05862	9.556	-.00372	250	23.24419	9.720	-.0034

JUNE 1970 IPTS-68 TABLE FOR RESISTANCE THERMOMETER 819

TEMP. KELVIN	RESISTANCE ABS. OHMS	INVERSE DIFF.	REC diff.	TEMP. KELVIN	RESISTANCE ABS. OHMS	INVERSE DIFF.
250	23.24419	9.720				
251	23.34704	9.723				
252	23.44985	9.727				
253	23.55263	9.730				
254	23.65537	9.733				
255	23.75809	9.736				
256	23.86077	9.739				
257	23.96343	9.742				
258	24.06605	9.745				
259	24.16863	9.748				
260	24.27119	9.751	-.00332			
261	24.37372	9.754				
262	24.47621	9.757				
263	24.57867	9.760				
264	24.68110	9.763				
265	24.78350	9.766				
266	24.88587	9.769				
267	24.98821	9.772				
268	25.09051	9.775				
269	25.19279	9.778				
270	25.29503	9.781	-.00323			
271	25.39724	9.784				
272	25.49942	9.787				
273	25.60157	9.790	-.00284			
274	25.70369	9.793				
275	25.80577	9.796				
276	25.90783	9.799				
277	26.00985	9.802				
278	26.11184	9.805				
279	26.21380	9.808				
280	26.31573	9.811	-.00265			
281	26.41763	9.814				
282	26.51950	9.817				
283	26.62133	9.820				
284	26.72314	9.823				
285	26.82491	9.826				
286	26.92665	9.829				
287	27.02836	9.832				
288	27.13004	9.835				
289	27.23169	9.838				
290	27.33330	9.841	-.00256			
291	27.43489	9.844				
292	27.53644	9.847				
293	27.63796	9.850				
294	27.73946	9.853				
295	27.84092	9.856				
296	27.94235	9.859				
297	28.04374	9.862				
298	28.14511	9.865				
299	28.24645	9.868				
300	28.34775	9.871	-.00246			

Manufacturer's Calibration Data

MODEL 162D SERIAL 819 3/27/70

T(68) KELVIN	RESISTANCE OHMS	OHMS PER KELVIN	T(68) KELVIN	RESISTANCE OHMS	OHMS PER KELVIN
80	5.111913	.110967	130	10.618734	.108385
81	5.222951	.111039	131	10.727044	.108310
82	5.334050	.111098	132	10.835280	.108236
83	5.445193	.111143	133	10.943443	.108163
84	5.556371	.111178	134	11.051534	.108091
85	5.667572	.111201	135	11.159554	.108019
86	5.778786	.111215	136	11.267502	.107949
87	5.890006	.111219	137	11.375381	.107878
88	6.001221	.111215	138	11.483190	.107809
89	6.112424	.111203	139	11.590931	.107741
90	6.223224	.110800	140	11.698603	.107673
91	6.334394	.111169	141	11.806209	.107606
92	6.445531	.111138	142	11.913748	.107539
93	6.556632	.111101	143	12.021222	.107474
94	6.667690	.111058	144	12.128631	.107409
95	6.778702	.111012	145	12.235976	.107345
96	6.889662	.110960	146	12.343257	.107281
97	7.000568	.110905	147	12.450476	.107219
98	7.111415	.110847	148	12.557633	.107157
99	7.222200	.110785	149	12.664728	.107095
100	7.332921	.110721	150	12.771763	.107035
101	7.443575	.110654	151	12.878738	.106975
102	7.554159	.110584	152	12.985654	.106916
103	7.664672	.110513	153	13.092511	.106857
104	7.775112	.110440	154	13.199310	.106799
105	7.885477	.110365	155	13.306052	.106742
106	7.995765	.110288	156	13.412737	.106685
107	8.105977	.110212	157	13.519366	.106629
108	8.216111	.110134	158	13.625940	.106574
109	8.326165	.110055	159	13.732458	.106519
110	8.436140	.109975	160	13.838923	.106464
111	8.546034	.109894	161	13.945333	.106411
112	8.655847	.109813	162	14.051691	.106357
113	8.765580	.109732	163	14.157996	.106305
114	8.875230	.109651	164	14.264248	.106253
115	8.984800	.109569	165	14.370450	.106201
116	9.094288	.109488	166	14.476600	.106150
117	9.203694	.109407	167	14.582699	.106099
118	9.313020	.109325	168	14.688748	.106049
119	9.422264	.109244	169	14.794748	.106000
120	9.531428	.109164	170	14.900699	.105951
121	9.640512	.109084	171	15.006600	.105902
122	9.749515	.109004	172	15.112454	.105853
123	9.858440	.108924	173	15.218259	.105806
124	9.967285	.108845	174	15.324018	.105758
125	10.076052	.108767	175	15.429729	.105711
126	10.184742	.108689	176	15.535393	.105665
127	10.293354	.108612	177	15.641012	.105618
128	10.401889	.108536	178	15.746584	.105572
129	10.510349	.108460	179	15.852111	.105527
130	10.618734	.108385	180	15.957593	.105482

MODEL 162D SERIAL 819 3/27/70

T(68) KELVIN	RESISTANCE OHMS	OHMS PER KELVIN	T(68) KELVIN	RESISTANCE OHMS	OHMS PER KELVIN
180	15.957593	.105482	230	21.180058	.103542
181	16.063030	.105437	231	21.283565	.103507
182	16.168422	.105392	232	21.387038	.103473
183	16.273770	.105348	233	21.490477	.103439
184	16.379075	.105305	234	21.593882	.103405
185	16.484336	.105261	235	21.697253	.103371
186	16.589554	.105218	236	21.800591	.103337
187	16.694729	.105175	237	21.903895	.103304
188	16.799862	.105132	238	22.007165	.103270
189	16.904952	.105090	239	22.110402	.103237
190	17.010000	.105048	240	22.213606	.103204
191	17.115007	.105006	241	22.316777	.103171
192	17.219972	.104965	242	22.419915	.103138
193	17.324895	.104924	243	22.523019	.103105
194	17.429778	.104883	244	22.626091	.103072
195	17.534620	.104842	245	22.729130	.103039
196	17.639422	.104802	246	22.832137	.103007
197	17.744183	.104761	247	22.935111	.102974
198	17.848905	.104721	248	23.038052	.102942
199	17.953587	.104682	249	23.140962	.102909
200	18.058229	.104642	250	23.243838	.102877
201	18.162832	.104603	251	23.346683	.102845
202	18.267395	.104564	252	23.449496	.102813
203	18.371920	.104525	253	23.552276	.102780
204	18.476406	.104486	254	23.655025	.102748
205	18.580854	.104448	255	23.757741	.102717
206	18.685263	.104409	256	23.860426	.102685
207	18.789635	.104371	257	23.963079	.102653
208	18.893968	.104333	258	24.065700	.102621
209	18.998264	.104296	259	24.168289	.102589
210	19.102522	.104258	260	24.270847	.102558
211	19.206743	.104221	261	24.373373	.102526
212	19.310926	.104184	262	24.475868	.102495
213	19.415073	.104147	263	24.578332	.102464
214	19.519183	.104110	264	24.680764	.102432
215	19.623256	.104073	265	24.783164	.102400
216	19.727292	.104037	266	24.885533	.102369
217	19.831293	.104000	267	24.987871	.102338
218	19.935257	.103964	268	25.090177	.102306
219	20.039185	.103928	269	25.192452	.102275
220	20.143077	.103892	270	25.294696	.102243
221	20.246933	.103856	271	25.396908	.102212
222	20.350754	.103821	272	25.499088	.102181
223	20.454540	.103785	273	25.601283	.102195
224	20.558290	.103750	274	25.703402	.102119
225	20.662005	.103715	275	25.805489	.102087
226	20.765685	.103680	276	25.907545	.102056
227	20.869330	.103645	277	26.009570	.102025
228	20.972941	.103611	278	26.111563	.101993
229	21.076517	.103576	279	26.213525	.101962
230	21.180058	.103542	280	26.315456	.101931

MODEL 162C SERIAL 819 3/27/70

T(68) KELVIN	RESISTANCE OHMS	OHMS PER KELVIN	T(68) KELVIN	RESISTANCE OHMS	OHMS PER KELVIN
280	26.315456	.101931			
281	26.417355	.101899			
282	26.519223	.101868			
283	26.621059	.101837			
284	26.722864	.101805			
285	26.824638	.101774			
286	26.926381	.101743			
287	27.028092	.101711			
288	27.129772	.101680			
289	27.231421	.101649			
290	27.333039	.101618			
291	27.434625	.101586			
292	27.536180	.101555			
293	27.637704	.101524			
294	27.739197	.101493			
295	27.840658	.101462			
296	27.942089	.101430			
297	28.043488	.101399			
298	28.144856	.101368			
299	28.246193	.101337			
300	28.347499	.101306			

Manufacturer's Calibration Data

MODEL 162D SERIAL 828 3/30/70

T(68) KELVIN	RESISTANCE OHMS	OHMS PER KELVIN	T(68) KELVIN	RESISTANCE OHMS	OHMS PER KELVIN
80	5.102199	.110757	130	10.598962	.108170
81	5.213027	.110828	131	10.707058	.108096
82	5.323915	.110888	132	10.815080	.108022
83	5.434848	.110933	133	10.923029	.107949
84	5.545814	.110967	134	11.030906	.107877
85	5.656805	.110990	135	11.138712	.107806
86	5.767809	.111004	136	11.246448	.107735
87	5.878817	.111008	137	11.354113	.107666
88	5.989822	.111004	138	11.461710	.107597
89	6.100814	.110993	139	11.569238	.107528
90	6.212299	.111485	140	11.676699	.107461
91	6.323241	.110942	141	11.784093	.107394
92	6.434151	.110910	142	11.891421	.107328
93	6.545025	.110874	143	11.998683	.107263
94	6.655856	.110832	144	12.105881	.107198
95	6.766642	.110785	145	12.213015	.107134
96	6.877376	.110734	146	12.320086	.107071
97	6.988056	.110680	147	12.427094	.107008
98	7.098677	.110622	148	12.534041	.106947
99	7.209237	.110560	149	12.640927	.106886
100	7.319734	.110496	150	12.747752	.106825
101	7.430163	.110429	151	12.854518	.106766
102	7.540523	.110360	152	12.961224	.106707
103	7.650813	.110289	153	13.067872	.106648
104	7.761029	.110217	154	13.174463	.106590
105	7.871171	.110142	155	13.280996	.106533
106	7.981237	.110065	156	13.387473	.106477
107	8.091226	.109990	157	13.493894	.106421
108	8.201138	.109912	158	13.600260	.106366
109	8.310971	.109833	159	13.706571	.106311
110	8.420724	.109753	160	13.812828	.106257
111	8.530397	.109673	161	13.919032	.106203
112	8.639990	.109593	162	14.025182	.106150
113	8.749502	.109512	163	14.131280	.106098
114	8.858933	.109431	164	14.237326	.106046
115	8.968283	.109350	165	14.343321	.105995
116	9.077552	.109269	166	14.449265	.105944
117	9.186739	.109188	167	14.555158	.105893
118	9.295846	.109107	168	14.661002	.105843
119	9.404872	.109026	169	14.766796	.105794
120	9.513818	.108946	170	14.872541	.105745
121	9.622684	.108866	171	14.978237	.105696
122	9.731471	.108786	172	15.083886	.105648
123	9.840178	.108707	173	15.189486	.105601
124	9.948807	.108629	174	15.295040	.105553
125	10.057358	.108551	175	15.400546	.105507
126	10.165831	.108473	176	15.506007	.105460
127	10.274227	.108396	177	15.611421	.105414
128	10.382548	.108320	178	15.716789	.105368
129	10.490792	.108245	179	15.822112	.105323
130	10.598962	.108170	180	15.927390	.105278

MODEL 162D SERIAL 828 3/30/70

T(68) KELVIN	RESISTANCE OHMS	OHMS PER KELVIN	T(68) KELVIN	RESISTANCE OHMS	OHMS PER KELVIN
180	15.927390	.105278	230	21.139834	.103344
181	16.032623	.105233	231	21.243143	.103309
182	16.137812	.105189	232	21.346419	.103275
183	16.242957	.105145	233	21.449660	.103241
184	16.348059	.105101	234	21.552867	.103208
185	16.453117	.105058	235	21.656041	.103174
186	16.558132	.105015	236	21.759181	.103140
187	16.663104	.104972	237	21.862288	.103107
188	16.768034	.104930	238	21.965361	.103073
189	16.872922	.104888	239	22.068401	.103040
190	16.977768	.104846	240	22.171408	.103007
191	17.082572	.104804	241	22.274382	.102974
192	17.187335	.104763	242	22.377323	.102941
193	17.292057	.104722	243	22.480231	.102908
194	17.396738	.104681	244	22.583106	.102875
195	17.501379	.104641	245	22.685949	.102843
196	17.605979	.104600	246	22.788759	.102810
197	17.710539	.104560	247	22.891536	.102778
198	17.815059	.104520	248	22.994281	.102745
199	17.919540	.104481	249	23.096994	.102713
200	18.023981	.104441	250	23.199675	.102681
201	18.128383	.104402	251	23.302324	.102649
202	18.232746	.104363	252	23.404941	.102617
203	18.337071	.104324	253	23.507524	.102584
204	18.441356	.104286	254	23.610077	.102553
205	18.545604	.104247	255	23.712598	.102521
206	18.649813	.104209	256	23.815087	.102489
207	18.753984	.104171	257	23.917544	.102457
208	18.858117	.104133	258	24.019969	.102425
209	18.962213	.104096	259	24.122363	.102394
210	19.066271	.104058	260	24.224725	.102362
211	19.170292	.104021	261	24.327056	.102331
212	19.274277	.103984	262	24.429355	.102299
213	19.378224	.103947	263	24.531624	.102269
214	19.482134	.103910	264	24.633861	.102237
215	19.586008	.103874	265	24.736066	.102205
216	19.689845	.103837	266	24.838240	.102174
217	19.793647	.103801	267	24.940382	.102142
218	19.897412	.103765	268	25.042493	.102111
219	20.001141	.103729	269	25.144573	.102080
220	20.104834	.103693	270	25.246622	.102049
221	20.208492	.103658	271	25.348639	.102017
222	20.312115	.103622	272	25.450625	.101986
223	20.415702	.103587	273	25.552625	.102000
224	20.519253	.103552	274	25.654548	.101923
225	20.622770	.103517	275	25.756439	.101891
226	20.726252	.103482	276	25.858299	.101860
227	20.829699	.103447	277	25.960128	.101829
228	20.933112	.103413	278	26.061925	.101797
229	21.036490	.103378	279	26.163691	.101766
230	21.139834	.103344	280	26.265426	.101735

MODEL 162C SERIAL 828 3/30/70

T(68) KELVIN	RESISTANCE OHMS	OHMS PER KELVIN	T(68) KELVIN	RESISTANCE OHMS	OHMS PER KELVIN
280	26.265426	.101735			
281	26.367130	.101704			
282	26.468802	.101672			
283	26.570443	.101641			
284	26.672053	.101610			
285	26.773632	.101579			
286	26.875179	.101547			
287	26.976695	.101516			
288	27.078181	.101485			
289	27.179635	.101454			
290	27.281057	.101423			
291	27.382449	.101392			
292	27.483810	.101361			
293	27.585139	.101329			
294	27.686437	.101298			
295	27.787705	.101267			
296	27.888941	.101236			
297	27.990146	.101205			
298	28.091320	.101174			
299	28.192463	.101143			
300	28.293575	.101112			

Manufacturer's Calibration Data

MODEL 162D SERIAL 833 3/30/70

T(68) KELVIN	RESISTANCE OHMS	OHMS PER KELVIN	T(68) KELVIN	RESISTANCE OHMS	OHMS PER KELVIN
80	5.107079	.110863	130	10.609018	.108276
81	5.218013	.110935	131	10.717220	.108202
82	5.329007	.110994	132	10.825348	.108128
83	5.440046	.111039	133	10.933403	.108055
84	5.551120	.111073	134	11.041386	.107983
85	5.662216	.111097	135	11.149297	.107912
86	5.773327	.111110	136	11.257138	.107841
87	5.884442	.111115	137	11.364909	.107771
88	5.995553	.111111	138	11.472611	.107702
89	6.106652	.111099	139	11.580244	.107633
90	6.218000	.111348	140	11.687810	.107566
91	6.329053	.111053	141	11.795309	.107499
92	6.440075	.111022	142	11.902741	.107433
93	6.551060	.110985	143	12.010109	.107367
94	6.662003	.110943	144	12.117411	.107302
95	6.772899	.110896	145	12.224649	.107238
96	6.883744	.110845	146	12.331825	.107175
97	6.994535	.110791	147	12.438937	.107113
98	7.105267	.110732	148	12.545988	.107051
99	7.215938	.110671	149	12.652978	.106990
100	7.326544	.110606	150	12.759907	.106929
101	7.437084	.110540	151	12.866776	.106869
102	7.547555	.110470	152	12.973587	.106810
103	7.657954	.110399	153	13.080338	.106752
104	7.768280	.110326	154	13.187032	.106694
105	7.878532	.110252	155	13.293669	.106637
106	7.988707	.110175	156	13.400249	.106580
107	8.098806	.110099	157	13.506774	.106524
108	8.208827	.110021	158	13.613243	.106469
109	8.318769	.109942	159	13.719657	.106414
110	8.428631	.109862	160	13.826017	.106360
111	8.538413	.109782	161	13.932323	.106306
112	8.648115	.109701	162	14.038576	.106253
113	8.757735	.109620	163	14.144777	.106201
114	8.867274	.109539	164	14.250926	.106149
115	8.976732	.109458	165	14.357023	.106097
116	9.086109	.109377	166	14.463070	.106046
117	9.195405	.109296	167	14.569065	.105996
118	9.304619	.109215	168	14.675011	.105946
119	9.413753	.109134	169	14.780907	.105896
120	9.522807	.109053	170	14.886755	.105847
121	9.631780	.108973	171	14.992553	.105799
122	9.740674	.108894	172	15.098303	.105750
123	9.849488	.108814	173	15.204006	.105703
124	9.958224	.108736	174	15.309661	.105655
125	10.066882	.108658	175	15.415270	.105608
126	10.175462	.108580	176	15.520831	.105562
127	10.283965	.108503	177	15.626347	.105516
128	10.392391	.108427	178	15.731817	.105470
129	10.500742	.108351	179	15.837241	.105424
130	10.609018	.108276	180	15.942621	.105379

MODEL 162D SERIAL 833 3/30/70

T(68) KELVIN	RESISTANCE OHMS	OHMS PER KELVIN	T(68) KELVIN	RESISTANCE OHMS	OHMS PER KELVIN
180	15.942621	.105379	230	21.160059	.103442
181	16.047955	.105335	231	21.263467	.103408
182	16.153245	.105290	232	21.366841	.103374
183	16.258492	.105246	233	21.470181	.103340
184	16.363694	.105203	234	21.573487	.103306
185	16.468853	.105159	235	21.676760	.103272
186	16.573969	.105116	236	21.779998	.103239
187	16.679043	.105073	237	21.883204	.103205
188	16.784074	.105031	238	21.986375	.103172
189	16.889062	.104989	239	22.089514	.103138
190	16.994009	.104947	240	22.192619	.103105
191	17.098914	.104905	241	22.295691	.103072
192	17.203777	.104864	242	22.398730	.103039
193	17.308600	.104822	243	22.501736	.103006
194	17.413381	.104782	244	22.604709	.102973
195	17.518122	.104741	245	22.707650	.102941
196	17.622823	.104701	246	22.810558	.102908
197	17.727483	.104660	247	22.913434	.102876
198	17.832104	.104621	248	23.016277	.102843
199	17.936685	.104581	249	23.119088	.102811
200	18.041226	.104541	250	23.221867	.102779
201	18.145728	.104502	251	23.324613	.102746
202	18.250191	.104463	252	23.427328	.102715
203	18.354616	.104424	253	23.530010	.102682
204	18.459001	.104386	254	23.632660	.102650
205	18.563348	.104347	255	23.735278	.102618
206	18.667657	.104309	256	23.837865	.102587
207	18.771928	.104271	257	23.940420	.102555
208	18.876161	.104233	258	24.042943	.102523
209	18.980357	.104195	259	24.145435	.102491
210	19.084515	.104158	260	24.247894	.102460
211	19.188635	.104121	261	24.350323	.102428
212	19.292719	.104084	262	24.452720	.102397
213	19.396765	.104047	263	24.555086	.102366
214	19.500775	.104010	264	24.657420	.102334
215	19.604749	.103973	265	24.759723	.102303
216	19.708685	.103937	266	24.861994	.102271
217	19.812586	.103900	267	24.964234	.102240
218	19.916450	.103864	268	25.066442	.102209
219	20.020278	.103828	269	25.168619	.102177
220	20.124071	.103793	270	25.270765	.102146
221	20.227828	.103757	271	25.372880	.102115
222	20.331549	.103721	272	25.474963	.102083
223	20.435235	.103686	273	25.577060	.102097
224	20.538886	.103651	274	25.679082	.102021
225	20.642502	.103616	275	25.781072	.101990
226	20.746083	.103581	276	25.883030	.101959
227	20.849629	.103546	277	25.984958	.101927
228	20.953140	.103511	278	26.086854	.101896
229	21.056617	.103477	279	26.188718	.101865
230	21.160059	.103442	280	26.290551	.101833

MODEL 162C SERIAL 833 3/30/70

T(68) KELVIN	RESISTANCE OHMS	OHMS PER KELVIN	T(68) KELVIN	RESISTANCE OHMS	OHMS PER KELVIN
280	26.290551	.101833			
281	26.392353	.101802			
282	26.494124	.101771			
283	26.595863	.101739			
284	26.697571	.101708			
285	26.799248	.101677			
286	26.900894	.101646			
287	27.002508	.101614			
288	27.104091	.101583			
289	27.205643	.101552			
290	27.307163	.101521			
291	27.408653	.101489			
292	27.510111	.101458			
293	27.611538	.101427			
294	27.712934	.101396			
295	27.814298	.101365			
296	27.915632	.101334			
297	28.016934	.101302			
298	28.118206	.101271			
299	28.219446	.101240			
300	28.320655	.101209			

REFERENCES

1. J.C. Carson ; et al: Feasibility Design of an Instrument System for Measurement of the Horizon Radiance in the CO_2 Absorption Band, Horizon Definition Study. NASA CR-66429, May 1967.

2. J.S. Titus and R.N. Schmidt: Feasibility Investigation of a Low-Temperature, Variable Infrared Source, Horizon Definition Study. NASA CR-66614, March 1968.

3. R.P. Heinisch, J.K. Anderson, and R.N. Schmidt: Emittance Measurement Study, Final Report. NASA CR-1583, June 1969

4. J.R. Thomas; et al: Attitude - Referenced Radiometer Study. Volume II, Precision Radiometric System. NASA CR-66855, August 1969.

5. V.G. Padalka and I.N. Shklyarevskii: Determination of the Microcharacteristics of Silver and Gold from the Infrared Optical Constants and the Conductivity at 82 and 295°K. Optics and Spectroscopy, Volume 11, No. 4, October 1961, page 285.

6. Thomas Altshuler: Procedure for Calculation of Atmospheric Transmission of Infrared. General Electric Report No. R57ELC15, May 1957.

7. John L. Riddle: Notes to Supplement Resistance Thermometer Reports on the International Practical Temperature Scale of 1968. National Bureau of Standards, April 1969.

NASA-Langley, 1971 – 14
Coml., Newport News, Va.